AMERICAN UNIVERSITY OF BEIRUT

Towards a computationally efficient model of working memory: a case study on vocabulary acquisition

by
Nadine Jamil Hajj

A thesis
submitted in partial fulfillment of the requirements
for the degree of Doctor of Philosophy
to the Department of Electrical and Computer Engineering
of the Faculty of Engineering and Architecture
at the American University of Beirut

Beirut, Lebanon
April 2019

AMERICAN UNIVERSITY OF BEIRUT

TOWARDS A COMPUTATIONALLY EFFICIENT MODEL OF WORKING MEMORY: A CASE STUDY ON VOCABULARY ACQUISITION

by

NADINE JAMIL HAJJ

Approved by:

Dr. Zaher Dawy, Professor Electrical and Computer Engineering, AUB	Committee Chair
Dr. Mariette Awad, Associate Professor Electrical and Computer Engineering, AUB	Advisor
Dr. Fadi Karameh, Associate Professor Electrical and Computer Engineering, AUB	Member of Committee
Dr. Arne Dietrich, Professor Psychology, AUB	Member of Committee
Dr. Wassim Nasreddine, Assistant Professor Neurology, AUB	Member of Committee
Dr. Taous-Meriem Laleg-Kirati, Assistant Professor KAUST	Member of Committee
Dr. Donatello Materassi, Assistant Professor Electrical and Computer Engineering, AUB	Member of Committee

Date of thesis/dissertation defense: April 24, 2019

AMERICAN UNIVERSITY OF BEIRUT

THESIS, DISSERTATION, PROJECT RELEASE FORM

Student Name: Hajj Nadine Jamil
Last First Middle

○ Master's Thesis ○ Master's Project ⊗ Doctoral Dissertation

☐ I authorize the American University of Beirut to: (a) reproduce hard or electronic copies of my thesis, dissertation, or project; (b) include such copies in the archives and digital repositories of the University; and (c) make freely available such copies to third parties for research or educational purposes.

☒ I authorize the American University of Beirut, to: (a) reproduce hard or electronic copies of it; (b) include such copies in the archives and digital repositories of the University; and (c) make freely available such copies to third parties for research or educational purposes after: **One ___ year from the date of submission of my thesis, dissertation or project.**
Two ___ years from the date of submission of my thesis , dissertation or project.
Three X years from the date of submission of my thesis , dissertation or project.

Nadine Hajj 12/5/2019
Signature Date

This form is signed when submitting the thesis, dissertation, or project to the University Libraries

Acknowledgements

First and foremost I am grateful for my advisor Professor Mariette Awad for her continuous support and guidance throughout this long journey. As my teacher and mentor, Dr. Awad provided me extensive personal and professional guidance and taught me a great deal about both scientific research and life in general, she has taught me more than I could ever give her credit for here. She has shown me, by her example, what a good scientist (and person) should be.

I would like to extend my gratitude towards the committee members for this dissertation for their valuable input and comments; in particular to the chair of the committee Professor Zaher Dawy for his relevant feedback.

I am grateful to all of those with whom I have had the pleasure to work during this and other related projects and have helped me grow and learn throughout my residency at the American University of Beirut.

Last but not least, to my family and friends who stood by me during the tough times in the past five years and have shown me unconditional love and support.

An Abstract of the Thesis of

Nadine Jamil Hajj for Doctor of Philosophy
Major: Electrical and Computer Engineering

Title: A multi-modal stochastic and reinforcement deep learning framework inspired by the biological working memory

Seamlessly integrating today's advanced technologies into our life requires intelligent systems capable of handling various types of inputs such as images and audio; which calls for multi-modal learning. While creating a unique delineation of a concept based on different modalities such as visual and phonological representation is a seemly effortless task for humans, deep learning models often struggle to successfully implement a unified structure capable of handling multiple modalities due to their specialized structures that process a specific type of data. Challenges in multi-modal learning tasks include forming a homogeneous representation of the different modalities, translating signals from one modality to another, identifying overlapping information across inputs, fusing these inputs into one form, and employing the different inputs in learning a unique model.

This dissertation presents a biologically inspired multi-modal deep learning stochastic based computational model of working memory adhering to Baddeley's mutli-component model. The model is composed of three loops playing the role of phonological short term processing store, visual short term analysis store and central executive. The loops employed are inspired by their biological counterpart at the structural and operational levels. Three training algorithms to learn the network's connections are proposed: an iterative Bayesian solution, a stochastic spike timing dependent reinforcement learning strategy and a two stage algorithm with an unsupervised phase and a reinforcement learning phase.

The proposed network and algorithms are tested on publicly available datasets. The phonological loop is tested on a collection of English word recordings with the proposed network achieving an average recognition rate of 92.45%. The visual loop tested on the Amsterdam Library of Object Images achieved an average

accuracy of 95.3%. The central executive is tested on the 1-2-AX task with a 97.5% accuracy reported in our results. The multi-modal network attained an overall accuracy of 98.25% - an improvement of 6.64% over the best performing deep architecture - for an increase of 44% in training epochs with a reduction of 14.4% in the number of parameters needed by our model thus saving about 7 GB in storage space. Complexity and sensitivity analysis are conducted to show the merit of the proposed solution. In addition, a case study using the proposed visual loop is conducted for security applications. The network is tested in the tasks of person identification, abandoned luggage detection and crime classification. Superior performance was obtained compared to state of the art algorithms.

Contents

List of Figures

List of Tables

Chapter 1

Introduction

As humans, we heavily rely on our senses to perform a multitude of daily tasks ranging from simple object identification to complex higher order decision making. Losing a sensory function often leaves the subject at a disadvantage and presents a challenge for both technology and humans to maintain swift communication. Integrating today's advanced technologies into our life requires intelligent systems capable of handling various types of inputs such as images and audio; which calls for multi-modal learning. While creating a unique delineation of a concept based on different modalities such as visual and phonological representation is a seemly effortless task for humans, deep learning models often struggle to successfully implement a unified structure capable of handling multiple modalities due to their specialized structures that process a specific type of data. Challenges in multi-modal learning tasks include forming a homogeneous representation of the different modalities, translating signals from one modality to another, identifying overlapping information across inputs, fusing these inputs into one form, and employing the different inputs in learning a unique model [5].

The deep learning community has attempted in the past decade to present efficient solutions to multi-modal learning problems using deep neural networks [6, 7, 8], deep Boltzmann machines [9], and recurrent neural networks such as LSTM [10, 11, 12]. Applications targeted by multi-modal learning span a variety of types including audio-visual speech recognition and synthesis, action classification, event detection, emotion recognition and synthesis, image and video description, and multimedia cross modal retrieval and hashing [13]. Early work in multimodal machine learning focused on audio-visual speech recognition [14] and employed a hidden Markov models approach with various extensions [15, 16]. Recently deep neural networks were employed in audio-visual classification with marginal improvement in noisy settings [6]. With the exponential growth in multimedia data, context indexing and retrieval has been targeted by multimodal learning using a variety of rule based methods and classification techniques such as support vector machines, estimation methods such as Kalman filtering and neu-

ral networks [17, 18]. The fields of emotion recognition and synthesis emerged as applications to affective computing with multi-modal learning applied to applications such as face detection and expression classification. A range of techniques were employed for that purpose including Bayesian modeling, Markov models, Kalman filters and some voting rules [19, 20]. Image captioning is another application that has seen some interest in health care problems targeting visually impaired patients and has been tackled using a variety of classification, correlation and image processing techniques [21, 22].

An interesting application that would greatly benefit from a multi-modal learning system is assisted living robots. Given the challenges in financial assistance and insurance coverage, as well as the shortage in caregivers, assistive robots are becoming an integral if not necessary part of patient care for the elderly population. Today's robots fall into several categories: telerobots which primary goal is effective communication with health care professionals and patient monitoring [23]; mobile manipulators which service older patients with disabilities by fetching requested items [24]; assistive walking devices which support patients in their transportation needs preventing falls and injuries [25, 26]; animal-like robots which provide entertainment and stress-relief to emotionally and mentally challenged patients [27, 28, 29]; home health care robots which provide multiple medical services including monitoring and treatment [30]; and humanoid robots which alleviate the burden of constant care by identifying patient needs, providing medications and managing health care plan [31].

In an attempt to tackle the problem of multi-modal learning, we present a biologically inspired multi-modal computational model of working memory, a function responsible for maintaining and manipulating information for a temporary period, crucial for the execution of multiple simple and complex cognitive tasks [32]. Baddeley's working memory model, the most influential to date, dissects working memory into three basic components: a visuo-spatial sketchpad holding visual and spatial information, a phonological loop holding phonological information and a central executive acting as a "control structure" [33, 34, 35]. A mutli-modal approach where separate storage and processing units are employed for visual and phonological processing and an integration and analysis unit that mimics the role of the central executive is adopted.

Given the often limited computer proficiency of patients interacting with these robots, ease of use requires the developed systems to swiftly analyze, store and recall inputs generated by the patient and/or environment which can take various forms. A basic task such as fetching an object requires a system capable of identifying these objects using inputs such as visual and verbal cues (such as images captured by a camera mounted on the robot arm and words uttered by the patient). Efficiently executing these tasks require an intelligent system which can

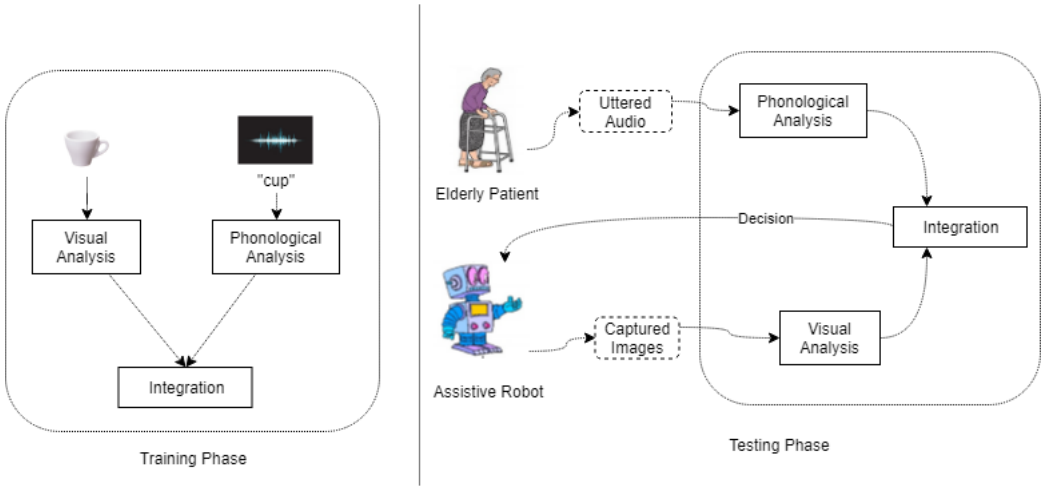

Figure 1.1: Motivational example of a multi-modal object recognition assistive robot

efficiently interpret information generated by sensors and/or humans in a timely manner. Learning such system often occurs using some learned models which can be static mostly and provided by the designer during system pre-training, or dynamic through an online learning mechanism that adapts to the environment and iteratively adapts and improves its performance. Given the nature of assisted living setups, robots which can efficiently communicate and adapt to such environment would benefit from a multi-modal system capable of incorporating concepts represented by different modality inputs into a robust representation instead of using the trendy deep networks that pre-train on massive datasets. An illustration of a possible deployment of such a system for an assistive robot framework is shown in figure 1.1. During the training phase, the model is trained on a sequence of visual and phonological cues (in the form of audio) representing objects which can be found in domestic environments. For example, the model learns to associate images of a cup and the uttered word "cup" with the concept of a cup. During the testing phase, an elderly patient utters a word (such as "cup) representing an object present while a camera mounted on the robot is capturing images of the surrounding objects, the different images captured as well as the auditory cue are hence passed to the model which produces a decision once the correct image is found (the robot picks up the object requested by the patient once the camera locates it).

Other than in assisted living environments which require conversational robots and human-machine interfaces to perform specific tasks while efficiently communicating with the patient via multi-modal (image and/or audio) cues, our work has direct implications for better understanding executive dysfunction in neurological disorders such as attention deficit-hyperactivity disorder (ADHD),

Parkinson's disease, Multiple Sclerosis (MS), and other neurodegenerative disorders. More importantly, it would provide a simple and easy platform for medical practitioners to simulate and associate symptoms of these diseases with biological phenomena such as neural degeneration, and neural hyperactivity. Manipulations of the neural substrate can mimic lesions or pharmacological interventions using a set of parameters such as cell type, firing rate and learning rate. As an easy alternative to invasive recording techniques which can be crucial to brain-machine interfaces for locked-in patients, our work is a step towards shedding light into the neurological basis of challenged learners.

To learn the connections of our network we present three learning algorithms. The first a simplification employing a Bayesian inference scheme in which two assumptions can be made: a deterministic setup in which weights are considered deterministic unknown variables and a probabilistic approach where rather than learning a tremendous number of variables, weights are assumed to be drawn from a normal distribution of unknown parameters (i.e. mean and standard deviation) rendering the number of optimization variables (and hence the cardinality of the search space) a reduced one. Furthermore, the problem is tackled from two perspectives: a global approach where the entire network optimizes a global objective function - and hence individual loops may not be optimal with respect to their own performed task -, and a localized approach where each loop achieves a local solution minimizing a local objective function - the overall objective function is hence not necessarily minimized). The second, a spike timing dependent plasticity based reinforcement learning strategy in which a modification of the partially observable Markov decision process is introduced to implement a reinforcement learning algorithm in which neurons act as agents and actions taken are firing decisions. And the third a two-stage learning algorithm in which the basic assumption we take is that while smaller subpopulations of neurons reach a local solution using a Hebbian-like learning, larger associations employ a reinforcement learning strategy to optimize their collaboration.

While security cameras are widely spread in areas ranging from commercial shops, to airports, to streets; the sense of security remains diminished among the general populace, in part due to the increasing threads from malicious individuals or groups and in other part due to the lack of constant monitoring of these cameras. While ensuring around the clock surveillance staff may be expensive and impractical, implementing intelligent systems capable of detecting security breaches and/or recognizing suspects is an efficient and desirable solution.

With the tremendous increase in computational power provided by the development of GPUs and other distributed architectures, deep learning has attained considerable success in a variety of computer vision tasks including but not limited to face recognition, object identification and scene understanding. One field

that has benefited tremendously from the evolution of deep learning algorithms is security applications. With convolutional neural networks exceeding human performance levels [36] in the ImageNet LSVRC 2010 context, a various set of convolutional architectures are now ready-made for use in image related machine learning tasks. Such models have been widely and successfully employed for tasks such as face detection [37, 38], person re-identification [39, 40, 41], abandoned luggage detection in airports and public settings [42, 43], and criminal event classification[44, 45, 46].

We present a case study using the proposed visual processing deep network inspired by the human's visual system which encompasses the eye, the lateral geniculate nucleus and the primary visual cortex on three security related tasks: person re-identification, abandoned luggage detection and event classification.

In summary the contributions of this dissertation are as follows:

- A biologically inspired multi-modal deep learning network modeled after Baddeley's multi-component model.
- Three algorithms for learning the weights of the network: a Bayesian iterative algorithm, a stochastic spike timing dependent reinforcement learning strategy, and a two-stage learning algorithm composed of a stochastic unsupervised Hebbian phase and a stochastic reinforcement learning phase
- A case study using the proposed visual network on security visual tasks

This dissertation is organized as follows: Chapter 2 discusses the state of the art on cognitive and computational models of working memory, Chapter 3 summarizes background information on electrical signaling in neurons the neurological basis of learning and memory, and the organization of the cerebral cortex. Chapter 4 presents the structure of our proposed multi-modal network. Chapter 5 details the three proposed algorithms for learning our model. Chapter 6 presents our experimental results while chapter 7 concludes the draft.

Chapter 2

Literature Review

2.1 Introduction

Understanding the ability of the human brain to perform complex cognitive tasks in a timely and efficient manner has always been the goal of researchers in multiple fields with applications including medical care, artificial intelligence and education [47, 48, 49]. While an abundance of evidence provided by electrophysiological data and brain lesions shaped our understanding of the cortex functionality, a detailed description of the mode of operation of the different subsystems employed during complex tasks is yet to be provided, mainly due to the unfeasibility of employing invasive recording techniques in humans [50]. Of interest to our research is working memory (WM), a short term capacity limited buffer for temporary storage and processing of information. This core executive function has been proven to play a central role in processing sensory inputs, retrieving stored information from the long term memory as well as carrying out complex tasks such as problem solving, creative thinking and language production [51].
Questions that arise when attempting to describe the functionality of WM mainly incorporate three aspects: the cognitive aspect concerned with providing a general workflow scheme to the information processing occurring in WM; the computational aspect which attempts to model the neurological phenomenon underlying the WM function; and the anatomical aspects which discerns brain areas or regions involved in WM tasks and their respective roles; as well as the effect of a brain lesions or malfunction in a particular node on the overall operation of the WM network.
The aim of this chapter is to provide a combined view of WM from the three described perspectives; an effort that to the best of our knowledge is yet to be accomplished. This review is intended to equip researchers from various disciplines with a general outlook to WM while pointing out relevant references for those seeking further information.
The rest of this chapter is organized as follows: section 2.2 presents a summary

of the cognitive models of WM with emphasis on Baddeley's multi-component model [33] and Cowan's embedded processes model [52]; section 2.4 surveys the latest computational models of WM including neurocomputational studies focusing on the functioning of elementary units as well as artificial models relying on large-scale networks; section 2.5 describes the anatomical aspect of WM by summarizing the evidence collected in neuroimaging studies towards disseminating brain areas involved in WM tasks in addition to the neural correlates of WM related impairments; section 2.6 reports on the applications of WM in cognition, education, and artificial intelligence.

2.2 Cognitive models

According to the International Handbook of Psychology [53], the term 'working memory' (WM) refers to a platform capable of holding and manipulating information for a limited period of time. While a consensus regarding domain specific resources is yet to be reached; the definition of WM has shifted from the earlier concept of a short-term memory (STM) - a buffer of temporary storage - to a system that plays a crucial role in a variety of cognitive tasks ranging from simple recall to vocabulary acquisition. Many models for the mode of operation of WM has been proposed. This section summarizes the most prominent ones.

2.2.1 Baddeley's multi-component model

The original multi-component model initially proposed by Baddely and Hitch [33] - the most influential to date - is composed of 3 limited capacity components: the phonological loop, the visuospatial sketchpad and the central executive. The phonological loop holds speech-based and acoustic information in a temporary store lasting to a few seconds and refreshed by rehearsal. The visuospatial sketchpad has a similar functioning processing visual and spatial information. The central executive plays the role of integration and controls the flow of information between the loops.
The phonological loop presents multiple properties observed during verbal memory tasks:

- The phonological similarity effect: Similarity in spoken items improves serial recall of lists proving the existence of a phonological storage facility. The phonological loop is hence better understood by repeatedly using the same limited set.

- The word length effect: Longer words result in a poorer performance as was shown in [54]. This is due to the fact longer words require more time for rehearsal and thus are more affected by decay which in turn reduces performance. Another possible hypothesis is that longer words are more

sensitive to interference. Both explanations do not contradict the theory of a phonological loop [55].

- Articulatory suppression: The word length effect can be avoided by removing subvocalization [54, 56]. Written information requires subvocalization (i.e. uttering the word) for registration as opposed to uttered words which are directly registered in the phonological store. A contradictory view of this effect is provided by Jones et al. [57] claiming that this is the result of a mere perceptual effect linked to the recency effect of immediate serial recall; a rebuttal of such explanation was later provided in [55] showing that this effect is prominent across the serial position curve for short lists.

- Irrelevant Sound Effects: Irrelevant sounds have a greater effect on the recall of written digits as compared to white noise [58]; furthermore irrelevant sounds and nonsense syllables equally disturb the visual STM hinting at a prelexical level of interference [59]. Additionally, Jones et al. [60] showed that other range of sounds such as fluctuating tones have equal disruptive capacity as irrelevant words suggesting that a 'changing state' (or fluctuation) is a crucial feature in disruptive stimuli [61].

- Retaining Serial Order: Memory span is measured as the amount of digits that can be correctly recalled in order. A typical memory span is around six or seven digits [62]. Maintaining order in serial recall is critical to a variety of applications such as language and skilled performance. The theory of sequential association to retain order is far from accurate as pointed out by Lashley [63]; in fact partial recall is possible when an item is lost (the rest of the chain can be correctly recited). A possible explanation links items with a series of internal markers [64, 65]; another model assumes a degrading degree of excitation (emerging from a shared limited capacity of excitation) linked to the order of items. Recall hence occurs based on a decreasing strength of activation (in other terms, when encoded items are represented with a decreasing order of excitation)[66].

The fact that the phonological loop has been proven to be crucial for vocabulary learning [67] strongly supports the existence of a link between working memory and long term memory, with similar conclusions drawn for the visuospatial sketchpad. As a result a revised multi-component model was devised by [62].
The visuospatial sketchpad is a capacity-limited storage for processing visuospatial information with a span about five [62]. While further distinction between a visual and a spatial buffer is yet inconclusive, a number of studies support this dichotomy [68, 69, 70].
The central executive is regarded as a homunculus capable of attentional focus, storage and decision making. It is involved in situations where switching between tasks is required. Furthermore it has an important role in interfacing with long

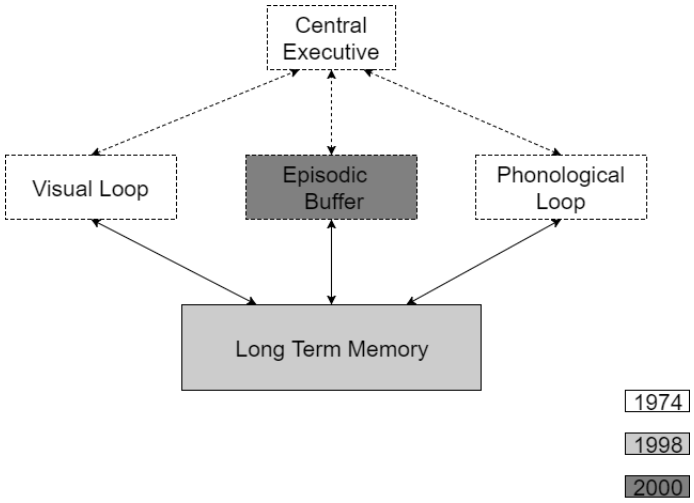

Figure 2.1: Evolution of Baddeley's model of WM

term memory [71]. This led to the addition of a fourth component in Baddeley's model of working memory: the episodic buffer a limited-capacity storage assumed to hold integrated episodes linking working memory to long term memory. An estimate of the capacity of this component is of four chunks [62, 72]. Figure 2.1 shows an illustration of the evolution of Baddeley's model of WM. Solid lines represent permanent systems and dashed lines represent temporary blocks.

2.2.2 Cowan's embedded processes model

Cowan's view of working memory is that activated memory and the focus of attention cannot be identical; the number of items activated in the short term memory is greater than that in the focus of attention hence items can be activated outside the focus of attention [73]. Cowan postulates that auditory stimulus undergoes two phases of processing: a brief period of activation (up to a few hundred milliseconds) and an extended stage up to about 30 seconds as illustrated in figure 2.2. Furthermore Cowan claims that his processing is common for other modalities, the first period of persistence of excitation being equivalent to an encoding process, the second phase viewed as a vivid recollection of the stimulus [74]. Cowan's view of activated memory equals that of Baddeley's phonological and visuospatial loops and has the advantage of representing temporary storage as one subsystem rather than distinct stores accounting for possible further additions or segmentation of domain specific units [72]. Cowan's structure is a focus of attention embedded within activated memory (hence the nomenclature embedded process model)[73, 75, 52]

The main assumptions and features of the embedded process model are summarized below [1]:

- Though the distinction between a verbal and visuospatial forms of memory is valid, interference between these two tasks is possible. Moreover, further dissection of types of temporary buffers are equally plausible (auditory versus verbal versus tactile source of stimulation is a valid illustration). It is hence advantageous to represent the temporary storage as one unit where different types of stimulus are processed and interference is facilitated.

- According to Cowan, the term focus of attention represents the subset of memory currently active and being attended to. The term short-term memory or activated memory is used in the literature to refer to the entire activated area or to the subset within the focus of attention. An association of voluntary (emerging from central executive) and automatic (due to environmental interventions) processes are responsible for the control of the focus of attention (as shown in figure 2.2).

- Whereas some theories consider working memory as the portion of long term memory that is being activated Cowan goes beyond this definition to account for episodic links between simultaneously presented stimuli. These links in form of objects, chunks or events are mediated by attention before encoding into long term memory.

- When rehearsal or grouping of multiple stimuli is kept from occurring, links between the corresponding encoded items are not formed and each stimulus is represented as a separate chunk in working memory. An estimate of the capacity limit ranges from three to five chunks of information (see section 2.3.2 for a short review on measuring the capacity of working memory). Cowan's understanding of working memory limit is that of the focus of attention [76].

- Parietal lobes are the hub responsible of the focus of attention, whereas frontal lobes are the main site of the central executive controlling attention. An antagonism arises between storage and processing of information due to the involvement of the focus of attention in retention of both data and task goal and processing controlled by the central executive (emerging from frontal lobes) [77]. A partial resolution of this issue results from practice which redirects processing towards automatic an phenomenon and storage within long term memory.

- Focus of attention can hold the maximum number of chunks (capacity limit of around four) or can be redirected towards one task to enhance its processing. Information storage within activated memory outside of the scope of attention relieves the load on attention and hence avoids the storage

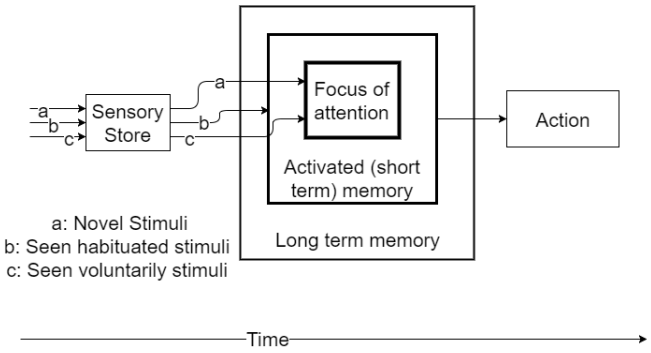

Figure 2.2: Cowan's model of information processing [1]

limitation problem. Ability to control attention is thought of as highly dependent on the capacity of the focus of attention.

2.2.3 Long term working memory model

The main argument in this hypothesis states that the concept of a short-time temporary buffer must be extended to include some form of long term storage to meet the large load on working memory during certain tasks such as text comprehension and expert performance. The skilled memory theory postulates that cognitive functions are regarded as a end results of information processing stored in the long-term memory and are recalled by cues into the short-term memory by acquiring memory skills (hence the terminology of skilled memory). The process of working memory under skilled memory theory termed "long-term working memory" includes a temporary buffer namely the short-term working memory [78]. Information is kept in the long-term working memory and accessed by cues into the short-term working memory. The two types of memory are differentiated at the level of duration: while short-term working memory is only transient, information in the long-term memory are kept in a stable more permanent state [79].

Encoding of stimuli is the result of specific processes responsible of creating episodic representations in a "retrievable form" (a form which allows a particular cue of reactivating the corresponding trace). Acquired knowledge and cues are the core of recall and influence both learning and encoding stages. Information is stored in a long-term form in a manner that allows traces and episodes to remain stored and be easily retrieved using a retrieval cue.

Acquiring the correct skills that allow "experts" to skillfully manipulate domain-specific information is underlined by two phenomena: recency and elaborative encoding. As a result reliable retrieval remains possible even when multiple related cues are presented or when multiple representations are activated as a result of

a cue. This can be achieved by learning associations between presented stimuli, retrieval cues and long term representations stored in memory. Expert skills are maintained by repetitions ad long term learning.

2.2.4 Time-based resource-sharing model

While other models mention the importance of time in cognition through forgetting from short term memory, the time-based resource-sharing model [80, 81] presents a time-based framework for working memory based on four assumptions. The first defines the role of attention as a limited shared capacity module, gating both the processing and maintenance of information. The second postulates that decay of memory or forgetting is due to the attention being switched away, with attention being required for refreshment of these traces. The third proposes that disruption occurs when an attention requiring process causes attention to shift hence averting memory refreshment. The fourth assumes a time aspect of attentional resources sharing: attention is fully engaged within certain tasks during a short period of time and memory refreshment is totally prevented during these periods. Resources are shared via a rapid and frequent switching between the processing and the maintenance of information during the execution of a task.
Short-term memory is defined as being the part of long-term memory activated beyond a threshold via attention, while working memory includes traces of short-term memory as well as the parts of long term memory activated outside the focus of attention. Maintenance or refreshment of memory traces requires a frequent switching from processing to holding of information. As a consequence, decay is directly correlated with the amount of time allocated to processing rather than maintenance and is related to attention switching. Hence, high cognitive loads are not due to the complexity of the task or the amount of time required for the completion of the task, but rather are the result of a frequent switching of attention towards maintaining the corresponding information hence inhibiting attention and thus memory from processing other tasks. During a low cognitive load, other tasks are attended to when a lower rate of switching occurs allowing the processing of new information rather than maintenance of current traces. According to this theory cognitive load is a function of the amount of time spent during which attention is prevented from switching to processing to allow retention of information. The higher the load the less the capacity of memory of processing of other tasks [82].

The functionality of Baddeley's central executive loop under the time based resource sharing model framework was investigated through a series of experimental studies [83]. Barrouillet argues that most of the fractionations of working memory assumed by Baddeley's standard multi-component model tend to disappear when temporal factors are carefully controlled, and that the system known as the central executive is in charge of both functions of processing and storage.

Results clearly indicate that processing and storage interfere in working memory and, therefore, they rule out a strong version of the multi-component model assuming a sharp distinction between executive control and storage.

2.2.5 Discrete-slots models

According to the discrete-slots view, visual WM makes available some number of slots for storing to-be-remembered items. The slot-based memories are conceptualized as being all-or-none: When memory is probed, if the test item occupies one of the discrete slots, then the observer can judge its presence with no loss in resolution, regardless of the number of other items in the set of to-be-remembered objects. By contrast, if the object has not been stored in one of the discrete slots, then there is a complete loss of resolution, that is, no information about the presented object remains. Specific members of the family of discrete-slots models differ according to whether the number of slots is presumed to be fixed or variable across trials and/or conditions.

An alternative view proposes that visual WM consists of a pool of resources that is allocated in continuous fashion through sharing of the resources. Thus, if the number of memory items is small, then the observer can maintain high-resolution representations of all of them. By contrast, if a large number of items must be maintained, then the continuous sharing of resources leads the observer to have lower-resolution representations of the individual items when memory is probed. The slots model of visual working memory, despite its simplicity, has provided an excellent account of data across a number of change detection experiments.

In a study by Donkin et. al [84], the slots model is investigated for the ability to account for the increased prevalence of errors when there is a potential for confusion about the location in which items are presented during study. Under the assumption that such location errors in the slots model occur when the feature information for an item in one location is swapped with the feature information for an item in another location, location errors were shown to be due to two reasons: whether the test item changes to an "external" item not presented at study, or to an "internal" item presented at another location during study and the number of items in the study array. By manipulating these variables it was shown that the slots model with location errors fails to provide a satisfactory account of the observed data.

Conversely, this model was tested in [85] by assessing the receiver operating characteristics (ROC) of participants in a visual-working-memory change-detection task. ROC plots yielded straight lines with a slope of 1.0, a tell-tale characteristic of all-or-none mnemonic representations, highly consistent with a

discrete fixed-capacity model of working memory for this task.

2.2.6 Other models

Previously detailed models are specific theories devised to explain the functionality of working memory. The literature provides an abundance of models that treat this function as a subpart of a complete model of human thinking. In what follows, we briefly mention the most related frameworks that model working memory as part of a cognitive human thinking model.

Controlled attention framework [86]

Working memory consists of active traces of long term memory, process required to maintain said activation and attention. Attention is a domain-free, limited capacity, controlled resource. Working memory reflects the ability to activate representations in memory, 'bring' and maintain them in focus. Fluid intelligence emerges from individual differences in capacity for controlled processing. Experts acquire the ability to overcome attentional limitations in their field of expertise while said limitations reemerge in novel situations. Controlled processing is required to maintain goals and block interference. The prefrontal cortex and related structures are the hub for controlled processing. Individual differences reflect that of the operation of the prefrontal cortex.

ACT-R model [87]

Adaptive Character of Thought-Rational theory is a cognitive architecture of human thinking. Complex cognition is the by product of the interaction of procedural and declarative knowledge. Procedural knowledge consists of units termed production rules while declarative knowledge consists of chunks. Objects in the environments are encoded in chunks while their transformation and interactions are represented in production rules. Human cognition relies on the amount and the deployment of encoded knowledge.

EPIC model [88]

EPIC's working memory has several complementary parts as illustrated in figure 2.3.

- Modal stores: temporary stores which hold encoded information from perceptual (visual, auditory, and tactile)processors.

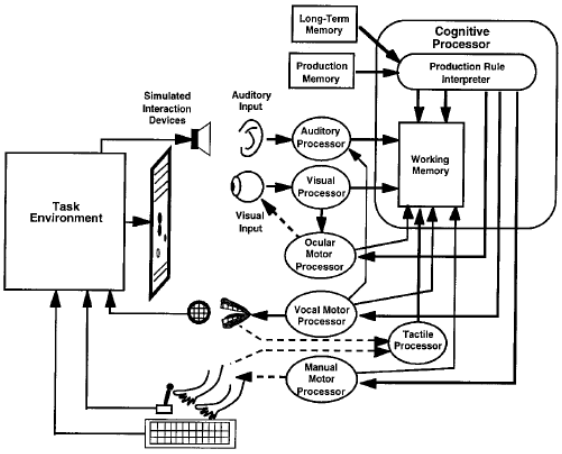

Figure 2.3: EPIC model of human thinking

- Control store: holds information regarding the goals and steps, which cause goals to be executed in specified sequences, as well as strategy notes which manipulate goals and status notes which refer to the status of processes.
- Tag store: contains labels which associate roles to modal store items.
- Storage capacity: a temporary buffer which holds information that can be kept from decay after random amounts of time if refreshed. The capacity of EPIC's working memory if a function of decay times and refresh rates.

Soar architecture [89]

Soar can be thought of as an engine for applying knowledge to situations to yield behavior. All behavior is seen as occurring in a problem spaces, made up of States and Operators. Fluent behavior is a cycle where an operator is selected, and is applied to the current state resulting in a new state. Each decision cycle ends with some kind of change to the context stack. If the knowledge available specifies a unique next operator, then that change is made, otherwise an impasse occurs. Soar learns to overcome impasses using a reinforcement learning based scheme.

Interactive cognitive subsystems model [90]

A general framework for human behavior composed of 9 subsystems falling under two categories: peripheral and central. Peripheral subsystems include sensory and perceptive modules - namely acoustic, visual and body state subsystems - as well

as effectors - namely articulatory and limb subsystem. Central subsystems include morphonolexical (speech forms), object (entities in visual space), propositional (entities in semantic space) and implicational (abstract relationship).

2.3 Discussion

2.3.1 Domain specific resources

A major question in cognitive science concerns the nature and the functional organization of the working memory system, particularly that related to the specificity of storage resources. Baddeley's dissemination of storage capacities into separate phonological and visuospatial loops has been widely investigated with contradicting results.
In a study by Feforenko et. al [91], the results of a dual-task experiment which investigates the nature of working memory resources used in sentence comprehension are reported. Participants read sentences of varying syntactic complexity (containing subject- and object-extracted relative clauses) while remembering one or three nouns (similar to or dissimilar from the sentence-nouns). A significant on-line interaction was found between syntactic complexity and similarity between the memory-nouns and the sentence-nouns in the three memory-nouns conditions, such that the similarity between the memory-nouns and the sentence-nouns affected the more complex object extracted relative clauses to a greater extent than the less complex subject-extracted relative clauses. The results argue against the domain-specific view of working memory resources in sentence comprehension.
Vergauwe et. al [92] examined trade-offs in four dual-task situations in which participants maintained verbal or visuospatial information while concurrently processing either verbal or visuospatial information. Results revealed that both verbal and visuospatial recall performance decreased as a direct function of increasing cognitive load, regardless of the nature of the information concurrently processed. The observed trade-offs suggest strongly that verbal and visuospatial activities compete for a common domain-general pool of resources.
On the other hand, Chein et. al [93] conducted an fMRI study to identify brain regions making domain-general contributions to working memory task performance. For both verbal and spatial versions of the task, complex working memory span performance increased the activity in lateral prefrontal, anterior cingulate, and parietal cortices during the Encoding, Maintenance, and Coordination phase of task performance. Meanwhile, overlapping activity in anterior prefrontal and medial temporal lobe regions was associated with both verbal and spatial recall from working memory. These findings serve to support the distinction between verbal and visuospatial resources.
Further evidence towards this dissemination is shown in [94] where two experi-

ments are reported in which participants were required to perform pairwise combinations of a verbal memory task, a visual memory task, and perceptuomotor tracking, and pairwise combinations of the two memory tasks and articulatory suppression. Tracking resulted in no disruption of the verbal memory preload over and above the impact of a delay in recall and showed only minimal disruption of the retention of the visual memory load. Performing an ongoing verbal memory task had virtually no impact on retention of a visual memory preload or vice versa, indicating that performing two demanding memory tasks results in little mutual interference. Results also showed minimal disruption when the two memory tasks were combined, although verbal memory (but not visual memory) was clearly disrupted by articulatory suppression interpolated between presentation and recall. These data suggest that a multiple-component working memory model provides a better account for performance in concurrent immediate memory tasks than do theories that assume a single processing and storage system.

2.3.2 Limited capacity

The concept of limited capacity has been the target of multiple studies over the last two decades. According to Cowan [95], quantifying the capacity of WM can be regarded in three aspects: the number of "items" that can be held in memory, the limited time these items can be held and the "energy" limit (neuronal aspect). The first view regards WM as a buffer with limited amount of "slots" that are occupied by memory traces, also termed chunks. The second approach characterizes WM as a limited-time resource where items held decay over time. The third aspect considers the neuronal resources (hence the terminology of "energy") employed to hold representations which are limited in nature and hence are altered by competition and interference.
The first attempt to quantify memory span dates back to 1956 [96], when Miller quantified memory limit to seven (plus or minus 2) items. Digit span was widely employed as a mean to characterize WM capacity which was thought to be around seven until Cowan revised this number to the "magical four" [97]. Further dissemination of WM components following the Baddeley and Hitch model [33] attempted to quantify limits of the different modality specific resources following a large amount of evidence strongly suggesting independent components. For example disturbing the phonological loop would disrupt verbal memory but not spatial memory while the reverse is true for a spatial disruption [67, 55].
Capacity of verbal memory was estimated at four to six chunks of information. This number remained constant regardless of the type of stimuli used (words or digits). Increasing the complexity of retained information did not affect the amount of chunks retained but rather altered the complexity of the chunks which became larger [96]. However Baddeley et. al [54] contradicted this view by arguing that a subject's recall is enhanced when short words are retained and stipulated that capacity limit is rather related to the amount of time items are

stored and not the length.
Similar results where obtained for the visuo-spatial memory. Memory span is measured by presenting and array of objects to be retained. Performance was unaltered for different complexities (color, orientation, size, and presence or absence of a black segment in the center) [98].
Furthermore, Cowan argues for a cross-modality capacity limit stemming from the attention control process: holding information is an attention-requiring process which cannot be unlimited [76].

2.4 Computational models

Modeling cognitive functions requires a good understanding as well as providing answers on the operation of the neural substrate from the molecular aspect to the global abstract functioning of the involved areas. We survey in this section the state of the art computational models tackling working memory at the elementary level as well as at the global scale.

2.4.1 Neurocomputational models

At the cellular scale, working memory models tackles the behavior of single cell neurons and aim at developing artificial models generating spikes with relatively high resemblance to those observed in single cell recordings [99, 100]. The main underlying mechanism allowing for memory function is persistent activity observed in working memory cells even after removal of stimuli [101]. The main theories explaining this phenomenon are: recurrent excitation within cell assemblies [102], synfire chains [103] and single-cell bistability [104].

Persistent activity through recurrent excitation

The underlying assumption behind this theory is that activity may be maintained in a neural network through recurrent excitation [105]. Memory traces are stored in the network via the synaptic strength of connections and are retrieved as fixed-point attractors. To achieve such representation neurons encoding a particular pattern are connected via strong excitatory recurrent connections, while nodes encoding different traces are linked through weak connections (i.e. inhibitory weights). Such model can be learned using a Hebbian rule which strengthen connections between co-firing neurons. During retrieval, a stored pattern is recalled by the activation of the stored pattern. The Hopfield model is simple and has the potential to explain several aspects of human memory such as similarity based generalization, fault tolerance and content addressability (retrieval of patterns from partial cues) [106, 107, 108]. Computationally speaking, these models

[109, 110, 111, 112], characterize a neuron by its total synaptic input current, and the resulting, monotonically related mean firing rate.

Persistent activity through synfire chains

The synfire chain theory stipulates that sustained activity at delay-period rates can be achieved via synfire chains - a wave of synchronous activity propagated through feedforward connections linking a collection of neurons arranged in a chain [113, 114]. These loops are maintained via symmetric connections while independent loops are linked via asymmetric connections which maintains activity in a large scale network [115, 116, 117, 118]. A major drawback of such approach is its susceptibility to decay or blowup but can be overcome through limiting total activity and dispersion. Recordings in the motor cortex has shown the validity of this theory through waves of synchronous activity observed in neuronal populations during different tasks [119], consistent with activity in a synfire chain. However, these observations do not contradict other theories. Furthermore, synfire chains may require larger neuronal populations to achieve the desired memory function due to the absence of dense recurrent connections which result in a higher sensitivity to loss of information in feedforward connections [120, 121].

Persistent activity through cellular bistability

A common drawback of the previously described models is that novel stimuli can be only processed through synaptic learning, a slow process which cannot explain the humans' ability to generalize from previously acquired information [122]. The cellular bistability theory provides an alternative solution by incorporating a two-state property into single neurons: a cell is characterized by a resting state and a continuously spiking up state. Sustained activity is hence achieved without requiring synaptic learning. This theory has been used in connectionist and spiking neural network models and have been successful in achieving sustained activity [123, 124]. A biological explanation of this phenomena is through the non linear current–voltage relationship of the NMDA receptor [125]. A limitation of this approach is its high sensitivity to noise due to the inherent instability of neurons. Despite limited evidence supporting this theory, experimental studies have shown basis for cellular bistability specifically in the prefrontal cortex [126, 127, 128, 104].

Activity-Silent WM

While an abundance of evidence explains working memory function through sustained activity, recent observations contradict the assumed correlation between the two phenomena [129]. A deeper look into neuronal activity [130] show a high activity during maintenance phases of WM tasks but low correlation during other stages [100]. Such behavior may optimize resources in anticipation of resource

requiring tasks. Maintenance of input during "silent" periods is achieved via synaptic weights patterns. In a computational model employing a combination of sustained activity and synaptic strength encoding during silent periods [131], activity silent WM has been found to be more efficient and less energy requiring than the classical sustained activity theory. Biologically, memory traces are stored within synaptic weights rather than in activation patterns which can be less energy consuming.

2.4.2 Artificial models

This section summarizes the most prominent computational models of WM that have been proposed in the past decade. Table 2 compiles a list of previous work tackling this topic, showing the basic assumptions of the models, the tasks used for validation, the learning algorithm employed as well as the number of citations received by each work.
A notable work in this scope is the Long Short-Term Memory (LSTM) [132, 133, 134, 135] . The model relies on a recurrent neural network architecture modified to account for long-time dependencies in time sequences. The network is composed of assembled blocks named memory blocks in the recurrent layer. These cells are nodes with self-recurrent connections to act as buffers as well as multiplicative nodes gating the input to these buffers. An output node controls the output of the buffers passed on to connected cells. A later addition included a "forget" cell aiming at modeling the decay of information with time. The goal of network is to learn mappings between a time sequence presented to the model and the output sequence generated at the output via learning the connections' weights using the truncated backpropoagation through time learning algorithm.
A computational model relying on the interaction of subcortical structures in an actor-critic structure is presented in [136]. A reinforcement learning strategy is implemented to train the critic system to recognize "important representations" driving the actor to act as a gating structure controlling the processes of update and maintenance in the network. Takac et. al introduced a self-organizing map to model the operation mode of working memory [137]. Input signals emerging from sensorimotor regions are mapped into the input signal area, then are fed to a signal encoding SOM. The network learns to identify signals and patterns observed in certain sequential context. During recall, representations acquired are activated at the presentation of a stimuli with different degrees and compete to retrieve the best match.
A biologically inclined computational model of working memory is FROST (short for FROntal–Striatal–Thalamic) [138]. The model implements a set of differential equations fitted using single-cell recording data. Different equations are implemented to model different types of neurons in diverse brain areas. The model conserves two biological properties of the neural substrate: saturation imposed via a maximum firing rate and decay in the absence of input. Parallel prefrontal

cortical connections spread activation throughout the network connections. Areas such as the prefrontal cortex, the posterior parietal cortex and the medial dorsal nucleus interact with the basal ganglia to create a working memory network. Experiments show the ability of FROST to successfully replicate neuron activity as well as behavioral data.
A recurrent neural network (RNN) based model of WM model is described in [103]. Echo state networks - a type of RNNs with a reservoir and a recurrent layer to which inputs and outputs are connected - are modified to obtained WM-like behavior by adding "WM-units" (binary states output nodes employing sharp threshold functions that possess trainable feedback connections to the reservoir). The network is trained using a two-stage algorithm in which memory (reservoir) connections' weights are first learned using the alpha rule followed by the learning of output weights in a similar manner. The model is tested using a generated database of sequences of characters where the target is to count open curly braces. Experimental results over 30 runs show an error rate of 25%.
Oberauer et. al [139] present a neural network based model of complex span (a task designed to study the functioning of WM). The model extends the "serial-order-in-a-box" (SOB) theory which employed an auto-associator, to include context related information in the form of a two-layer network: an item layer and a serial position layer. The model accounts for the time-based resource-sharing observations by assuming that capacity is a by-product of interference and decay. Inputs are represented via a distributed (network scale) activation with overlapping nodes representing similarities in context. The network is trained using Hebbian learning on a database of complex span tasks with results mimicking those observed in cognitive tests.

Reference	Date	Task	Learning algorithm	Basic assumptions	citations
Cohen et. Al	1999	AX-task	Reward based	Based on the interactions of the PFC, HCMP and PMC PMC performs inference processing PFC performs maintenance control HCMP performs rapid learning	415
Frank et. Al	2001	1-2-AX task	Hebbian based	Based on the interactions between frontal cortex and basal ganglia	697

				Implements hierarchical strips allowing parallel processing	
Goela et. Al	2001	Tower of Hanoi	Optimization of number of moves	Based on the frontal lobe Employs a hybrid symbolic-connectionist architecture	78
O'Reilly et. Al	2006	1-2-AX task Serial recall	Reinforcement Learning	Relies on interactions between prefrontal cortex and basal ganglia basal ganglia implements dynamic gating PFC maintains information	693
LSTM	1997-2017	Multiple pattern recognition tasks	Gradient descent	Artificial structure based on recurrent neural networks Forget gates mimic memory decay Convolutional LSTM employs convolution to deal with images	5500
Takac et. Al	2015	Episodic representations	Hebbian based	Maps sensorimotor mechanisms which perceive episodes and the hippocampal structures which store these representations Employs a self organizing map with recurrent connections	10
Frost	2005	Maintenance of representations	Least squares	Based on the FROntal–Striatal–Thalamic circuitry	118

				Representations are encoded in the lateral prefrontal cortex and sustained via parallel, prefrontal cortical–thalamic loops.	
Pascanu	2011	AX-task	Hebbian based	Employs a recurrent neural network of the echo state network type	44
Oberauer et. al	2012	Complex span	Hebbian based	Employs a two-layer neural network which associates distributed item representations with distributed, position marker Based on the time-based resource-sharing cognitive theory	136
Cano et. Al	2012	Visual span	second-order Runge-Kutta algorithm	Uses populations of leaky integrate-and-fire neurons	19

Table 2.1: Computational Models of WM

2.4.3 Neuromorphic based models

The mode of operation of the human brain observes multiple differences to that traditional artificial neural networks adopt. One of the main differentiators is the brain's parallel pathways allowing cognitive processes to be streamlined in parallel and processed in a swift and robust manner. On the other hand, in neural network architectures data is processed via queues in a limited number of streams. Such approach renders learning a task much more computationally expensive and requiring complex structures. Neuromorphic engineering, also known as neuromorphic computing [140, 141] is a concept describing the use of very-large-scale integration (VLSI) systems containing electronic analog circuits to mimic neuro-biological architectures present in the nervous system. A key aspect of neuromorphic engineering is understanding how the morphology of individual neurons, circuits, applications, and overall architectures creates desirable computations, affects how information is represented, influences robustness to damage, incorporates learning and development, adapts to local change (plasticity), and facilitates evolutionary change.

Perhaps the main driving force behind development of neuromorphic chips is the necessity of power efficient brain simulator. A highly detailed simulation of the entire brain, down to the gene expression level, needs processing power on the order of an exaflop (10^{18} operations per second) [142] a staggering amount considering that the human brain requires around 20 watts to function [143]. Today's supercomputers would consume an average of 1 gigawatts of power to deliver a full fledged brain simulation [144]. Accordingly, supercomputers might not be the optimal power efficient platforms for large-scale brain simulations. Therefore, integrated circuits architectures seemed like a plausible solution for implementation of neural simulations since they reduce power consumption and increase processing speed. Elementary units are optimized for a specific function such as the number of transistor delays and register access are minimized. The result is a low power architecture simulating brain spikes. We summarize here some of the most prominent work on neuromorphic computing.

Neurogrid One of the early successful neuromorphic chips that could simulate 1 million neurons with 1 billion synapses with 100,000 times less power consumption compared to a Blue Gene supercomputer. Neurogrid was a chip designed in 2006 for energy efficient and fast neural simulations [145], and was trained using a backpropagation algorithm in 2014 [146]. Connection weights are stored in a memory table, and nodes can represent a neuron with a single or multiple synapse.

BrainScaleS BrainScaleS uses wafer-scale integration, a hardware approach which allows dense connectivity patterns within the architecture. The archi-

tecture is composed of units called HICANNs (High Input Count Analog Neural Network). Each HICANN comprises 128,000 synapses and 512 membrane patches [147].

SpiNNaker A standard SpiNNaker chip is a 10×10 cm board with 18 cores ($\approx$ 1,000 spiking neurons each) and the biggest SpiNNaker machine (composed of a collection of chips) can simulate 1 billion neurons [148]. SpiNNaker is used in different applications such as building a line follower robot, representing information through spiking activity of neurons, and solving partial differential equations of heat flow.

SyNAPSE This chip is a scalable neuromorphic chip with the end goal of building cognitive computers rather than simulating brain functions which can be combined together to form a large scale network. This chip contains 4096 cores with 256 neurons each (around 1 million in total) and each neuron can have 256 synapses. Applications implemented with this structure range from energy efficient object recognition to audio signal processing and multisensory fusion [149]. A commercial implementation of this structure is that of IBM TrueNorth.

Google's tensor processing units (TPU) TPUs are an architecture in which data moves in the array in a pulse like fashion developed for machine learning purposes using tensorflow. This specific architecture enables the TPUs to be efficient in matrix multiplication which is a vital part of artificial neural networks. The user can program TPUs to run convolutional, LSTM models, and large, fully connected models. Conceptually, this chip is designed based on the insight that artificial neural networks heavily rely on matrix multiplication operations hence the need for an efficient chip designed for that purpose. This design is more focused on computational practicality rather than biological realism needed for neural simulation.

The major limitation of these architecture is that the number of neurons and synapses realized cannot be varied independently: If the number of synapses increases, that of neurons decreases. While our approach bares resemblance to neuromorphic structures at the level of the elementary unit, key differentiators are denoted: (1) neuromorphic structure are analog (though a digital hardware was made available by IBM TrueNorth) programmable low power circuits learned mostly using unsupervised learning while our approach is that of a software based neural network which unlike it artificial counterpart looks beyond implementing a very complex structure capable of learning from massive amounts of data. (2) Neuromorphic approaches often incorporate a much smaller number of neurons justified by the fact that the percentage of neurons that actually fire are much smaller than that observed in deep networks. (3) While neuromorphic computing

Table 2.2: Comparison of Neuromorphic Architectures

Platform	No. of compartment Neurons	No. of Synapses	Neuron type	Learning Algorithm
Neurogrid	1M	1B	Spiking	Backpropagation
SpiNNaker	18K	arbitrary	Spiking	Backpropagation
BrainScales	196K	50M	Spiking	Backpropagation
SyNAPSE	1M	268M	Spiking	Backpropagation
Google's TPU	64K		ANN type	Backpropagation
Proposed structure	21M		Stochastic	Stochastic Reinforcement Learning

focuses on low power consumption, our approach relies heavily on high performance computing and could benefit from distributed architecture to gain speed advantage. Table 2.2 summarized the main properties of the above discussed platforms in comparison to our proposed method.

In this thesis, we propose a deep learning multi-modal biologically inspired model mimicking the functionality of the working memory network. While the elementary computational unit - the neuron - we adopt presents similarities to that of the spiking neuron neuromorphic architectures implement, our adopted neuron is represented as a stochastic system which encodes inputs via firing patterns while neuromorphic structures implement a binary neuron. Additionally, while our proposed model organizes neurons in columns spreading through layers and grouped in populations and subpopulations according to the organization of the brain structures responsible of the implemented functions, neuromorphic architectures implement large-scale brain networks by realizing low-power chips which can be grouped together to mimic a large brain structure with no particular structure enforced. Furthermore, our proposed model is trained using a biologically inspired algorithm using a spike timing dependent plasticity approach which achieves a local solution which implements a Hebbian learning and a global solution which implements a reinforcement learning strategy.

2.5 The anatomy of working memory

The humans' ability to robustly and efficiently execute WM tasks can hardly be attributed to one brain region. Rather, complex functions such as WM are thought to be performed by a large scale network widespread across the brain (see large scale theory in [150, 151]). Such network identified using neuroimaging techniques is composed of nodes each performing a particular function crucial to execution of the higher WM task. Furthermore, evidence from brain lesions and trauma has provided valuable evidence towards a deeper understanding of the mode of operation of these regions. This section summarizes the latest efforts in answering two fundamental questions: what brain regions/areas are involved in WM and what role does each node play? What abnormalities/disorders are a result of the malfunctioning or sectioning a particular part of the WM network?

2.5.1 The WM network

The core network

The "core" WM network is regarded as involved in different types of WM tasks irrespective of the aspect of the processed stimulus. A coordinate-based meta-analysis study comprising a set of 189 fMRI experiments by Rottschy et. al [2] attempted to identify the core WM network - also attributed to the central executive function - and resulted in a spectrum of regions summarized in table 2.3 also illustrated in figure 2.4. The conjunction analysis conducted across n-back, Sternber, verbal and non verbal tasks across the encoding, maintenance and recall components showed a strong bilateral correlation in the dorsal area 44 (extending into the premotor cortex), anterior insula, (pre-) SMA, and IPS (areas hIP1–3). The intraparietal areas hIPl-3 and area PFt of the left hemisphere as well as the hIP3 region of the right hemisphere were also identified as nodes of the core network.
The relative stability of this network irrespective of the WM task [152] suggests its role as a central executive [33]. This result is in accordance with the large scale theory challenging the previous findings of Posner et. al [153] pointing towards a centralized execution of WM components. Recent evidence from brain lesions and WM disorders converge towards this view. Pathologies spreading across multiple areas and/or their connectivity are often observed in deficits such as schizophrenia [154], attention deficit hyperactivity disorder [155] and dementia [156]. Overlap between the core WM network and other large scale networks involved in selective attention [157], motor orientation [158] and planning [159] suggest a larger role of the core WM network in the execution of higher level functions.
Further dissemination of this network into update, inhibition, shifting and dual-task coordination networks indicate the involvement of the dorsolateral prefrontal

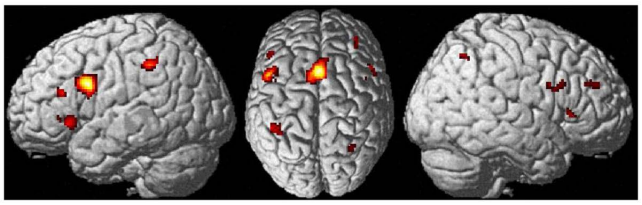

Figure 2.4: The core WM network

Table 2.3: Areas of the core WM network [2]

Macroanatomical location	Cytoarchitectonic location	MNI coordinates		
		x	y	z
Left posterior medial frontal cortex		0	14	52
Right posterior medial frontal cortex		6	24	42
Left intraparietal sulcus intraparietal cortex	hIP1 hIP2 hIP3 PFt	-44	-40	42
Left anterior insula		-36	22	-2
Left inferior frontal gyrus pars opercularis	Area 44	-46	10	26
Left IFG caudal lateral prefrontal gyrus	Area 45	-46	30	20
Right anterior insula		38	24	4
Right caudal lateral prefrontal cortex		34	44	26
Right inferior frontal gyrus pars opercularis	Area 44 45	50	16	26
Right intraparietal sulcus	hIP3	30	-60	50

cortex BA 9/46 in update tasks; the right inferior prefrontal area BA 45/44 in inhibition tasks; the anterior cingulate BA 24, pre-SMA BA 6 and inferior parietal BA 40 in shifting tasks. Neural correlates of dual-task coordination remain unclear with contradicting evidence obtained in multiple studies [160].

Verbal WM network

Verbal specified regions that are selectively active during verbal tasks are comprised mainly of Broca's area. A correlation analysis comparing phonological short-term memory tasks with visual tasks shows considerable activation in the left premotor frontal gyrus and adjacent Broca's area, in the left superior temporal gyrus and in left and right insula [161]. Comparing working memory up-

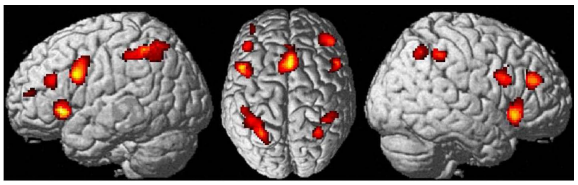

Figure 2.5: The verbal WM network [2]

dating with phonological tasks activity was recorded in the right middle frontal gyrus, in the right inferior parietal and angular gyri and in the left supramarginal gyrus[162]. Juxtaposing activity during verbal and non-verbal tasks, results indicate that verbal WM tasks considerably invoke left Brodmann areas while non-verbal tasks employ the left supplementary motor area and bilateral dorsal premotor cortex. Speech production has also been highly associated with the supplementary motor association areas and the cerebellum suggesting a role for these areas in subvocal rehearsal function. In contrast, storage of phonological information may not be localized in one area but rather in a network comprising the anterior prefrontal and inferior parietal areas [2]. Figure 2.5 shows the activation obtained using a conjunction analysis on verbal vs non-verbal tasks obtained by [2]. Areas of activation are also summarized in table 2.4.

The visuo-spatial loop network

Visual encoding neurons are mainly concentrated in the area of the principal sulcus but showcase different patterns of activity in the presence of a visual stimulus, during the delay period and during the reactivation phase. Such behavior is crucial to maintain the time aspect in visual tasks [163]. Furthermore, neuronal populations encoding simple, complex or categorical memoranda are distinct. Patterns of activity exhibited by prefrontal neurons depend on the goals of registration, memory and control. Further dissemination is observed for neurons involved in memory for object identity (ventral ares) and those evoked in location (dorsal areas)[164]. Figure 2.6 shows the activation observed in a object identity versus object location experiment conducted by [2]. Table 2.5 summarizes the main regions activation in a conjunction analysis of object identity and object location tasks.

2.5.2 WM related impairment

The challenge in drawing conclusions on the neural correlates of memory impairment or disorders lies in the diversity of the type of deficit, the type of assessment used, the limited number of cases as well as the individual differences between reported patients. However, overlap and similarities in observed symptoms and/or

Table 2.4: Areas of verbal WM network [2]

Macroanamtomical location	Cytoarchitectonic location	MNI coordinates		
		x	y	z
Posterior medial frontal cortex		2	16	48
Left anterior insula		-32	22	-2
Left inferior frontal gyrus	Area 44/45	-46	10	30
Left caudal lateral prefrontal cortex		-42	34	22
Left rostral lateral prefrontal cortex		-38	52	12
Right anterior insula		38	24	-6
Right caudal lateral prefrontal cortex		42	40	22
Right inferior frontal gyrus pars opercularis	Area 44/45	46	10	26
Left intraparietal sulcus	hIP1/hIP2/hIP3	-32	-56	44
Left superior parietal lobule/IPS	7A/7P/hIP3	-28	-58	50
Left SPL/IPS	7PC/hIP1/hIP2	-42	-52	55
Left inferior parietal lobule/intraparietal cortex	Area 2/PFt	-46	-38	49
Right intraparietal sulcus	hIP1/hIP2/hIP3	42	-44	44
Right intraparietal cortex	PF/PFt	48	-40	46
Right SPL/IPS	7A/hIP1/hIP3	32	-58	46

Table 2.5: Areas of visual WM network [2]

Macroanamtomical location	MNI coordinates		
	x	y	z
Posterior medial frontal cortex	-2	20	48
Left anterior insula	-30	20	-4
Left caudal lateral prefrontal cortex	-44	38	22
Right anterior insula	36	24	-4
Right caudal lateral prefrontal cortex	44	34	30
Left posterior superior frontal gyrus	-28	4	50
Right posterior superior frontal gyrus	28	8	54

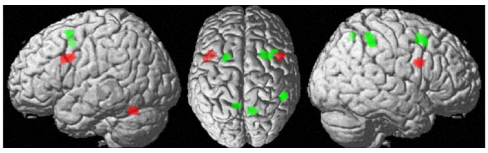

Figure 2.6: The visual WM network [2]. Areas highlighted in green are correlated with object location while red colored areas are associated with object identity.

affected brain regions provided strong evidence towards identifying areas responsible for certain patterns [165].
Non-fluent aphasia has mostly been associated with lesions in the left inferior frontal gyrus (Broca's area) and the anterior insula. Conduction aphasia is mostly correlated with malfunctions in the inferior parietal cortex. Patients with working memory deficit have globally shown prefrontal dysfunction with multiple neurological disorders such as Parkinson, schizophrenia and age related memory deficit. Lesions in the right anterior temporal lobe often led to impairment in object recognition with no effect on spatial tasks [166]. Frontal lobe malfunctions have also been associated with ADHD which is mainly manifested in WM impairment. In particular parieto-occipital reduced activity accounts for limited alerting capabilities, while fronto-central abnormalities are responsible for encoding related limitations [167]. Reduced cognitive control over WM in Schizophrenia was associated with reduced activation in mid ventrolateral prefrontal cortex [168].

2.6 Applications

There's little to no doubt that working memory is a crucial function in the execution of tasks ranging from simple object recognition to abstract and complex thinking. As such, interest in WM has spanned multiple fields and motivated research in cognitive applications, in education as well as in artificial intelligence. This section aims at briefly describing the importance of WM in these fields as well as present the state of the art outcomes in corresponding research.

2.6.1 Applications in cognition

One important question raised in cognitive development is the evolution of working memory proficiency during an person's life. A common procedure to measure the capacity of WM is through digit span - a test in which subjects are asked to iterate a sequence of randomly generated digits. Capacity is hence considered as the maximum number of digits a subject can hold (without error). Studies have shown that digit span witnesses an increase from childhood to maturation [169]. Another link to working memory is control: efficient learning requires staying on

task (focusing on relevant tasks). Research points out that subjects with good WM proficiency have a higher tendency at staying on task and execute control more efficiently [170].
A key aspect in acquiring long term memories is a prompt functioning of WM and hence impairment in modality-specific resources or in general control of WM can have devastating results on learning and long-term memory. WM was shown to be an essential in vocabulary acquisition, language comprehension, concept formation and strategy planning [171].

2.6.2 Applications in education

The direct link between WM and learning raises multiple questions in the applications of WM in education; specifically tackling children with learning disabilities, subjects with limited WM capacity as well as tailoring education to achieve desired performance. As a result, considerable effort has been consecrated to adapting the material to the learner's abilities such as delaying the introduction of arithmetic until students master the concept of one-to-one correspondence [172, 170]. Another approach deals with individual differences within age groups and attempts to devise more personalized learning strategies to better suit learners' needs. For example students with limited capacity may benefit from information conveyed at a shallower level while integration of technology is better reserved for individuals with higher abilities [173, 174]
A debatable method attempts to train or improve working memory abilities by emphasizing WM requiring tasks. Such scheme requires an adaptive training invoking long-term learning and had resulted in arguable results. While there has been an indication that WM training can improve performance on WM tasks, little effect was seen on tasks requiring higher reasoning [175, 176]
Overall, the aim of such research is to help children with disabilities to acquire skills that would be put to use in learning outside of the school environment. While this subject continues to be at the heart of recent studies, it remains a controversial topic as a consensus on its efficacy has yet to be reached.

2.6.3 Applications in artificial intelligence

The tremendous increase in computational resource and the introduction of deep learning as a powerful solution to various artificial intelligence problems has transformed the field of machine learning. However, deep learning remains less than ideal: it relies on large amount of data employed to train a large neural network with a high number of hyperparameters. Recent research has shifted towards incorporating aspects of human intelligence in artificial models rendering those more efficient. As stated by Will Knight in MIT technology review [177] "What Happens When You Give an AI a Working Memory? It solves puzzles in a surprisingly human-like way." Perhaps the most prominent application is Google's

DeepMind AI which was recently equipped with a WM module. Other applications include arithmetic [178] and pattern matching [179].

2.7 Conclusion

This chapter presented a survey on working memory models, summarizing the most prominent cognitive theories - notably Baddeley's and Cowan's models, discussing the latest evidence on domain specific resources and measuring working memory capacity, reporting on the state of the art of computational models, describing the underlying anatomy of related impairment and briefly presenting applications of working memory.

Chapter 3

Background Information

3.1 Functional Anatomy of Neurons

Neurons are the elementary computational unit employed by the central nervous system to produce complex behavior responsible for higher order functions. Neurons exist in different types and shapes but are all characterized by a cell membrane, a cytoplasm, branches that serve as synaptic termination of incoming connections, and an axon that transmit signals to neighboring cells. The semi-permeable membrane (permeable to different ions with different conductivity) separating inner from outer mediums is electrically polarized with a resting potential (when no ions are flowing) of $-65mV$ (the inside is negative with respect to the outside by a differential of $65mV$. Due to the aqueous aspect of the neuronal medium, electric current is carried by movements of ions and not electrons. Neurons employ two main communication means for conveying information: graded, locally summed slow potentials that decay close to the membrane (synaptic potentials) and fast, short-lived actively propagated signals (action potentials) that relay data over long distances. The mechanisms governing both mode of operations are described below.

3.1.1 Electric Signaling by Neurons

The semi-permeable membrane outlining the cell body of a neuron is a complex bilayer of lipids in which protein molecules constituting perforated ion channels (through which ions diffuse) are incorporated. Ionic flow across the membrane is a byproduct of selective conductivity to different ions and active ion pumps. Membrane potential is controlled by both the number and the selectivity of ion channels; and is altered by changes to the latter. Ions such as K^+ and Na^+ in addition to Ca^{2+} and Cl^- constitute the basic data-carrying elements in electric signals generated by neurons. A current exciting a neuron (through post-synaptic potentials) result in a slow, local alteration of the membrane voltage. Properties of the response to a neuron (speed and amplitude) to an input pulse are func-

tion of the electrical characteristics (namely capacitance and conductance) of the membrane (for a complete mathematical description see [180]).
These voltage are however not suitable to conduct information over to connecting neurons (typically die within few millimeters of their site of generation); hence efficient communication relies on action potentials taking place when a threshold exceeding response is observed. Such phenomena is possible due to temporal and spatial summations; the former occurring occurs as a result of partial overlap between signals over time, the latter taking place when physically close signals are exciting a cell. Action potentials are spikes or impulses that are similar in shape. Firing patterns however can vary among brain areas depending on the type of neuronal population. Furthermore, nerve pulses are characterized by an "all or none" response; i.e. if a threshold crossing current is presented, the cell exhibits an action potential, failing that these pulses are not generated. Properties of a train of action potentials following a sequence of stimuli are function of the ion channels in a membrane as well as the frequency of stimulation: while some neurons have a linear input-output relationship, other respond with complex bursts. An action potential traveling along an axon terminating at a synaptic button of a cell's dendrite causes a sequence of events denoted by "synaptic transmission" to occur; this phenomenon involving the the action of neurotransmitters is the key to continuation of flow between neurons.

3.1.2 Synaptic Transmission between Neurons

A the synaptic boutton at which terminates the axon or dendrite of another cell is a synaptic cleft separating the pre and the post synaptic mediums. Though not physically in contact, the synaptic cleft is the site of transmission between neurons which occurs in five essential steps: the synthesis of a neurotransmitter, the packing of neurotransmitter in the presynaptic cell, the release of neurotransmitter into the cleft, the binding of the neurotransmitter into the postsynaptic cell (via neuroreceptors), and the termination of the neurotransmitter function. The effect of a neurotransmitter diffusing on the connected membrane can either bring this membrane closer to its firing threshold (excitatory) or away from said threshold (inhibitory). The type of synapses is determined by the type of neuroreceptor to which the transmitter binds. At the post-synaptic membrane, the resulting potential is governed by the summation of all efferent connections and depends on the concentration of transmitter released as well as the distance to the site of initial excitation. The synaptic strength mainly characterized by the amount of neurotransmitter released can be altered through the processes of potentiation and depression which are highly influenced by the synapse firing history. This constitutes the basis of learning and memory which alter the response of neurons to a stimuli. Long term memory is characterized by long term or even permanent changes of synaptic strength while short term memory is characterized by temporary altering of the membrane's conductivity.

3.1.3 Learning and Memory

The mechanisms that alter the synaptic strength of a connection, shape the functional anatomy of the brain from a collection of a very large number of neurons and synapses during early development to an optimal structure. At birth, both connections and neurons are in surplus. About half the newborn neurons die by adulthood with various factors influencing the number and connectivity of surviving ones. The main aspect determining the number of remaining connections is the load of target tissue terminating at these neurons during development. Connections and neurons follow a competition scheme that prune the less efficient ones and maintain the optimal combination matching functional demands with various results across brain areas. After adulthood, synaptic connections continue to be altered via a combination of potentiation and depression that allow the brain to acquire knowledge. Short term memory is exhibited as a result of a transient altering of a membrane's selectivity to Ca^{2+} ions, while long term memory involves the activation of certain neuroreceptor.

3.2 Cerebral Cortex

The cerebral cortex is a collection of an estimated 25 billion neurons strongly connected via a staggering 10^{14} synapses via over $100,000$ km of axons. With a surface area of approximately $1800cm^2$ made possible by the corrugation into gyri and sulci, the cerebral cortex weighs about 50% of the entire brain. Over the course of evolution, the cerebral cortex is among the parts of the vertebrate brains that has witnessed the most growth in size in conjunction with the development of complex and higher order cognitive functions specially in humans. Involved in a collection of tasks ranging from simple perception and movement functions to abstract level of thinking, the cerebral cortex remains in large the most elusive organ of the human body with efforts from various fields converging towards a better understanding of its functionality.
Visible on top of cerebral cortex is a type of structure referred to as the neocortex due to its relatively recent appearance in the evolution of the cortex. While mammals possess little of the neocortex, primates show a larger expansion of the neocortex. In humans, the neocortex amounts to around 95% of the total cortical area. Neurons constituting the neocortex are of the pyramidal type; the terminology resulting from their triangular-like shape. Pyramidal neurons are cone-shaped cells from which stem vertical dendrites terminating at the cortical surface as well as a collection of dendrites branching out horizontally. Long axons exciting multiple cortical and subcortical areas via glutamate activated synapses. Pyramidal cells range from less than $10\mu m$ in diameter to up to $100\mu m$. Non pyramidal cells are found with a smaller quantity and are of several types and generally synapse within cortex areas (referred to as interneurons) with the ma-

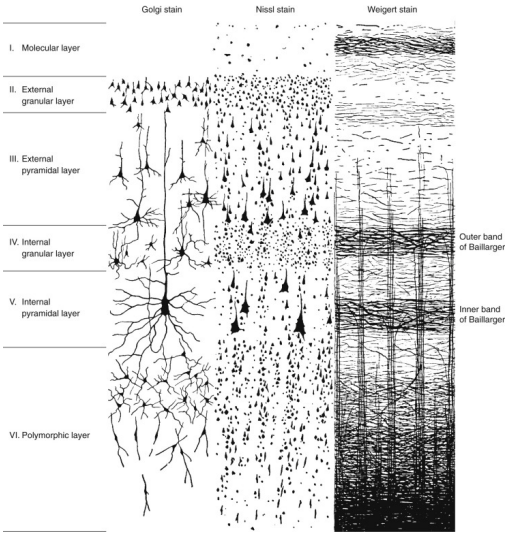

Figure 3.1: Layers of the cortex as shown using three stains [3]

jority forming inhibitory synapses.
Neurons in the neocortex are organized in an hexa-layered structure with each distinguished by the properties of its constituting neurons and connections. Layers are numbered using roman numbers with decreasing order from the bottom to top. Illustrated in figure 3.1 is a cross section of the neocortex revealed by three different stains.

Layers in the cortex receive projections of neurons originating from cortical and subcortical ares. Efferent connections from cortical areas terminate in the same or in the contralateral hemisphere. Subcortical afferent connections are of thalamic origin in the vast majority. Connections to the neocortex exhibit different shapes of ramifications in different layers. As a result layers of the cortex are non-uniform in nature. In addition to the layered structure, the cortex is also characterized by a columnar organization. The former is in the form of horizontal lamination while the latter is manifested in the arrangement of pyramidal cells in vertical columns. Cortical columns are about 50 to 500 μm wide and share parameters of the stimuli exciting its neurons. These "mini-columns" are regarded as the basic computational unit in the cortex and are composed of an association of around 100 neurons. Mini-columns appear to connect via horizontal intracortical connections to form a higher order computational unit referred to as hypercolumn.
Areas in the neocortex appear to exhibit function dependent activity and hence are regarded as specialized modules. While these modules alone are only responsible for the execution of simple tasks, complex and higher order functions arise as a byproduct of the collaboration of several of the specialized areas widespread across the cortex. Lesions or damage to any of these regions can have serious

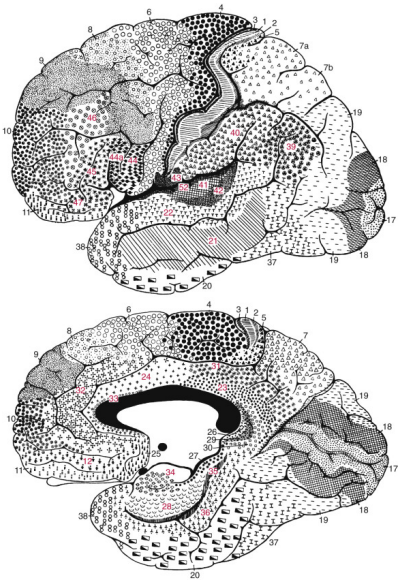

Figure 3.2: Brodmann's mapping of the cerebral cortex [4]

impact of the performance of individuals in a range or tasks. Brain lesions in addition to neuroimaging are a powerful tool in discerning the role of specialized areas in multiple functions.
The mapping of specialized structures in the cortex is the result of the work of Brodmann that devises each of the hemispheres into 44 areas as shown in figure 3.2 and summarized in table 3.1. While the mapping is somehow approximate (specially when involving higher order functions) it remains widely accepted and supported by evidence. Each hemisphere is split into primary sensory areas (at which terminate thalamic sensory projections), a primary motor area, association areas as well as limbic areas. The visual cortex resides in the calcarine sulcus, the motor cortex is lodged in the precentral gyrus, the auditory cortex is found in the transverse temporal gyri and the somatosensory cortex is localized in the postcenral gyrus.

Lobe	Number	Location	Other Names
Frontal	4	Precentral gyrus, anterior paracentral lobule	Primary motor area; M1
	6	Superior and middle frontal gyri, precentral gyrus	Premotor area, supplementary motor area
	44, 45	Inferior frontal gyrus (opercular and triangular parts)	Broca's area (on the left)

Parietal	3, 1, 2	Postcentral gyrus, posterior paracentral lobule	Primary somatosensory area; S1
	5, 7	Superior parietal lobule	Somatosensory association area
	39	Inferior parietal lobule	Angular gyrus
	40	Inferior parietal lobule	Supramarginal gyrus
Occipital	17	Banks of calcarine sulcus	Primary visual area; V1
	18, 19	Surrounding 17	Visual association areas; V2, V3, V4, V5
Temporal	41	Transverse temporal gyri	Primary auditory area; A1
	42	Transverse temporal gyri	Auditory association area; A2
	22	Superior temporal gyrus	Auditory association area; posterior portion (on the left) = Wernicke's area

Table 3.1: Mapping of cortex by Brodmann

Chapter 4

Multi-modal Network Structure

Our proposed structure stems from Baddeley's model: it incorporates separate substructures processing verbal and visual stimuli and a unifying structure integrating processed inputs and generating a combined representation of the presented information. We assume that the verbal information to be processed is cued in the form of an auditory input, while the visuospatial data is presented in an image. The central executive merges the representations of the two modalities to create one "unique" encoding of the stimuli presented.
Each of the loops is a deep specialized neural network composed of populations of neurons arranged in columns mimicking the columnar organization of the neocortex. We first describe the operation of a neuron and cortical column, and then describe the distribution of populations within each loop. The proposed structure is shown in figure 4.4.

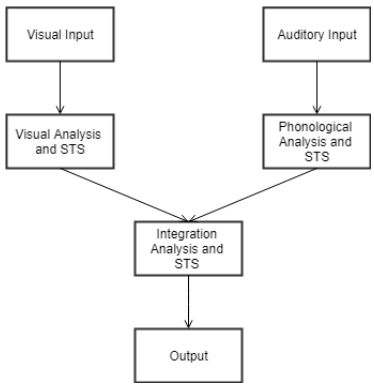

Figure 4.1: Proposed Hybrid Structure

4.1 Neuron and Cortical column

Many models has been proposed in the literature to model the activity of a single neuron. These models generally fall under two types: biological models which attempt to replicate the firing patterns observed in single cell recordings and artificial models which abstract from the biology and model neurons as a computing unit implementing a simple function. While the former expresses firing rate as an often complex function of an input current, the latter deals with a numerical output in response to a numerical input. Our method relies on modifying the elementary computational unit as well the connectivity of the network to include recurrent connections. Unlike existing neural network models where excitation and inhibition alter the weight of a connection based on the response of the cell to an input, we adopt a more biologically plausible approach by hard coding these processes in the synapses mimicking the role of GABA, the main neurotransmitter responsible for inhibitory action, and NMDA receptors, which act as gators of information flow and play a crucial role in memory function [104]. NMDA receptors are ion channels protein that bind to glutamate causing the cell membrane to undergo a depolarization hence is believed to be crucial for maintaining synaptic - a property underlying the cellular mechanisms of learning and memory [181]. In contrast, GABA receptors are considered the chief inhibitory actor in the brain due to its hyperpolarization effect on the cell membrane, inhibiting neurons from generating action potentials [182]. Recurrent connections serve as a mean to maintain neural activity history and hence account for temporal patterns found in the data, an important aspect in time series prediction. The elementary computing unit we adopt borrows the concept of strength encoding from the anatomy: the strength of a stimuli is reflected at the output of the neuron by the firing rate observed. In other terms, a "strong input" leads to a higher frequency of spikes at the output of the neuron.
Mathematically, let $[x_1, x_2, ..., x_n]_t$ be a vector representing n synapses connecting to a neuron at time t, weighted by the vector $[w_1, w_2, ..., w_n]; w_i >= 0$ representing the corresponding synaptic strength, the output y of the neuron is expressed as:

$$y = \begin{cases} \frac{1}{1+exp(\sum_i p_i x_i w_i)} \ for\ t = t+1, ..., t+m \ \ if \ \sum_i p_i x_i w_i > \theta \\ 0 \ for\ t = t+1 \ \ else \end{cases} \tag{4.1}$$

The response of a neuron to the total stimulus is a train of spike sustained for m time steps where $m = \sum_i p_i x_i w_i$. Following this train of spikes is a refractory period, represented by r time steps of zero activity, where no input can excite the neuron to generate an action potential. In other terms, during the refractory period, the neuron is not responsive to stimuli. π is a type encoding parameter set to 1 if the synapse is excitatory and 0.01 if the synapse is inhibitory.
Figure 4.2 shows an example of the activity of a neuron following a sequence of

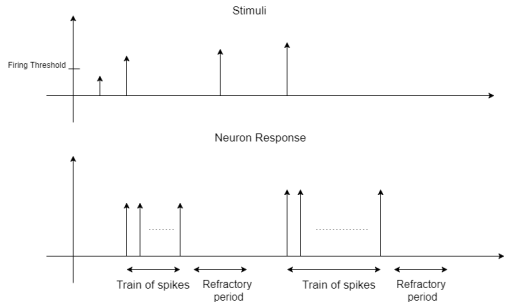

Figure 4.2: Illustration of a neuron's activity

stimuli. The first stimuli applied is lower than the firing threshold and hence no activity is observed. The second stimuli crosses the action potential and a train of spikes is recorded. The third stimuli occurs during the refractory period hence no response is generated (despite a threshold exceeding input). The last stimuli excites the cell after recovery from refractory period and generate a longer train of spikes due to its higher amplitude compared to the second pulse.

In addition, the neurons are arranged in a columnar-like organization [183]. In our model, a column is considered a collection strongly connected - physically close - neurons. While the number of neurons in a column varies across areas and layers, an accepted average of this number is about 200 [184]; for simplicity we adopt this number as constant throughout all our model.
To illustrate the functionality of a column and its ability to encode patterns, we consider in figure 4.3 a column of five neurons, four of which are excitatory (shown in green) and one being inhibitory (shown in red). The figure shows the status of the column following a sequence of events (stimuli). Levels of input to the column is shown as gradients of blue. The level of the total input to a node is computed as a weighted sum of incoming connections with weights chosen at random. An active node is highlighted in yellow. Connection weights are reflected in shades of grey. For simplicity, the connections' weights are considered constant in figure 4.3.

4.2 Phonological Analysis and STS

Phonological processing refers to mechanisms involved in representing, accessing, or manipulating information related to the sound structure of language. Verbal short-term memory relies on auditory-motor integration networks. Verbal short-term memory is often held to comprise at least two components: a storage component of some form and a mechanism for active maintenance of this information. In Baddeley's model, for example, the storage mechanism is the "phonological store", a dedicated buffer, and active maintenance is achieved by the "articulatory rehearsal" mechanism [67]. While the neural bases of phono-

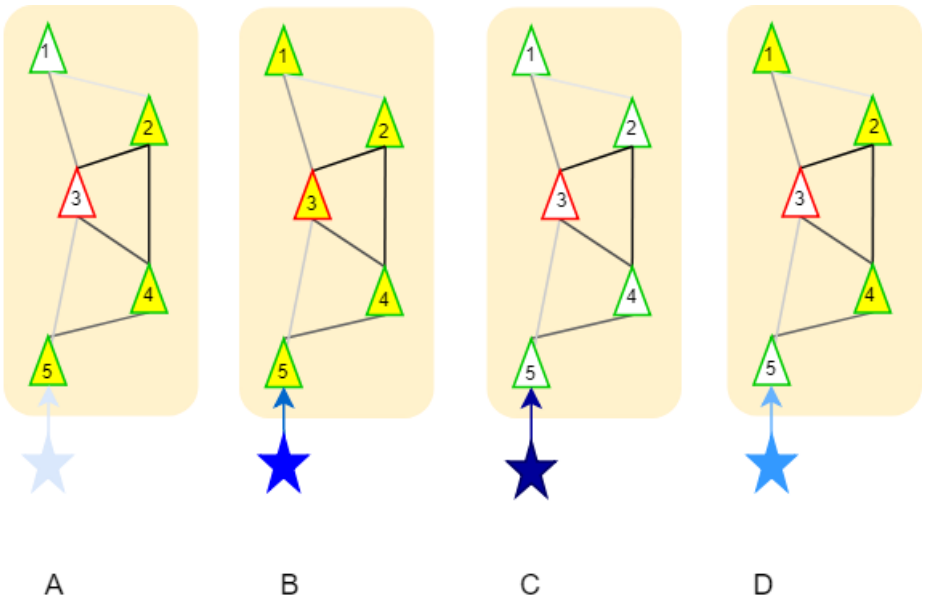

Figure 4.3: Response of a column to a sequence of events. In (A), only neurons 5, 4 and 2 have threshold crossing output and hence generate a sequence of spikes (illustrated by yellow highlight). In (B), a stronger input stimuli is presented which causes all five neurons to fire. In (C), the input is presented while the neurons are within the refractory period and hence no activity can be observed. In (D), the neurons have recovered and the stimuli causes neurons 4,2 and 1 to fire.

logical processing are far from confined to one area or brain region; we assume that the phonological loop can be assimilated to a network that bares certain resemblance to the auditory system (given that the verbal input in our model takes the form of an auditory cue).
The auditory system comprises: the outer and middle ear which combined function is to amplify frequencies in a pseudo-uniform manner; the middle ear characterized by a tonotopic organization; the auditory nerve which encodes information in patterns of firing (in a similar manner to the proposed neuron model); and the auditory cortex where tonotopic mapping is maintained. The auditory cortex possesses similar properties to that of the visual cortex in that its organization is hexa-layered with columnar aspect.
Areas identified as parts of the auditory cortex (ACx) are shown to be grouped in 3 major regions: the core group composed of tonotopically organized areas (includes the primary auditory cortex); the medial belt referred to as secondary auditory cortex receiving connections from core areas; and the parabelt areas - tertiary auditory cortex - with incoming projections from the lateral belt areas. Approximately, 10-15 areas constitute the ACx [185].
In our model, we model the phonological loop via a network inspired by the audi-

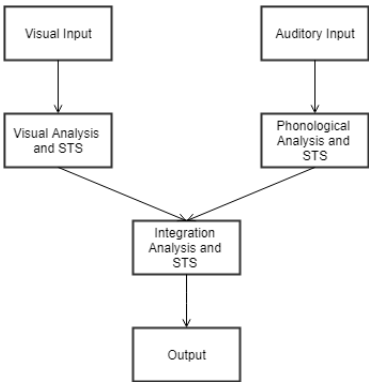

Figure 4.4: Proposed structure architecture

tory cortex (ACx). While a consensus on the areas composing each region of the ACx is yet to be reached, we adopt a dissection similar to that proposed by [186]: the auditory system is composed of 3 main associations of areas: the core region further divided into three subdivisions, the belt region disseminated into seven areas - two of which fall in the medial belt, the remainder in the lateral belt -, and the parabelt region split into two regions. Further branching of these areas is considered beyond the scope of this work; instead we elect to model individual areas as one subpopulation and regions as one population .
The connections of our network follow that of its biological counterpart. Individual core areas are characterized by a tonotopic organization in which connections between layers form strips that process a range of frequency. These strips connect to neurons of other areas associated with the same frequency range. For that, the raw audio stimuli goes through a frequency analysis stage mimicking the processing of the ear. The resultant spectrum is fed to the core areas in a parallel stream (i.e. frequency strips from different areas receive copies of the input) which output is fed to the secondary then tertiary areas. While core areas are tonotopically organized, belt and parabelt subpopulations are fully connected subpopulations.
A total of $100,000,000$ neurons are distributed with decreasing density from bottom to top. This number is chosen as a rough estimate matching that in the A1 areas of monkey primates [187]. The density of neurons is reduced by half between consecutive layers and inhibitory and excitatory synapses are randomly distributed throughout with a ratio of 1/5 inhibitory cells. Figure 4.6 shows the organization of the audio processing network. The tonotopic organization of core subpopulations is further detailed in figure 4.7.

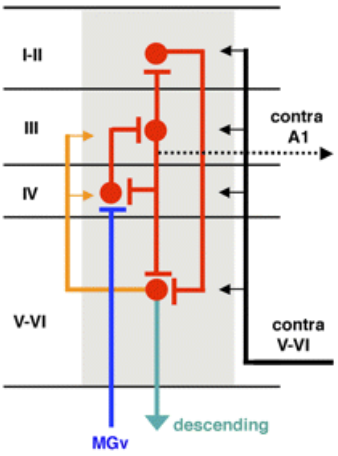

Figure 4.5: Connections of the primary auditory cortex

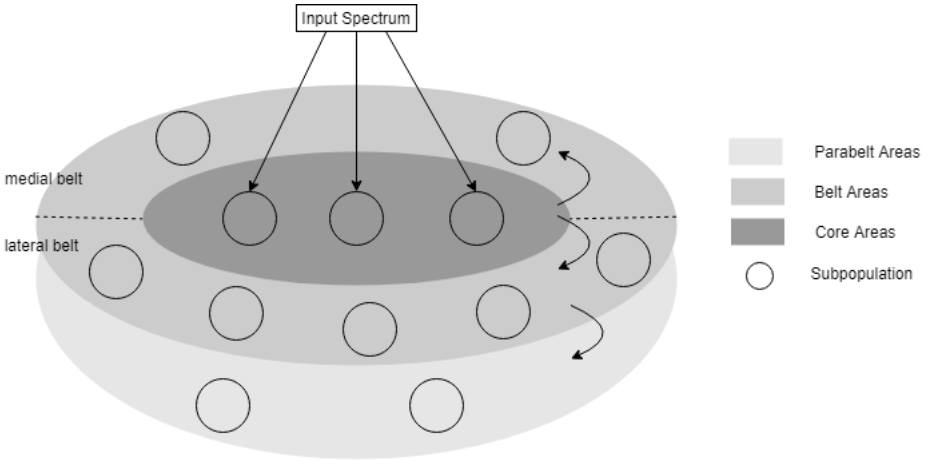

Figure 4.6: Organization of phonological loop populations. Shaded areas represent core, belt and parabelt groups and are modeled as populations. Circles represent subpopulations. The input spectrum is fed to the core areas (parallel paths) as further detailed in 4.7; the output of core areas is summed and fed (distributed) to all medial and lateral belt populations; the latter connect (also via parallel paths) to parabelt populations.

4.3 Visual Analysis and STS

4.3.1 The visual system in the brain

Because our model takes roots in the biological visual processing system, we begin by describing the various structures in the brain involved in visual tasks starting with the eye, retina, lateral geniculate nucleus up to the primary visual cortex [50]. Anatomically, the eye is a three-layered structure comprising a lens. The inner most layer is the first neural-based module (the outer layer is an extension

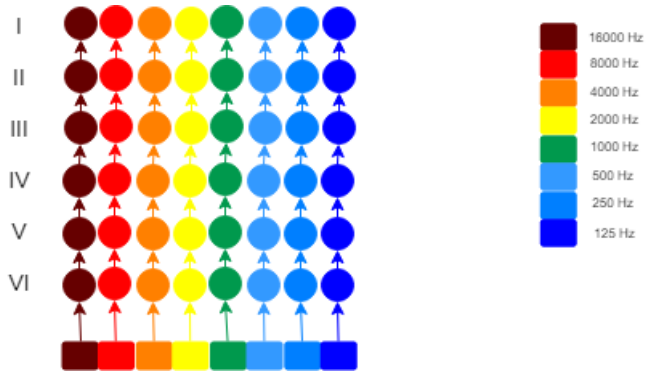

Figure 4.7: Tonotopic organization of a core area (subpopulation)

of the dura matter and the middle layer serves as a medium for blood nerves) inside which the retina is suspended [51]. The retina is an association of neurons arranged in five alternating layers of synapses and interneurons. At a functional level, the retinal process extracts from the visual input elementary features such as boundaries, lines and basic shapes. Rather than levels of intensities, retinal neurons respond to patterns of lights rendering the structure an inherent feature extraction stage [188]. The optic nerves conduct information to the lateral geniculate nuclei (LGN) crossing at the optic chiasm. Each LGN is composed of a six-layered structure receiving projections from the retina in a retinotopic matter. As a result, any location in the visual field is mapped to a column of neurons projecting throughout the six layers of the nucleus. The nucleus is not fully connected: layers 1, 4 and 6 receive projections from the contralateral eye (that of opposite hemisphere), while layers 2, 3, and 5 connect from the ipsilateral eye (same hemisphere). The primary visual cortex receives connections from the lateral geniculate nucleus and projects processed visual information to higher order cortical areas. Information extracted includes orientation, color depth and motion. The primary visual cortex is characterized by a columnar organization in which cortical columns constitute the elementary computing unit. Increasingly complex information is extracted from input data to achieve robust invariant representations of visual information [189].

4.3.2 Proposed Structure

The proposed visual processing network follows an organization similar to that of the visual processing system in the brain. It starts by a 5-layer retinotopic structure mimicking the retina, projecting into a 6-layered network with similar structure to that of the lateral geniculate nucleus (LGN) followed by a 6-layered columnar-organized network with similar properties to that of the primary visual cortex. The retinal, LGN and primary visual cortex are each modeled as a population of neurons. The retinal population is divided into 5 supopulations - each

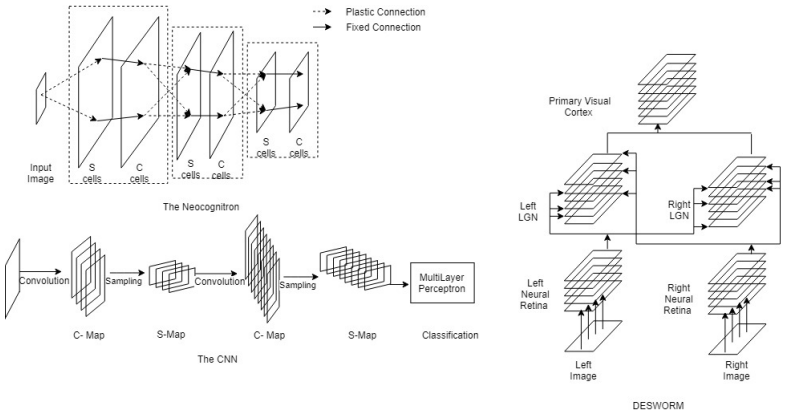

Figure 4.8: Comparison of CNN, Neocognitron and DESWORM structures

composing one layer - (matching the different neuronal types). The LGN population is composed of 3 subpopulations (to match the 3 types of neurons found in the LGN) while the primary visual cortex is considered as one subpopulation (corresponding to the V1 or Brodmann area 17 of the brain). Figure 4.10 shows the organization of the visual processing network. Figure 4.11 shows the organization of populations and subpopulations in a retinotopic manner illustrated via shades of grey: neurons of the same color process information extracted from the part of the visual field with the matching color. In addition, our model possesses some common properties with models widely used in the literature: (1) a retinotopic pattern as observed in convolutional neural networks [190], (2) excitatory and inhibitory synapses aligned with S and C cells of Fukishima's neocognitron [191, 192, 193], and (3) a columnar organization as proposed in cortical algorithms [194, 195, 196]. In our implementation, a total of $543,570,000$ neurons are used for visual processing: 5×10^6 for the retinal network, $570,000$ for the LGN and $538,000,000$ for the V1 area. The density of neurons is decreased throughout the structure and the ratio of inhibitory to excitatory synapses is maintained at $1/5$ in all layers.
Figure 4.8 shows an illustration of CNN, the neocognitron and DESWORM structures. Furthermore, figure 4.9 shows the connections of the retinal network of DESWORM whith the retinotropic organization (where columns throughout the network map to areas of the visual field; this is also maintained in the LGN networks.

4.4 Central Executive

The central executive function has long been associated with the basal ganglia. The latter can be thought of as a structure composed of three parts: an input nucleus, an intrinsic nucleus and an output nucleus. Input nuclei are the parts

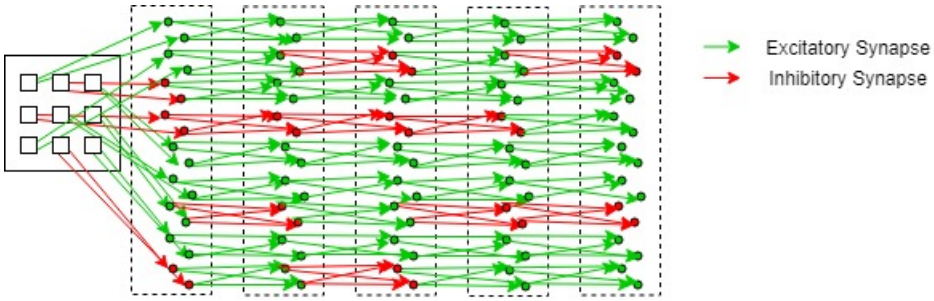

Figure 4.9: DESWORM retinal network with retinotropic mapping

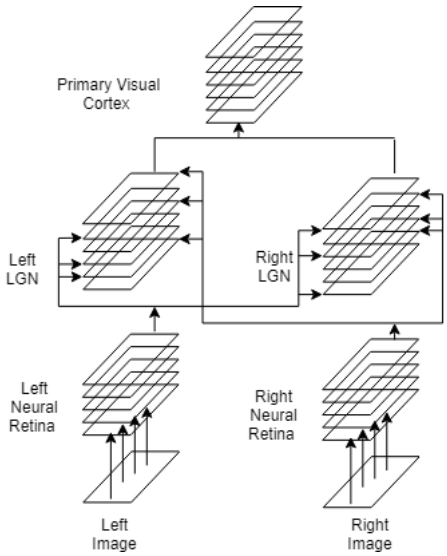

Figure 4.10: Visual Sketchpad Network

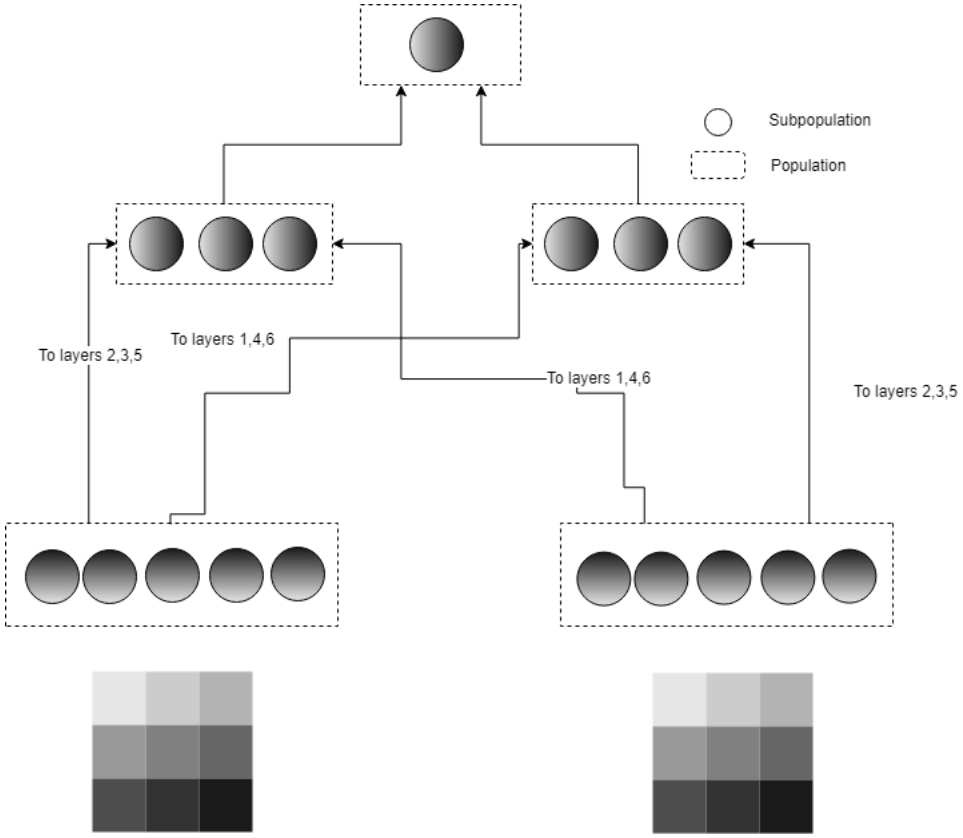

Figure 4.11: Retino-topic organization of visual network

where afferent connections from different sources (dominantly cortical, thalamic and nigral connections) terminate. The caudate nucleus (CN), the putamen (Put), and the accumbens nucleus (Acb) are all considered input nuclei (the association of these input structure is referred to as striatum). The output nuclei are the parts from which efferent connections emerge towards the thalamus and consist of the internal segment of the globus pallidus (GPi) and the substantia nigra pars reticulate (SNr). Intrinsic nuclei are composed of the external segment of the globus pallidus (GPe), the subthalamic nucleus (STN) and the substantia nigra pars compacta (SNc) located between the input and output nuclei involved in processing of basal ganglia information [197].

The central executive is modeled after the basal ganglia - to which the ability to focus attention is attributed - circuitry through a network constituted of 3 populations corresponding to the input network, consisting of the striatum which receives excitatory projections; the intrinsic network composed of the globus pallidus (GPe) which receives inhibitory connections from the striatum (association of the caudate nucleus (CN), the putamen (Put), and the accumbens nucleus (Acb)), the subthalamic nucleus (STN) which receives inhibitory connections from the GPe, and the substantia nigra pars compacta (SNc) constituting the dopamine system sending dopaminergic (modulatory) connections to other parts in the basal ganglia; and the output network consisting of the association of GPi and SNr receiving inhibitory projections from the GPe, the striatum and the STN. The input, intrinsic and output nuclei are each mapped as a population while individual areas are modeled as subpopulations. An illustration of the basal ganglia circuitry is shown in figure 4.12. Dopaminergic connections are accounted for by setting the parameter p_i introduced in section 4.1 to 0.5 (hence neither excitatory nor inhibitory).

Our model is an association of three networks: input, intrinsic and output, with the intrinsic network composed of three parts corresponding to the GPe, SNc, and STN. The input receives a stimulus processed by the intrinsic network which projects to the output network. The dopaminergic (or modulatory system) learns to indicate whether the output state needs to be maintained or updated. About 500×10^6 neurons (a number chosen to match that found in adult human brains [198]) constitute the central executive network.

Figure 4.13 illustrates the multi-modal proposed architecture.

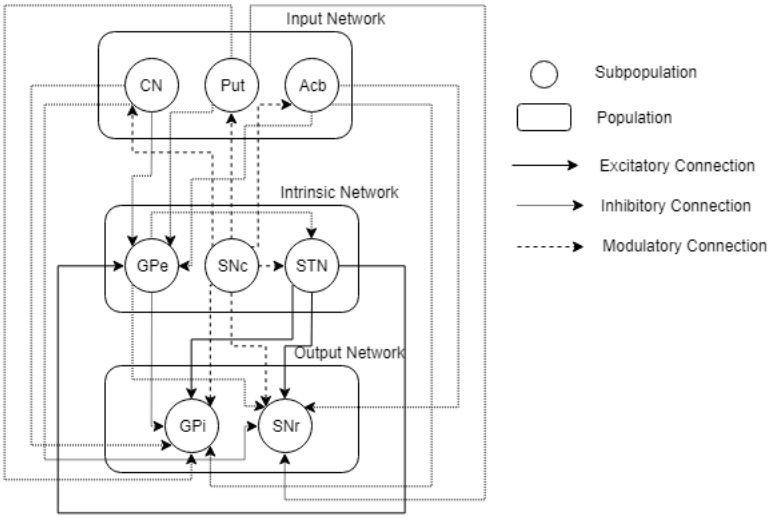

Figure 4.12: Central Executive Network.

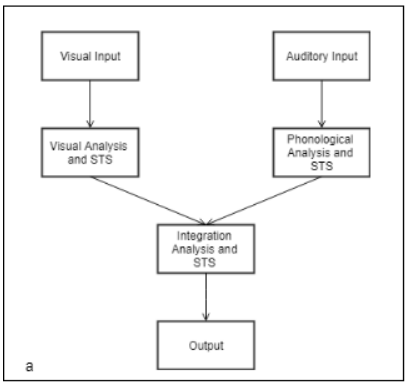
Visual Input
Auditory Input
Visual Analysis and STS
Phonological Analysis and STS
Integration Analysis and STS
Output
a

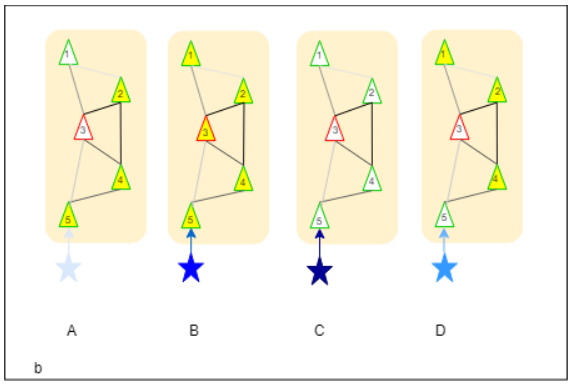
A
B
C
D
b

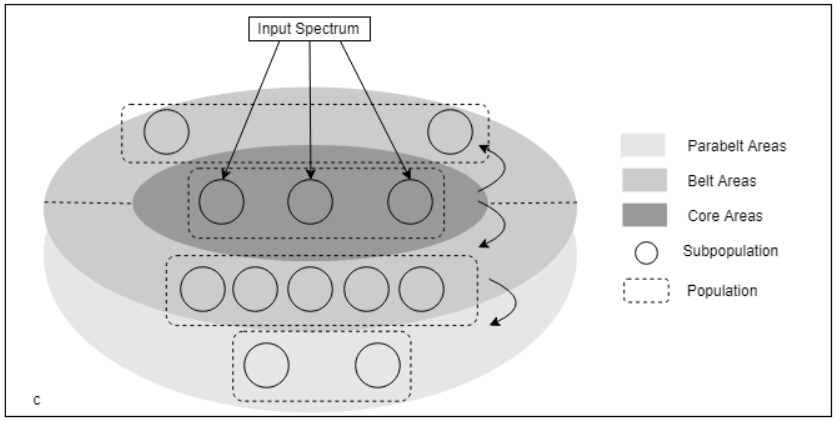
Input Spectrum
Parabelt Areas
Belt Areas
Core Areas
Subpopulation
Population
c

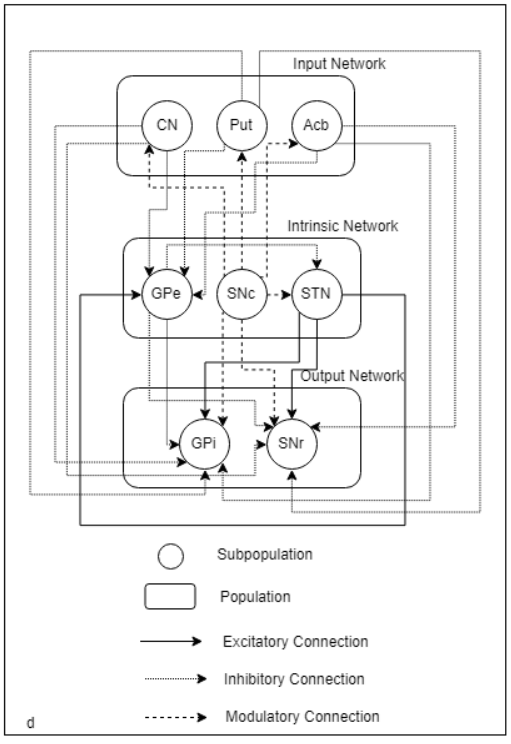
Input Network
CN
Put
Acb
Intrinsic Network
GPe
SNc
STN
Output Network
GPi
SNr
Subpopulation
Population
Excitatory Connection
Inhibitory Connection
Modulatory Connection
d

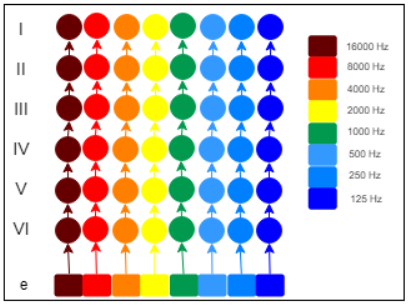
I
II
III
IV
V
VI
16000 Hz
8000 Hz
4000 Hz
2000 Hz
1000 Hz
500 Hz
250 Hz
125 Hz
e

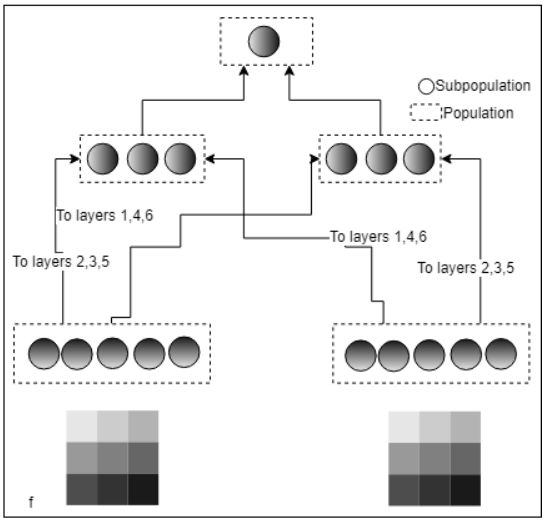
Subpopulation
Population
To layers 1,4,6
To layers 2,3,5
To layers 1,4,6
To layers 2,3,5
f

Figure 4.13 *(previous page)*: a. Proposed structure architecture. b. Response of a column to a sequence of events. In (A), only neurons 5, 4 and 2 have threshold crossing output and hence generate a sequence of spikes (illustrated by yellow highlight). In (B), a stronger input stimuli is presented which causes all five neurons to fire. In (C), the input is presented while the neurons are within the refractory period and hence no activity can be observed. In (D), the neurons have recovered and the stimuli causes neurons 4,2 and 1 to fire. c. Organization of phonological loop populations. Shaded areas represent core, belt and parabelt groups and are modeled as populations. Circles represent subpopulations. The input spectrum is fed to the core areas (parallel paths) as further detailed in e. ; the output of core areas is summed and fed (distributed) to all medial and lateral belt populations; the latter connect (also via parallel paths) to parabelt populations. d. Central Executive Network. e. Tonotopic organization of a core area (subpopulation). Frequency partition is color coded. f. Proposed visual network with retino-topic organization illustrated via shades of grey: neurons of the same color process information extracted from the part of the visual field with the matching color.

Chapter 5

Learning Algorithms

"Neurons that fire together wire together. Neurons that fire apart wire apart."

D.O. Hebb

5.1 Introduction

Learning is the basis of factual and episodic memories. It is believed that the cortex adapts itself such that more neurons are devoted to stimuli that appear more frequently or are more important and less neurons to less relevant ones [199]. This adaptation of cortex is also dubbed under the term of "learning" in the wider sense. All the different forms of learning are in one way or other related to changes in the strength of synapses [200]. The neural basis of synaptic learning often involve processes known as potentiation and depression; while the former results in an increased synaptic strength, the latter weakens said connection.

Hebbian models seem to be the most accurate in describing the change in synaptic strength of neurons' connections [201]. Hebbian models of development and learning require both activity-dependent synaptic plasticity and a mechanism that induces competition between different synapses. According to Hebb's rule [202], the interaction strength between two cells that are co-activated will facilitate synaptic efficacy. This rule has been extended to the temporal domain, where it is known as spike-timing dependent plasticity (STDP). In many cases, the following causal relationship is assumed to exist: an excitatory synapse undergoes long-term potentiation if presynaptic firing precedes postsynaptic firing, and long-term depression is induced when the temporal order of firing is reversed [203]; this relationship is termed temporally asymmetric Hebbian spike timing dependent plasticity. If a certain synaptic weight is large, a presynaptic spike is

more likely to elicit firing of the postsynaptic cell, following firing of the presynaptic cell. This will strengthen the synaptic weight, according to the STDP rule, which, in turn, will increase the likelihood of eliciting firing of the postsynaptic cell following firing of the presynaptic cell. On the other hand, if the synaptic weight is weak, then pre- and post-firing will be uncorrelated and the learning process will sample the STDP curve randomly. If the total depression is larger than the total potentiation, then the synapse will be further weakened. It has been argued that neurons in vivo operate in such a balanced regime. Synapses modifiable by STDP compete for control of the timing of postsynaptic action potentials. Inputs that fire the postsynaptic neuron with short latency or that act in correlated groups are able to compete most successfully and develop strong synapses, while synapses of longer-latency or less-effective inputs are weakened.

Though widely adopted, Hebbian learning is regarded as a "local" solution to the learning problem; mostly characterizing the behavior of smaller populations of neurons which can perform basic neural functions. When attempting to describe larger population activity performing higher order functions such as working memory, accumulating evidence suggest that human behavior involve a much more complex process in which reward and punishment play a crucial role, a.k.a reinforcement learning. Reinforcement Learning (RL) theory has contributed to a better understanding of dopamine reward signals in the brain [204], neural activities in other brain areas such as prefrontal cortex and basal ganglia [205, 206, 207], as well as alterations of brain activity and behavior in different pathologies [208, 209].

When tackling the problem of a learning algorithm for our multi-modal network, we initially attempted a simplification by adopting a Bayesian inference scheme in which two assumptions can be made: a deterministic setup in which weights are considered deterministic unknown variables and a probabilistic approach where rather than learning a tremendous number of variables, weights are assumed to be drawn from a normal distribution of unknown parameters (i.e. mean and standard deviation) rendering the number of optimization variables (and hence the cardinality of the search space) a reduced one. Furthermore, the problem is tackled from two perspectives: a global approach where the entire network optimizes a global objective function - and hence individual loops may not be optimal with respect to their own performed task -, and a localized approach where each loop achieves a local solution minimizing a local objective function - the overall objective function is hence not necessarily minimized). This approach is described in section 5.2.

Next, a spike timing dependent plasticity based reinforcement learning strategy is proposed in which a modification of the partially observable Markov decision process is introduced to implement a reinforcement learning algorithm in

which neurons act as agents and actions taken are firing decisions. A weight update rule is derived under this framework as formulated in section 5.3.

Finally, we describe a two-stage learning algorithm in which the basic assumption we take is that while smaller subpopulations of neurons reach a local solution using a Hebbian-like learning, larger associations employ a reinforcement learning strategy to optimize their collaboration. The first stage of the learning algorithm is presented in the framework of a stochastic dynamical model. We start by analyzing the stochastic learning dynamics of a single inhibitory synapse. Then we turn to investigate the learning dynamics of a population of inhibitory feed forward synapses. Finally we study a model that incorporates learning of both feed forward excitatory and inhibitory inputs to a single postsynaptic cell. Stability analysis is conducted to show convergence of the steady state solution. The second stage of the proposed algorithm tackles the problem of RL from an optimal control perspective. We reformulate the stochastic optimal control problem as an approximate inference one; applying the result to an RL framework. An iterative solution is drawn for a given path and proven to converge. The algorithm is detailed in section 5.4.

5.2 An Iterative Bayesian Solution

Let Ω_1, Ω_2, Ω_3 be the set of weights of the phonological loop, the visuo-spatial loop, and the central executive networks respectively. Denote by r an input of the phonological loop, v an input of the visuo-spatial loop, y and g the corresponding outputs of the phonological and visuo-spatial networks, and z the output of the central executive. The adopted nomenclature is illustrated in figure 5.1. A supervised learning setup aims at minimizing a cost function expressed as a form of discrepancy between a desired output and an actual output. In our case, the problem could be tackled in one of two ways: a "localized approach" and a "global approach". The localized approach aims at optimizing each of the loops separately (under the assumption that disturbing one does not alter the other) while a general approach optimizes the entire network as one entity aiming at processing the two modalities simultaneously. Additionally, we explore two possibilities for the set of weights representing the networks: a deterministic setup in which the optimal weights are considered unknown but fixed, and a probabilistic solution in which the optimal weights are derived from a probability distribution which parameters (mean and variance) are unknown. Below is a mathematical description of the four possible setups we explore. The nomenclature is summarized in table 5.1.

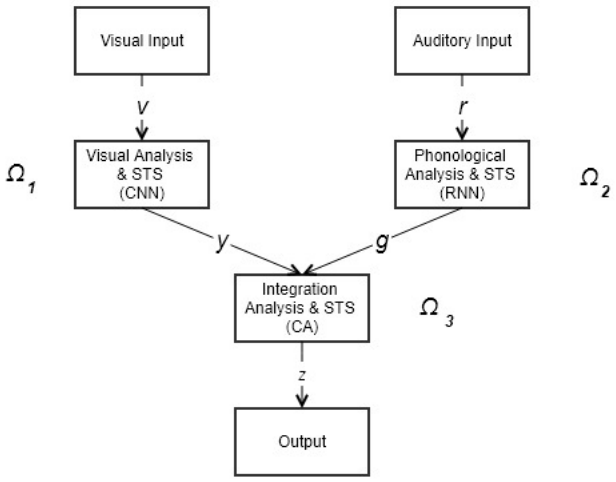

Figure 5.1: Proposed Hybrid Structure.

5.2.1 Deterministic Weights

In a deterministic approach, the problem is often reduced to finding the optimal set of weight which minimizes a certain objective function quantifying the offset between the predicted and the actual labels.

Localized approach

In a localized approach, each loop is assumed to be independent from the remainder of the network (i.e. achieves a local optimal solution); such approach is beneficial for cases of missing or noisy data as it allows for processing of modalities separately - a case for modality specific resources - . For a set of N training instances, i.e. a collection of input-output pairs $(r_j, y_j), (v_j, g_j), (y_j, g_j, z_j), j = 1, ..., N$ the multi-objective optimization problem can be written as:

$$\begin{cases} \min_{\Omega_1} E = \frac{1}{N}\sum_{j=1}^{N}(y_j - y_{jd})^2 \ \textit{subject to} & |\omega_{1i}| < \epsilon_1 \, |\omega_{1e}| > \epsilon_2 \\ \min_{\Omega_2} E = \frac{1}{N}\sum_{j=1}^{N}(g_j - g_{jd})^2 \ \textit{subject to} & |\omega_{2i}| < \epsilon_1 \, |\omega_{2e}| > \epsilon_2 \\ \min_{\Omega_3} E = \frac{1}{N}\sum_{j=1}^{N}(z_j - z_{jd})^2 \ \textit{subject to} & |\omega_{3i}| < \epsilon_1 \, |\omega_{3e}| > \epsilon_2 \end{cases} \tag{5.1}$$

where the subscripts i and e denote inhibitory and excitatory weights respectively and ϵ_1, ϵ_2 represent the maximum and minimum values an inhibitory and excitatory weight can take respectively.

Global approach

In this case, the optimization problem only minimizes the final output of the central executive as a function of the set of weights of all three subnetworks.

Mathematically it can be written as:

$$\begin{cases} \min_{\Omega_1,\Omega_2,\Omega_3} \frac{1}{N} \sum_{j=1}^{N} (z_j - z_{jd})^2 \\ \textit{subject to } \ |\omega_i| < \epsilon_1 \, |\omega_e| > \epsilon_2 \end{cases} \tag{5.2}$$

5.2.2 Probabilistic Weights

A probabilistic approach models the system as a stochastic process with random variables being characterized by their probability distributions. The assumption is inspired by the functionality of inhibitory and excitatory synapses: the former tends to attenuate the propagated signal while the latter tends to emphasize it. Assuming all synapses of the same type in a subnetwork are identical (a fairly reasonable assumption in the CNS) one can model inhibitory synapses as random variables drawn from a Gaussian distribution parametrised by a mean μ_{1i} and a standard deviation σ_{1i}; i.e. $\omega_{1i} \sim \mathcal{N}(\mu_{1i}, \sigma_{1i})$. Similarly, we can write $\omega_{1e} \sim \mathcal{N}(\mu_{1e}, \sigma_{1e})$. The same applies to all subnetworks.

Global approach

Solving the network is equivalent to finding the optimal set of weights maximizing the posterior distribution:

$$\begin{aligned} &\max_{\mu,\sigma} \log(p(z|v,r)p(\Omega_1,\Omega_2,\Omega_3)) = \log\left(\frac{p(v,r,z)p(z)}{p(v,r)} p(\Omega_1,\Omega_2,\Omega_3)\right) \\ &\textit{subject to } \mu_{1,2,3,e} \geq 5\mu_{1,2,3,i} \end{aligned} \tag{5.3}$$

where $\mu = [\mu_{1e}, \mu_{1i}, \mu_{2e}, \mu_{2i}, \mu_{3e}, \mu_{3i}]$, $\sigma = [\sigma_{1e}, \sigma_{1i}, \sigma_{2e}, \sigma_{2i}, \sigma_{3e}, \sigma_{3i}]$. Let $y = f(v, \Omega_1)$, $g = h(r, \Omega_2)$, and $z = t(y, g, \Omega_3)$ be the functions realized by the three subnetworks illustrated in figure 5.1; equation 5.3 can be written as:

$$\begin{aligned} &\max_{\mu,\sigma} \log\left[p(v)p(r)\int_y\int_g p(f(v,\Omega_1)|v)p(h(r,\Omega_2)|r)p(t(y,g,\Omega_3)|y,g)dgdy\right] \\ &+ \log\left[\int_v\int_r\int_y\int_g p(t(y,g,\Omega_3)|y,g)p(h(r,\Omega_2)|r)p(f(v,\Omega_1)|v)p(v)p(r)dgdydrdv\right] \\ &+ \log[p(\Omega_1,\Omega_2,\Omega_3)] \\ &\textit{subject to } \mu_{1,2,3,e} \geq 5\mu_{1,2,3,i} \end{aligned} \tag{5.4}$$

Localized approach

For a localized solution, the optimization problem to be solved can be written as:

Table 5.1: Nomenclature

Variable	Definition
Ω_1, Ω_2, Ω_3	Weights of phonological loop, visual loop and central executive respectively
r, v	Inputs of phonological and visual loops respectively
y, g, z	Outputs of phonological, visual loops and central executive respectively
ϵ_1, ϵ_2	Maximum value of an inhibitory connection weight, minumum value of an excitatory connection weight
μ, σ	Mean value of a network's connection weights, standard deviations of a network's connection weights

$$\begin{cases} \max_{\mu_1,\sigma_1} \log(p(y|v)p(\Omega_1)) \\ \textit{subject to } \mu_{1e} \geq 5\mu_{1i} \\ \max_{\mu_2,\sigma_2} \log(p(g|r)p(\Omega_2)) \\ \textit{subject to } \mu_{2e} \geq 5\mu_{2i} \\ \max_{\mu_3,\sigma_3} \log(p(z|y,g)p(\Omega_3)) \\ \textit{subject to } \mu_{3e} \geq 5\mu_{3i} \end{cases} \tag{5.5}$$

Given the complex and highly non linear functions implemented by the individual loops, a closed form solution for the values of the weights (for a deterministic case) or their probability distribution (for a probabilistic case) is unattainable. Instead, iterative solutions are sought. While most state of the art deep learning techniques employ an error backpropagation scheme or some derivative of it, we propose to make use of a heuristic search algorithm, GAs. Our choice is derived from the relative simplicity of (GAs) rendering their implementation for this complex problem a suitable alternative. While a guarantee of a convergence to a global solution cannot be claimed, searching the space for a possible solution satisfying the constrained optimization problem is a reasonable compromise.

5.3 A Spike Timing Dependent Plasticity Based Reinforcement Learning Approach

Reinforcement Learning (RL) theory has been successfully employed to model dopamine based reward learning in the brain [204], as well as the interactions between neural associations such as the prefrontal cortex and the basal ganglia [205, 206, 207], in addition to neural basis for a variety of neurological disorders [208, 209].
In this part, we propose a modification to the STDP framework which acts as

a reinforcement learning strategy. We apply the online version of the Partially Observable Markov Decision Model (POMDP) reinforcement learning algorithm [210] to the model at hand. A collection of interacting agents aiming at maximizing a common reward function is equivalent to each agent independently maximizing that function. A set of parameters $X_i = [x_{i1}, ..., x_{ij}, ...]$ relevant to an agent i are updated according to the following:

$$x_{ij}^{t+\Delta t} = x_{ij}^{t} + \alpha \mathcal{R}^{t+\Delta t} \tau_{ij}^{t+\Delta t} \tag{5.6}$$

$$\tau_{ij}^{t+\Delta t} = \gamma \tau_{ij}^{t} + \eta_{ij}^{t} \tag{5.7}$$

$$\eta_{ij}^{t} = \frac{1}{p_i^t(a_i)} \frac{\partial p_i^t(a_i)}{\partial x_{ij}^t} \tag{5.8}$$

where Δt is the time step, α is the learning rate parameter, τ is a trace of which changes are accumulated in η, and $p_i^t(a_i)$ denoted the probability of agent i choosing an action a_i at time t. In the case of our network, each neuron is a modeled as an independent agent which at each time step i fires with with a probability ρ. Hence takes an action $a_i = 1$ with a probability ρ_i^t or an action $a_i = 0$ with a probability $1 - \rho_i^t$. The neuron connects to a post synaptic cell through a connection of synaptic strength $x_i j$ defined as positive for excitatory synapses and negative for inhibitory synapses. Hence,

$$\eta_{ij}^{t} = \begin{cases} \frac{1}{\gamma_i^t} \frac{\partial \gamma_i^t}{\partial x_{ij}} \ \ if\ a_i^t = 1 \\ -\frac{1}{1-\gamma_i^t} \frac{\partial \gamma_i^t}{\partial x_{ij}} \ \ if\ a_i^t = 0 \end{cases} \tag{5.9}$$

Equations (5.6), (5.7) and (5.9) define a reinforcement learning strategy based on a stochastic binary cell assumption. However, the elementary computing unit we adopt borrows the concept of strength encoding from the anatomy: the strength of a stimuli is reflected at the output of the neuron by the firing rate observed. In other terms, a "strong input" leads to a higher frequency of spikes at the output of the neuron.
Mathematically, a neuron's output is described as

$$y_i^t = \delta_i^{t-t_i^h} + \sum_j x_{ij} \sum_{t_j^h \in \mathcal{T}} \theta_{ij}(t - t_i^h, t - t_j^h) \tag{5.10}$$

where t_i^h is the time of the last activity of the neuron and hence represents the history of firing, δ_i represents the refractory period due to the last firing and t_j^h represents the history of the activity of the presynaptic cell antecedent to t. $x_{ij}\theta_{ij}(t - t_i^h, t - t_j^h)$ is the response of the postsynaptic neuron to the firing of the j^{th} presynaptic neuron at time t_j^h. In other term, a post synaptic cell responds to the temporal summation of the firing of the collection of presynaptic neurons

connected to it taking into account a refractory period. From (5.10) we obtain

$$\frac{\partial y_i^t}{\partial x_{ij}} = \sum_{t_j^h \in \mathfrak{T}} \theta_{ij}(t - t_i^h, t - t_j^h) \tag{5.11}$$

Assuming a neuron fires with a probability $\rho_i^t = f_i(y_i^t - \epsilon$ where ϵ is the firing threshold and f_i is a probability density function, equation (5.9) can be written as

$$\eta_{ij}^t = \begin{cases} \frac{1}{f_i^t} f_i'^t \sum_{t_j^h \in \mathfrak{T}} \theta_{ij}(t - t_i^h, t - t_j^h) \ \textit{if } a_i^t = 1 \\ -\frac{\Delta t}{1 - f_i^t} f_i'^t \sum_{t_j^h \in \mathfrak{T}} \theta_{ij}(t - t_i^h, t - t_j^h) \ \textit{if } a_i^t = 0 \end{cases} \tag{5.12}$$

Let us now consider the case where the firing rate of both pre and postsynaptic cells are altered by a change in the synaptic strength x_{ij}. The algorithm is applied to an agent formed by the post synaptic cell i and all presynaptic cells j that connect to it. We can write

$$p_i(a_i)p_j(a_j) = \begin{cases} (1 - \rho_i)(1 - \rho_j) \ \textit{if } a_i = a_j = 0 \\ \rho_i(1 - \rho_j) \ \textit{if } a_i = 1,\ a_j = 0 \\ (1 - \rho_i)\rho_j \ \textit{if } a_i = 0,\ a_j = 1 \end{cases} \tag{5.13}$$

The probability of both pre and post synaptic neurons firing simultaneously in a short interval Δt is negligible and hence we do not consider the case of $a_i = a_j = 1$. By analogy we obtain

$$\eta_{ij}^t = \left(\frac{\Omega_i^t}{f_i^t} - 1\right) \frac{\partial f_i^t}{\partial x_{ij}} + \left(\frac{\Omega_j^t}{f_j^t} - 1\right) \frac{\partial f_j^t}{\partial x_{ij}} \tag{5.14}$$

If α and γ are chosen larger than the decay time β of τ, taking the limit of Δt to zero we obtain the following of equations which define the update rule under the STDP based reinforcement learning strategy:

$$\frac{dx_{ij}}{dt} = \alpha \mathcal{R}^t \tau_i j^t \tag{5.15}$$

$$\beta \frac{d\tau_{ij}}{dt} = -\tau_{ij}^t + \eta_{ij}^t \tag{5.16}$$

$$\eta_{ij}^t = \left(\frac{\Omega_i^t}{f_i^t} - 1\right) \frac{\partial f_i^t}{\partial x_{ij}} + \left(\frac{\Omega_j^t}{f_j^t} - 1\right) \frac{\partial f_j^t}{\partial x_{ij}} \tag{5.17}$$

5.4 A Two-Stage Stochastic Reinforcement Algorithm

5.4.1 Unsupervised Hebbian Learning

The first stage of the learning algorithm proposed consists of a sequence of weight update changes following a train of spikes propagating through a connection.

Table 5.2: Nomenclature

Variable	Description
ω_h	Inhibitory synaptic weight
β	Learning rate
$\Delta\omega_h$	Change in inhibitory synaptic weight
$g(\omega)$	Weight dependence of STDP rule
F	Temporal dependence of STDP rule
d, ν	Parameters in the range $[0, 1]$
$x_{1/2}$	Stochastic binary variable indicating status of pre/post
$t_{1/2,j}$	spike times of the pre/post jth cell synaptic cell
$\eta_{1/2}$	pre/post synaptic mean firing rate
$\bar{Y} = \int Y(t)dt$	Temporal average of a variable Y
$\gamma(t - t')$	decrease in firing rate after an inhibitory input at t'
N_I	Number of inhibitory cells
I_e	constant excitatory input to the cell
$\Omega_{h/e}$	Fixed point solution for inhibitory/excitatory population

We first consider a single inhibitory synapse and generalize our results for a population of inhibitory neurons and then a collection of inhibitory and excitatory neurons. Table 5.2 summarizes the nomenclature adopted. In our formulation, variables with subscript 1 denote presynaptic variables, while the subscript 2 designate post synaptic variables. The subscripts h and e distinguish inhibitory and excitatory synapses respectively.

Learning a single inhibitory synapse

For a single inhibitory synapse at which projects a set of pre-synaptic cells, learning such synapse is reduced to finding the optimal synaptic weight change following a train of spikes. For that, we adopt an STDP rule illustrated by equation (5.18) which describes a temporally asymmetric weight update rule for a single inhibitory synaptic weight ω_h.

$$\Delta\omega_h = \pm g(\omega_h)F(|t|) \tag{5.18}$$

$$g(\omega_h) = \begin{cases} g_2 = (1 - \omega_h)^d \textit{ for post synaptic cells} \\ g_1 = \nu(\omega_h)^d \textit{ for pre synaptic cells} \end{cases} \tag{5.19}$$

Equation (5.18) defines the synaptic change due to a single pair of pre-post spikes. We shall assume that the STDP rule is additive with respect to all pairs of pre-post spike times. Equation (5.18) describes a temporally asymmetric STDP rule. The temporal filter, $F(t)$, can be modeled by a decaying exponent or by a gamma distribution. Note that the STDP rule is temporally asymmetric and not antisymmetric due to the different scalings of depression and potentiation.

In our model, the strengthening and weakening of synapses follow equation (5.19).

A train of spikes in pre or post synaptic cells entitles a weight change expressed as a weighted summation of incoming synapses:

$$\omega_h(t+\delta_t) = \omega_h(t) + \beta g_2(\omega_h) x_2 \sum_{j=1}^{\infty} F(t - t_{1,j}) + \beta g_1(\omega_h) x_1 \sum_{j=1}^{\infty} F(t - t_{2,j}) \quad (5.20)$$

where $x_{1/2}$ is a stochastic variable which is one if the post/pre cell fired at time interval $[t, t+\delta_t)$ and zero otherwise; $t_{1/2,j}$ are the spike times of the post/pre synaptic neuron, respectively; the summation is over past times $t_{1/2,j} < t$. Note that the summation over all past spike times results from our assumption that the synaptic update rule, equation (5.18), is additive with respect to all pre-post spike time pairs. To derive the solution of this system we begin by expressing the derivative of ω_h using the short time limit:

$$\frac{\partial \omega_h(t)}{\partial t} = \lim_{\delta_t \to 0} \frac{\omega_h(t+\delta_t) - \omega_h(t)}{\delta_t} \quad (5.21)$$

$$\lim_{\delta_t \to 0} \frac{1}{\delta_t} x_1 = X_{1,h}(t) = \sum_j (t - t_{1,j}) \quad (5.22)$$

where $X_{1,h}$ describes the spike train of the inhibitory pre-synaptic neuron in terms of a series of delta function pulses at the spike times of the cell Similarly X_2 describes the post synaptic spike train. Replacing in (5.18):

$$\omega_h = \beta g_2(\omega_h) A_2(t) - \beta g_1(\omega_h) A_1(t) \quad (5.23)$$

$$A_2(t) = \int_{-\infty}^{t} dt' X_2(t) X_{1,h}(t') F(t - t') \quad (5.24)$$

$$A_1(t) = \int_{-\infty}^{t} dt' X_2(t') X_{1,h}(t) F(t - t') \quad (5.25)$$

In the limit of slow learning rate, the synaptic weight, ω_h, is relatively fixed over long periods of time, during which the right hand side of equation (5.23) is sampled by the dynamics such that we can neglect its fluctuations around its mean. This approximation yields deterministic dynamic equations for the mean synaptic weights expressed using (5.26),(5.27), and (5.28)

$$\omega_h = \beta g_2(\omega_h) \mathcal{A}_2 - \beta g_1(\omega_h) \mathcal{A}_1 \quad (5.26)$$

$$\mathcal{A}_2 = \int_{-\infty}^{t} dt' \langle X_2(t) X_{1,h}(t') \rangle F(t - t') \quad (5.27)$$

$$\mathcal{A}_1 = \int_{-\infty}^{t} dt' \langle X_2(t') X_{1,h}(t) \rangle F(t - t') \tag{5.28}$$

where $\langle . \rangle$ denotes averaging with respect to the distribution of the neural firing, for a given fixed synaptic weight, ω_h. To proceed with the analysis we need to specify the cross-correlation function between the pre-synaptic input and the post-synaptic response, and in particular its dependence on the synaptic weight, ω_h. However, the calculation of dependence of the temporal structure of the pre-post firing probability on the synaptic weight is not a trivial task. We assume that the cross-correlation of pre and post spikes can be written as a linear function as described in (5.29):

$$\langle X_2(t) X_{1,h}(t') \rangle = \begin{cases} \eta_2 \eta_1 (1 - \omega_h \gamma(t - t')) \ \textit{if } t > t' \\ \eta_2 \eta_1 \ \textit{if } t < t' \end{cases} \tag{5.29}$$

where $\eta_{1/2}$ is the average firing rate for pre/post cells. $\gamma(t - t')$ is a discount function decaying in time. Substituting (5.29) in (5.26) we obtain:

$$\omega_h = -\beta \eta_1 \eta_2 \bar{F} \left[\Delta g(\omega_h) + \omega_h \frac{\bar{\gamma F}}{\bar{F}} g_2(\omega_h) \right] \tag{5.30}$$

Where $\Delta g(\omega_h) \equiv g_1(\omega_h) - g_2(\omega_h)$ and $\bar{X} \equiv \int X(t) dt$.

Learning an inhibitory population

Consider now a population of inhibitory cells $\omega_{h,j}, j = 1 \ldots N_I$. A train of spikes traveling through the i^{th} cell at time t is described as $X_{h,i}(t) = \sum_{j=1}^{\infty} \delta(t - t_j)$. As before the post synaptic neuron responds to a train of spikes using a weighted summation:

$$X_2(t + \epsilon) = I_e - \frac{1}{N_I} \sum_{i=1}^{N_I} \omega_{h,i} X_{h,i}(t) \tag{5.31}$$

I_e represents the total excitatory input to the cell, ϵ is a small time delay assumed positive for causality.

For simplicity we assume that the correlations are instantaneous, $\langle X_{h,i}(t) X_{h,j}(t') \rangle = \eta^2 + \sigma_{ij} \delta(t - t')$. We shall further assume that the statistics of the input neuron responses are isotropic; i.e., no input neuron is statistically special. This assumption implies that:

1. The mean firing rate of all inhibitory presynaptic neurons is equal, $\eta_1 = \eta_2 = \eta$

2. The correlation structure of each input neuron with the rest of the input population (up to a permutation of indices) is the same. In particular, the correlation of a single input neuron with the total response of the population is equal for all input neurons; hence the uniform vector $v_o = [1, 1 \ldots, 1]$ is an eigenvector of the matrix σ.

Hence,

$$\omega_{h,i} = \beta g_2(\omega_{h,i}) A_{2,i}(t) - \beta g_1(\omega_{h,i}) A_{1,i}, i = 1, ..., N_I \tag{5.32}$$

$$A_{2,i}(t) = \int_{-\infty}^{t} dt' X_2(t) X_{1,h}(t') F(t - t') \tag{5.33}$$

$$A_{1,i}(t) = \int_{-\infty}^{t} dt' X_2(t') X_{1,h}(t) F(t - t') \tag{5.34}$$

Under the assumption of slow learning ($\beta \to 0$), the average inhibitory weight obeys:

$$\frac{1}{\beta \eta^2 \xi} = -\Delta g(\omega_{h,i}) \left[\omega_e - \frac{1}{N_I} \sum_{j=1}^{N_I} \omega_{h,i} \right] - g_2(\omega_{h,i}) \frac{1}{N_I} \sum_{j=1}^{N_I} \Gamma_{h,ij} \omega_{h,ij} \tag{5.35}$$

where $\xi = \int_0^\infty F(t)dt$, $\omega_e = I_e/\eta$ and $\Gamma_{h,ij} = \sigma_{ij}/\xi\eta^2$ is a nonnegative symmetric matrix. From the assumption of isotropy the uniform vector $v_0 = (1, 1, 1, ..., 1)$ is an eigenvector of the correlation matrix, $\Gamma_h v_0 = N_I \Gamma_0 v_0$, with eigenvalue $N_I \Gamma_0 = \sum_{j=1}^{N_I} \sigma_{h,ij}$.

A homogeneous solution $\omega_{h,i} = \Omega_h$ can be found as follows:

$$\frac{1}{\beta \eta^2 \xi} \Omega_h = -\Delta(\omega_h)(\omega_e - \Omega_h) - g_2(\Omega_h) \Gamma_h \Omega_h \tag{5.36}$$

The fixed-point equation for the homogeneous solution is given by:

$$\frac{g_1(\Omega_h)}{g_2(\Omega_h)} \equiv \nu \left(\frac{\Omega_h}{1 - \Omega_h} \right)^d = 1 - \Gamma_h \frac{\Omega_h}{\omega_e - \Omega_h} \tag{5.37}$$

The left hand side of equation (5.37), $\nu \left(\frac{\Omega_h}{1-\Omega_h} \right)^d$, starts from 0 at $\Omega_h = 0$, increases monotonically in the range of $\Omega_h, \log \left(\frac{\Omega_h}{1-\Omega_h} \right)^d, > 0 n \forall \Omega_h \in (0, 1)$, and diverges to infinity as $\Omega_h \to 0$. The right hand side of equation (5.37) decreases monotonically ($1 - \Gamma_h \frac{\Omega_h}{\omega_e - \Omega_h} < 0 \ \forall \Omega_h < \omega_e$) starts from the value of one at $\Omega_h = 0$, crosses zero at $\Omega_h = \frac{\omega_e}{1+\Gamma_h}$ and is continuous(5.37) has a unique solution

Ω_h^* in the range $[0, min(1, \omega_e)]$, implying a net positive input to the postsynaptic cell. For $\Omega_h < \Omega_h^*$ the temporal derivative of the homogeneous solution, equation (5.36), will be positive, and vice versa. Hence, the uniform solution is stable to fluctuations in the uniform direction.

To study the stability of the homogeneous solution to general perturbations, we consider an arbitrary (though small) deviation from the homogeneous solution $\epsilon = \omega_{h,i} - \Omega_h$. To first order in the deviations one obtains:

$$\frac{1}{\beta\eta^2\xi}\epsilon = -\theta\epsilon + \Delta g(\Omega_h)\frac{1}{N_I}\sum_{j=1}^{N_I}\epsilon - g_2(\Omega_h)\frac{1}{N_I}\sum_{j=1}^{N_I}\Gamma_{h,ij}\epsilon \equiv -\sum_{j=1}^{N_I}M_{ij}\epsilon \tag{5.38}$$

$$\begin{aligned}\theta = (I_e - \Omega_h)\frac{\partial}{\partial\Omega_h}\Delta g(\Omega_g) + \Gamma_h\frac{\partial}{\partial\Omega_h}g_2(\Omega_h) = d(I_e - \Omega_h)\left(\nu\Omega_h + (1-\Omega_h)^{d-1}\right) \\ - d\Gamma_h\Omega_h(1-\Omega_h)^{d-1}\end{aligned} \tag{5.39}$$

Replacing in equation (5.37) we obtain:

$$\theta = \nu\beta(\omega_e - \Omega_h)\frac{\Omega_h^{d-1}}{1-\Omega_h} \tag{5.40}$$

The eigenvalues M_n of the stability matrix M obey:

$$M_0 = \theta - \Delta g(\Omega_h) + g_2(\Omega_h)\Gamma_h \tag{5.41}$$

$$M_n = \theta + g_2(\Omega_h)\Gamma_{h,n} \tag{5.42}$$

where $\Gamma_{h,n}$ is an eigenvalue of Γ_h/N_I. At orthogonal directions $M_n > 0$, $\forall n \neq 0$ since $\Gamma_{h,n} > 0$ due to the positivity of the correlation matrix Γ_h. Hence, due to the negative feedback of Hebbian learning of inhibition, the uniform solution is always stable.
The STDP learning rule is an unsupervised learning rule and as such can learn salient features of the statistics of its inputs. The input statistics are expressed in the learning dynamics by the effective interactions between the synapses generated via the input correlations and the learning dynamics. Such sensitivity to input statistics may be manifested in solutions to the fixed point of the synaptic dynamics that reflect the correlations' structure of the input population.

Learning a mixed population

Consider now a population of N_E excitatory connection and N_I inhibitory connections. As per the adopted nomenclature, $X_{i,h/e} = \sum_{j=1}^{\infty} \delta(t - t_{i,h/e})$ represents a train of spikes in the i^{th} inhibitory/excitatory neuron. The response to a combination of inhibitory and excitatory inputs is modeled as:

$$X_2(t+\epsilon) = \frac{1}{N_E}\sum_{j=1}^{N_E} \omega_{e,j} X_{e,j} - \frac{1}{N_I}\sum_{j=1}^{N_I} \omega_{h,j} X_{h,j} \tag{5.43}$$

Under the assumptions that all neurons have similar properties (including firing rate) and uncorrelation of inhibitory and excitatory cells, the homogeneous solution is expressed as:

$$\frac{1}{\beta\eta^2\xi}\omega_{e,i} = -\Delta g(\omega_{e,i}) \left(\frac{1}{N_E}\sum_{j=1}^{N_E} \omega_{e,j} - \frac{1}{N_I}\sum_{j=1}^{N_I} \omega_{h,j} \right) + g_2(\omega_{e,i}) \frac{1}{N_E}\sum_{j=1}^{N_E} \Gamma_{e,ij}\omega_{e,j} \tag{5.44}$$

$$\frac{1}{\beta\eta^2\xi}\omega_{h,i} = (1-\nu) \left(\frac{1}{N_E}\sum_{j=1}^{N_E} \omega_{e,j} - \frac{1}{N_I}\sum_{j=1}^{N_I} \omega_{h,j} \right) - \frac{1}{N_I}\sum_{j=1}^{N_I} \Gamma_{h,ij}\omega_{h,i} \tag{5.45}$$

where $\Gamma_{h/e,ij} = \left(\sigma_{h/e,ij} - \eta^2\right)/\eta^2\xi$.

Under slow learning assumptions, the fixed point solution satisfies:

$$\Omega_h = \left(\frac{1}{1 + \frac{\Gamma_h}{1-\nu}} \right) \Omega_e \tag{5.46}$$

$$0 = -g_1(\omega_e)(\Omega_e - \Omega_h) + g_2(\omega_e)((1+\Gamma_e)\Omega_e - \Omega_h) \tag{5.47}$$

where from our assumption of isotropy the uniform vector is an eigenvector of the non-negative symmetric matrix Γ_e (for excitatory synapses) with the corresponding eigenvalue $N_I\Gamma_e = \sum_j \Gamma_{e,ij}$.

Fluctuation analysis around the homogeneous fixed point yields (a deviation of ϵ around the fixed point solution)

$$\frac{1}{\beta\eta^2\xi}\epsilon_e = -\theta\epsilon_e - \Delta g(\Omega_e)\epsilon_e + g_2(\Omega_e)\frac{1}{N_E}\sum_{j=1}^{N_E} \Gamma_{e,ij}\epsilon_{e,j} \tag{5.48}$$

where $\epsilon_{e,j}$ is the deviation of the j^{th} incoming excitatory synapse.

$$\frac{1}{\beta\eta^2\xi}\epsilon_h = (1-\nu)(\epsilon_e - \epsilon_h) + \frac{1}{N_I}\sum_{j=1}^{N_I} \Gamma_{h,ij}\epsilon_{h,j} \tag{5.49}$$

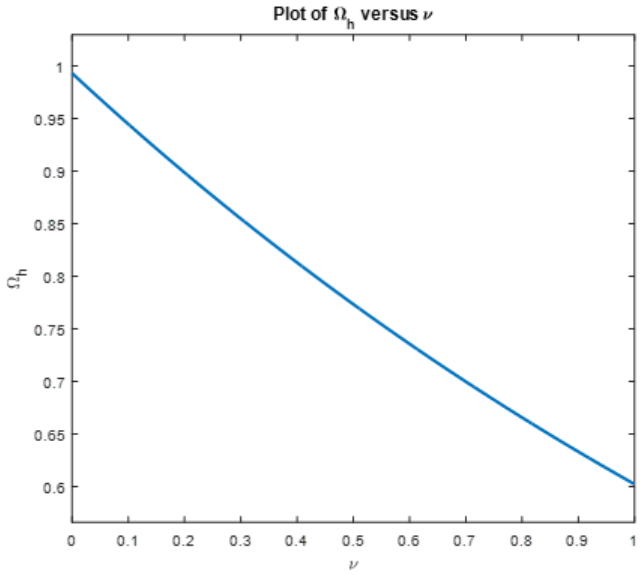

Figure 5.2: Effect of ν on steady state solution of single inhibitory synapse

where $\epsilon_{h,j}$ is the deviation of the j^{th} incoming inhibitory synapse.

$$\begin{aligned}\theta &= (\Omega_e - \Omega_h)\frac{\partial}{\partial \Omega_e} g_1(\Omega_e) - ((1+\Gamma_e)\Omega_e - \Omega_h)\frac{\partial}{\partial \Omega_e} g_2(\Omega_e) \\ &= 2(\Omega_e - \Omega_h)\frac{\partial}{\partial \Omega_e} g_1(\Omega_e) \geq 0\end{aligned} \tag{5.50}$$

Using the fixed point equations one can show that the homogeneous solution is always stable to fluctuations in the homogeneous direction. Additionally, similar to the analysis of the previous section, the homogeneous solution is always stable to fluctuations in directions of modifying the inhibition. Essentially, as the positive feedback of the STDP dynamics of the excitatory synapses becomes strong the homogeneous solution of the excitatory synapses loses its stability and the learning dynamics becomes more sensitive to the correlation structure of its excitatory inputs.

Theoretical simulation

We begin our experimental results by first investigating the effects of the parameters of our model on the stability and behavior of the synapses. Simulations were run on a set of 80 inhibitory neurons and 400 excitatory neurons (a ratio of 1/5 as in the cortex [211]. Figure 5.5 shows the evolution of the average neurons' weights versus time in minute for a collection of excitatory and inhibitory neurons.

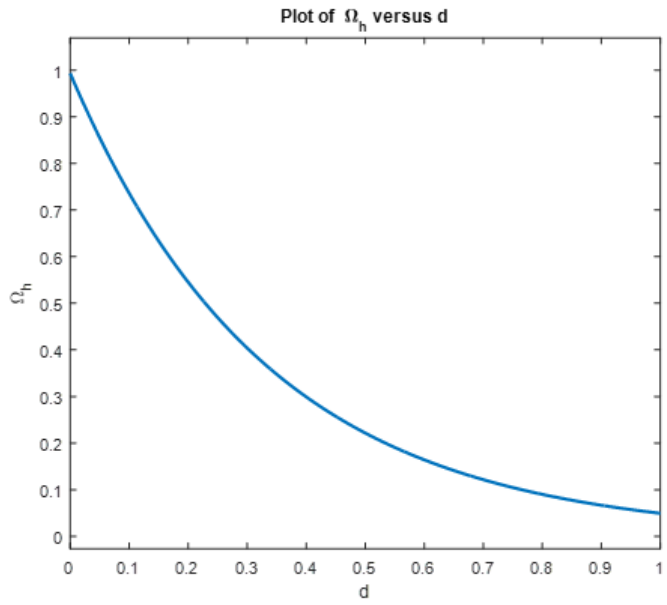

Figure 5.3: Effect of d on steady state solution of single inhibitory synapse

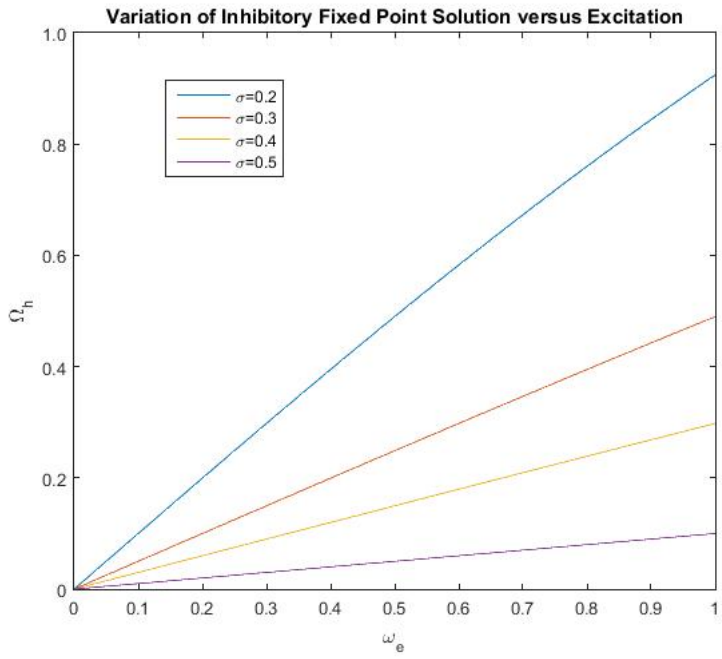

Figure 5.4: Effect of cross correlation on learning a population of inhibitory synapses

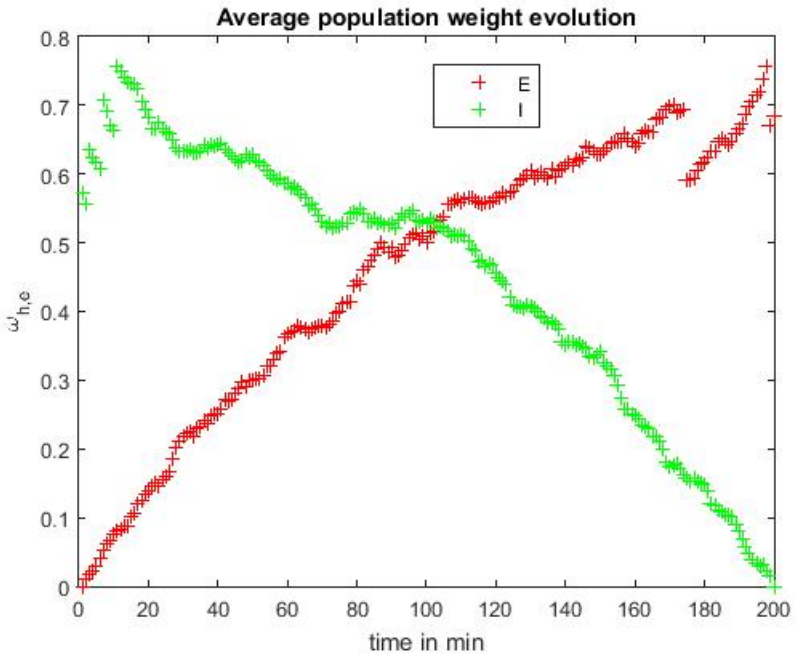

Figure 5.5: Evolution of weights in time

5.4.2 Stochastic Reinforcement Learning

The second stage aims at learning the connections between subpopulations using a stochastic reinforcement learning strategy. For that, we employ Bayesian inference approximation to model the optimal path finding problem and apply our result to a reinforcement learning framework. We first begin by defining a Markov decision process (MDP) as follows:

$$
\begin{aligned}
&MDP: \\
&\quad s_t \in \mathcal{S} : \text{set of states} \\
&\quad a_t \in \mathcal{A} : \text{set of actions} \\
&\quad \bar{s} = s_1, ..., s_T : \text{sequence of } T \text{ states} \\
&\quad \bar{a} = a_1, ..., a_T : \text{sequence of } T \text{ actions} \\
&\quad P(s_{t+1}|s_t) : \text{probability of moving from state } s_t \text{ to state } s_{t+1} \text{ given } a_t \\
&\quad \rho_t(s,a) \geq 0 : \text{ cost of state } s_t \text{ given } a_t \\
&\quad \pi(a_t, s_t) : \text{conditional probability of choosing } a_t \text{ given } s_t
\end{aligned}
\tag{5.51}
$$

An optimal policy π^* minimizes the expected cost of the Markov path λ_π (the

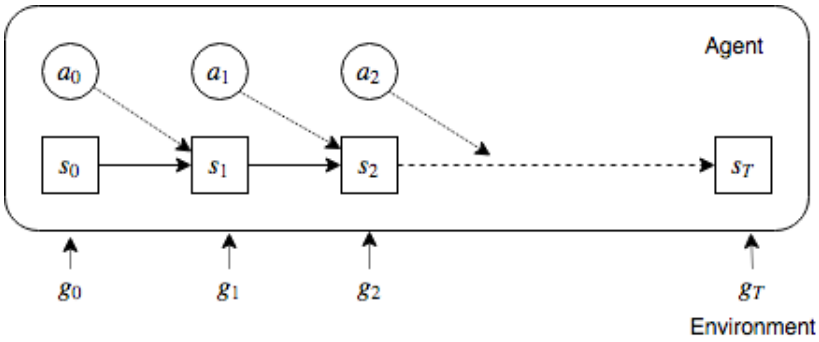

Figure 5.6: Bayesian approximation of the optimal path finding problem

subscript π denotes a path under a policy π):

$$\begin{aligned} \pi^* &= \arg\min_{\pi} \left\langle \sum_{t=0}^{T} \rho_t(s_t, a_t) \right\rangle_{\lambda_\pi} \\ \lambda_\pi(\bar{s}, \bar{a}|s_0) &= \pi(a_0|s_0) \prod_{t=1}^{T} \pi(a_t|s_t) P(s_{t+1}|s_t, a_t) \end{aligned} \tag{5.52}$$

where $\langle . \rangle_{\lambda_\pi}$ is the expected value operator computed over a path λ_π.

Under a reinforcement learning setup, it is reasonable to assume a discounted cost model; i.e. the cost of choosing a_t given s_t can be written as:

$$\rho_t(s_t, a_t) = \gamma^t \sigma(s_t, a_t) \tag{5.53}$$

where $\gamma \in [0, 1]$ is a discount factor and σ is a stationary function.

A Bayesian inference based approximation of the above control problem can be formulated as illustrated in figure 5.6, by introducing a binary task random variable g_t such as its probability is related to the cost function by: $P(g_t = 1|s_t, a_t) = \exp(-\eta\sigma(s_t, a_t))$ [212].

Given a policy π and observations $\bar{g} = g_{0...T} = 1$ the posterior probability of π is written as:

$$p_\pi(\bar{s}, \bar{a}) = P(\bar{s}, \bar{a}, \bar{g} = 1|s_0) = \lambda_\pi(\bar{s}, \bar{a}) \prod_{t=0}^{T} \exp(-\eta\rho_t(s_t, a_t)) \tag{5.54}$$

The problem defined in (5.54) is reduced to:

$$\pi^* = \arg\min_{\pi} KL\left[\lambda_\pi(\bar{s}, \bar{a}) || p_v(\bar{s}, \bar{a})\right] \tag{5.55}$$

with cost function

$$\hat{\rho}_t(s_t, a_t) = \rho_t(s_t, a_t) - \frac{1}{\eta} log(\upsilon(a_t, s_t)) \tag{5.56}$$

where υ is the uniform distribution.

The problems defined in (5.52) and (5.55) are equivalent.
Proof:
Let $\pi_t(a_t|s_t) = \delta_{a_t=\theta_t(s_t)}$ a deterministic policy (hence can be written in terms of the Dirac function), then

$$\begin{aligned} KL(\lambda_\pi||p_\upsilon) &= \log P(\bar{g}=1) + \int_{\bar{s}}\int_{\bar{a}} \lambda_\pi(\bar{s},\bar{a}) \log \frac{\lambda_\pi(\bar{s},\bar{a})}{\lambda_\upsilon(\bar{s},\bar{a})} \\ &+ \int_{\bar{s}}\int_{\bar{a}} \lambda_\pi(\bar{s})\pi(\bar{a}|\bar{s}) \sum_{t=0}^{T} \log \frac{1}{\exp(-\rho_t(s_t,a_t))} \\ &= \log P(\bar{g}=1|s_0;\upsilon) + KL(\lambda_\pi(\bar{s},\bar{a})||\lambda_\upsilon(\bar{s},\bar{a})) \\ &+ \int_{\bar{s}} \lambda_\pi(\bar{s}) \sum_{t=1}^{T} \rho_t(s_t, \theta_t(s_t)) \end{aligned} \tag{5.57}$$

$$\begin{aligned} KL(\lambda_\pi(\bar{s},\bar{a})||p_\upsilon(\bar{s},\bar{a})) &= \int_{\bar{s}}\int_{\bar{a}} \lambda_\pi(\bar{s},\bar{a}) \sum_{t=0}^{T} \frac{\log \delta_{a_t=\theta_t(s_t)}}{\upsilon(a_t|s_t)} \\ &= -\int_{\bar{s}} \lambda_\pi(\bar{s}) \sum_{t=0}^{T} \log \upsilon(\theta_t(s_t)|s_t) \end{aligned} \tag{5.58}$$

Hence,

$$KL(\lambda_\pi||p_\upsilon) = \log P(\bar{g}=1|s_0;\upsilon) + \left\langle \sum_{t=0}^{T} [\rho_t(s_t,\theta_t|s_t) - \upsilon(\theta_t(s_t)|s_t)] \right\rangle_{\lambda_\pi} \tag{5.59}$$

Although establishing an equivalency between the stochastic optimal control formulation and the Bayesian inference problem eases the former, the deterministic policy constraint - similarly to the classical formulation - requires solving Bellmann's equation. A relaxation of this assumption, allows a stochastic update, though does not guarantee an optimal policy. An proposed iterative solution for the above problem is given by:

$$\pi^{n+1} \leftarrow \arg\min_{\pi} KL(\lambda_\pi||p_{\pi^n}) \tag{5.60}$$

For any $\pi \neq \upsilon$ such as $KL(\lambda_\pi||p_\upsilon) \leq KL(\lambda_\upsilon||p_\upsilon)$ implies

$$\left\langle \sigma(\bar{s},\bar{u}) \right\rangle_{\lambda_\pi} \leq \left\langle \rho(\bar{s},\bar{u}) \right\rangle_{\lambda_\upsilon} \tag{5.61}$$

Proof:

$$KL(\lambda_{\pi^{n+1}}(\bar{s},\bar{a})||p_{\pi^n}(\bar{s},\bar{a})) = \int_{a_0} \pi^{n+1}(a_0|s_0)\Bigg[\log\frac{\pi^{n+1}(a_0|s_0)}{\pi^n(a_0|s_0)P(r_0|s_0,a_0)} + \int_{\hat{s}} P(\hat{s}|s_0,a_0)KL(\lambda_{\pi^{n+1}}(s_{2:T},a_{1:T}|s_1=\hat{s})||p_{\pi^n}(s_{2:T},a_{1:T}|s_1=\hat{s}))\Bigg] \tag{5.62}$$

Given three random variables a, b, and c such as $P(a,b,c) = P(a)P(b|a)P(c|b,a)$ then:

$$P(a)\exp\left(\int_b P(b|a)\log P(c=\hat{c}|b)\right) \propto \arg\min_{\lambda} KL(q(a)P(b|a)||P(a,b|c=\hat{c})) \tag{5.63}$$

and

$$\int_a P(a)\exp\left(\int_b P(b|a)\log P(c=\hat{c}|b)\right) \propto \min_{\lambda} KL(q(a)P(b|a)||P(a,b|c=\hat{c})) \tag{5.64}$$

Substituting (5.63) in (5.62) with $a = a_t|s_t$, $b = s_{t+1}$ and $P(c=\hat{c}|b) = \exp(\bar{\beta}_{t+1})P(g_t|s_t,a_t)$ the new policy can be written as a Gibbs distribution:

$$\pi^{n+1}(a_t|s_t) = \exp\left(\beta_t^{n+1}(s_t,a_t) - \bar{\beta}^{n+1}(s_t)\right) \tag{5.65}$$

with state energy

$$\beta_t^{n+1}(s_t,a_t) = \log\pi^n(a_t|s_t) + \log P(g_t=1|s_t,a_t) + \int_{s_{t+1}} P(s_{t+1}|s_t,a_t)\bar{\beta}_{t+1}^{n+1}(s_{t+1}) \tag{5.66}$$

and canonical partition function:

$$\bar{\beta}_t^{n+1}(s_t) = \log\int_a \exp\left(\beta(s_t,a_t)\right) \tag{5.67}$$

Hence, an iterative solution of a reinforcement learning problem given a path $(x,u,\mathcal{R},y)$ moving from state x to y for a control signal u and receiving a reward $\mathcal{R} = \log P(r=1|x,u)$, under a learning rate α is:

$$\beta(x,u) \leftarrow \beta(x,u) + \alpha\left[\mathcal{R} + \gamma\bar{\beta}(y) - \bar{\beta}(x)\right] \tag{5.68}$$

An update according to equation (5.60) can therefore be computed backwards in time using equations (5.65), (5.66), and (5.67).

Convergence analysis: let π^n be generated by (5.60) and let $\hat{\pi}$ be an arbitrary stochastic policy then,

$$KL(\lambda_{\hat{\pi}}||\lambda_{\pi^{n+1}}) - KL(\lambda_{\hat{\pi}}||\lambda_{\pi^n}) \leq \langle\eta\sigma(\bar{s},\bar{a})\rangle_{\lambda_{\hat{\pi}}} - \langle\eta\sigma(\bar{s},\bar{a})\rangle_{\lambda_{\pi^{n+1}}} \tag{5.69}$$

Summing over the horizon $0, 1, ..., T$ we obtain the following bound:

$$\frac{1}{T}\sum_{n=1}^{T}\langle\sigma(\bar{s},\bar{a})\rangle_{\lambda_{\pi^n}} \leq \langle\sigma(\bar{s},\bar{a})\rangle_{\lambda_{\hat{\pi}}} + \frac{1}{\eta T}KL(\lambda_{\hat{\pi}}||\lambda_{\nu}) \tag{5.70}$$

5.5 Conclusion

This chapter presented the three proposed learning algorithms investigated for our problem. The first employed a Bayesian inference scheme to develop optimization problems under deterministic or probabilistic weights and for a global or localized approach. The second implemented a reinforcement learning strategy using a spike timing dependent plasticity rule. The third constituted of two stages, the first being a Hebbian based learning implemented using a spike time dependent rule, the second being a stochastic reinforcement learning solved using a Bayesian inference problem.

Chapter 6

Results

6.1 The multi-modal network with the two-stage learning algorithm

6.1.1 Testing the visual loop

We tested our proposed visual processing network on the Amsterdam library of object images (ALOI). The dataset is composed of over 110,000 images of 1000 objects taken under different illumination, angle and color settings. Our network was compared against a pre-trained convolutional neural network (CNN) coupled with 3 different classifiers: multilayer perceptron (MLP), decision tree (DT), support vector machines with linear kernel (SVM-linear) and SVM with Gaussian kernel (SVM-rbf). The CNN employed is implemented using AlexNet [36] pre-trained on ImageNet [213] and fine-tuned on ALOI. Table 6.1 compiles the average accuracy, standard deviation over folds, and training epochs required for convergence. The reported number of epochs reflect that required for the fine tuning of the pre-trained network or that of the classifier used. Inhibitory and excitatory synapses are randomly distributed throughout our proposed network with a uniform ratio of 1/5 - to adhere to biological findings - kept throughout individual subpopulations. Parameters are chosen based on a grid search scheme ensuring maximum performance. Results are based on a 4 fold cross validation setup.

6.1.2 Testing the central executive

The 1-2-AX task is a complex working memory task where number and letter stimuli (1,2,A,X,B,Y) appear one at a time in sequence, and the participant is asked to detect one of two target sequences, depending on whether he or she last saw a 1 or a 2 (which thus serves as "task" stimuli). In the 1 task, the target is A followed by X, and for 2, it is B-Y. The task is hence reduced to correctly identify

when a stimulus requires to be maintained or updated. Each sequence of stimuli was generated by first randomly picking a 1 or 2, and then looping for one to four times over possible combinations of letters A, X, B and Y. A percentage of 50% of correct sequences is adopted. A uniform ratio of 1/5 of inhibitory synapses is maintained in these experiments.
We test the effect of each of the modifications proposed as well as the value of the proposed stochastic Hebbian learning algorithm (SHL) by performing our experiments on the following architectures:

- Network 1: 6 layer Deep Neural Network (DNN) with McCulloch-Pitts (summation/sigmoid activation function model) trained using regular Hebbian learning (HL)

- Network 2: 6 layer DNN with McCulloch-Pitts trained using SHL

- Network 3: 6 layer DNN with proposed neuron model trained using HL

- Network 4: 6 layer DNN with proposed neuron model trained using SHL

- Network 5: Proposed architecture with proposed neuron model trained using SHL

We report on the average recognition rate, the standard deviation across folds, as well as the total number of epochs required for convergence in table 6.2. Results are based on a 4 fold cross validation scheme.

6.1.3 Testing the phonological loop

To test our phonological loop, we train the proposed network on a collection of 4876 recordings of English words obtained from the Shtooka project [214]. We test the phonological similarity and the word length effects of the phonological loop by conducting three experiments:

- Experiment 1: The entire dataset of 4876 recordings is employed in a 4 fold cross validation scheme. Average recognition rate, standard deviation and average training epochs per fold are reported in table 6.3.

- Experiment 2: The uttered words are sorted by phonological similarity. For quantification purposes we measure the phonological similarity as the percentage of overlapping phonemes. To eliminate the word length effect, the dataset is further divided according to the number of phonemes in the uttered words. Results reported in table 6.3 are based on a 4 fold cross validation scheme. The average recognition rate is computed as the average across all levels of phonological similarity.

- Experiment 3: The dataset is split according to the words' length. Results reported in table 6.3 are based on a 4 fold cross validation scheme and a 1/5 inhibitory ratio.

Our proposed network is compared with a traditional artificial 3-layer neural network as well as a deep 6-layer recurrent neural network (RNN) with trained using backpropagation through time.

6.1.4 Testing the overall network

In this section, we test the multi-modal network on the MOBIO database - a collection of 152 videos (audio and image) - obtained from [215]. Though the database is originally designed for face recognition purposes, it can be suited for our purposes (for its bi-modal setup) by associating sequences of images of the same subject with speech uttered by the subject. The database includes a combination of short questions and free speech responses. We extract the audio parts corresponding to the subjects uttering their names only. The goal of our experiment is to predict whether a given image and uttered name correspond to the same person. Such setup mimics the working memory's ability to associate a verbal cue (the name) with a visual representation (image). To test and validate our proposed network., we conduct a series of experiments:

- Experiment 1: A network composed of 3 DNNs (one for each loop) with the image , and the audio spectrum vectorized as inputs; and each trained separately using stochastic backpropagation.

- Experiment 2: A network constructed from CNN for the visual loop, a RNN for the phonological loop and a 6-layer DNN for the central executive; each trained separately using stochastic backpropagation.

- Experiment 3: A network composed of 3 DNNs (as in experiment 1) each trained separately using the proposed STDP algorithm.

- Experiment 4: A network constructed as in experiment 2, with each loop trained separately using the proposed STDP algorithm.

- Experiment 5: A network as in experiment 1 with inter-loop connections trained using the proposed STDP algorithm and intra-loop connections trained using the proposed stochastic reinforcement learning algorithm. Each loop is divided into populations of about 2000 neurons.

- Experiment 6: A network constructed from CNN for the visual loop, a RNN for the phonological loop and a 6-layer DNN for the central executive with with inter-loop connections trained using the proposed STDP algorithm and intra-loop connections trained using the proposed stochastic reinforcement learning algorithm.

Table 6.1: Results on ALOI

Network	Accuracy	Standard Deviation	Training Epochs
CNN - MLP	92.5	3.2	612
CNN - DT	88.7	2.6	54
CNN - SVM-lin	85.6	3	243
CNN - SVM-rbf	92.9	3.6	358
Proposed Visual Loop	**95.3**	2.9	1029

Table 6.2: Results on 1-2-AX task

Network	Accuracy	Standard Deviation	Training Epochs
1	86.5	2.6	315
2	92.4	3.1	487
3	93.7	3.5	461
4	96.2	2.8	592
5	**97.5**	4.1	673

- Experiment 7: The proposed network described in 4 with inter-population connections learned using the proposed STDP and intra-population connections trained using the proposed stochastic reinforcement learning algorithm.

Table 6.4 summarizes the average accuracy per fold, the standard deviation between folds and the average number of training epochs for the experiments listed above. The metrics are computed per loop and for the overall network (for experiments 1-4, only the per loop connections are learned). In addition, figure 6.1 shows a bar plot of the number of parameters retained after training (using a sparse representation) for the individual and overall loops.

Table 6.3: Phonological Loop Testing

		ANN	RNN	Proposed network
Experiment 1	Recognition Rate	65.7	87.54	**92.45**
	Standard Deviation	7.8	4.3	5.8
	Training Epochs	1000	2097	2832
Experiment 2	Recognition Rate	54.85	64.99	**70.75**
	Standard Deviation	8.49	5.10	6.25
	Training Epochs	667	1736	2426
Experiment 3	Recognition Rate	43.9	53.94	70.75
	Standard Deviation	7.32	3.99	5.31
	Training Epochs	760	1802	2574

Table 6.4: Experimental comparison of multi-modal networks. Legend: V.L.: Visual Loop, P.L.: Phonological Loop, C.E.: Central Executive, O.A.: Overall

Exp.	Accuracy (%)				Std. Dev. (%)				Training Epochs			
	V.L.	P.L.	C.E.	O.A.	V.L.	P.L.	C.E.	O.A.	V.L.	P.L.	C.E.	O.A.
1	75.61	82.43	81.76	75.16	4.32	5.01	4.70	5.04	1024	1174	1096	-
2	85.39	90.63	83.14	80.98	3.81	4.16	3.95	4.29	1413	1559	1484	-
3	77.36	88.68	84.26	76.60	2.91	3.06	3.39	4.06	1323	1504	1340	-
4	89.65	91.64	85.04	80.06	4.50	5.22	4.62	4.88	1767	1911	2049	-
5	77.36	88.68	84.26	74.75	4.56	3.89	3.35	4.50	1323	1504	1340	2643
6	84.51	92.74	89.64	82.93	4.82	3.97	3.19	5.10	1793	1909	1708	3058
7	**85.95**	**94.38**	**90.79**	**87.32**	4.49	4.05	2.92	4.83	2214	2327	2167	3490

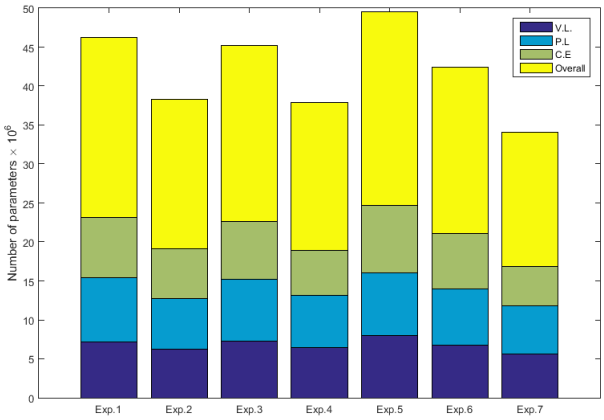

Figure 6.1: Memory Requirement Comparison.

6.1.5 Sensitivity analysis

We tested the sensitivity of our proposed architecture with respect to four parameters: the refractory period of neurons, the ratio of inhibitory to excitatory synapses, the average firing rate η, and the learning rate α of the proposed stochastic reinforcement learning. Each of these parameters are varied independently while the remainder are kept constant at their optimal values. The refractory period (RP) is varied in 5% increments from 5% to 20% (percentage of maximum firing rate). The inhibitory to excitatory ratio (I/E) is varied from 1/6 to 1/3. The average firing rate η is varied in 20% increment from 20% to 80% (percentage of maximum firing rate). The learning rate α is varied from 0.2 to 0.8 in increments of 0.2. The average recognition rate (over validation folds) and the number of training epochs till convergence are illustrated in figure 6.2.

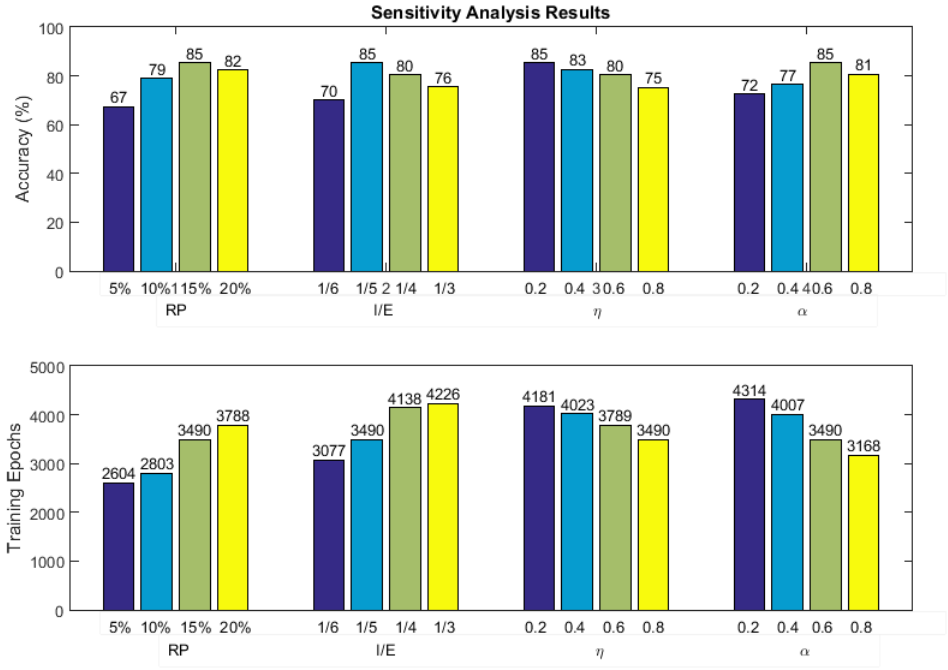

Figure 6.2: Sensitivity analysis results summary. The top figure illustrates the average recognition rate for different values of the four tested parameters as shown on the axis. The bottom figure shows the average number of training epochs.

6.1.6 Discussion

Artificial versus biological structures

Artificial structures such as DNN, ANN, RNN and CNN were consistently outperformed by the proposed biologically inspired structures. The visual loop saw an improvement of 2.8% in accuracy at the cost of an increase of about 1.7 folds in training epochs compared to the widely adopted CNN. The central executive saw an improvement of 11% in recognition rate compared to the generic DNN with Hebbian learning; a significant improvement despite the high computational cost of the proposed network. The proposed phonological loop outperformed both RNN and ANN by a range of 5% to 16% and witnessed a competitive drop in performance in the phonological similarity and word length effect test (an average of 21% decrease compared to 25% for RNN).
The multi-modal network presents similar properties: a superior performance at the level of individual loops and the overall network at the cost of an acceptable increase in training epochs.

Effect of parameters

The best performance was obtained for a refractory period of 15% (of the maximum firing rate), a inhibitory to excitatory ratio of 1/5, an average firing rate of 0.8 (80% of the maximum firing rate) and a learning rate of 0.6.
Both short and longer refractory periods worsen the performance of the model; while the former increases the sensitivity of the network to noise, the latter results in a lower time resolution (the ability of the network to respond to events separated by a certain period of time). An experimental compromise appears to be at about 15% of the maximum firing rate. From a computational complexity perspective, shorter refractory periods result in a speedier result in a speedier convergence: the network has the ability to recover from a particular state in a lesser amount of time.
The inhibitory to excitatory ratio observes a trade-off: limiting the number of inhibitory synapses increases excitability and hence alters the stability of the network while increasing this number limits the ability of the network to store and create representations. Higher values of I/E speed up the training of the network: encoding a pattern occurs in limited neural pathways.
The average firing rate has a reverse effect on performance: a lower firing rate improves the performance of the network at the expense of a lengthier training. Our stipulation is that a lower percentage of active nodes allows for a higher capacity and a lower memory footprint.
The effect of the learning rate is analogous to that observed in Hebbian learning algorithms: a trade-off must be made between complexity and local optima convergence. Higher values of α result in a faster convergence to a local optima and hence do not guarantee optimal performance.

Complexity Comparison

The visual loop: While CNNs present an advantage over the proposed network and training algorithms as illustrated in the number of convergence; AlexNet incorporated about has 62.3 million parameters, and requires around 1.1 billion computation units in a forward pass. In addition, the pre-training of AlexNet requires considerable computational resources and takes up to 3 weeks to reach convergence. Furthermore, in assisted living environments, one could argue that the visual stimuli encountered is limited to a restricted set of groups (mostly items found in domestic settings and/or medical related equipment) hence rendering the use of a pre-trained network (ImageNet contains 1 million images classified in over 1000 labels) obsolete and subject to overfitting. The proposed method, though requiring about 68% more epochs than a MLP (the fine tuning stage only taken into account) requires no pre-training and can be easily tailored towards the specifics of the data. The average firing rate being limited, a sparse representation of the network renders a forward pass more efficient than a CNN.

The central executive: A traditional DNN of the same size of the proposed structure trained using a Hebbian learning requires about half the number of epochs compared to that proposed, but attains a considerable 10% less in accuracy. The proposed structure is only 14% more computationally expensive for a 1.3% increase in accuracy compared to the best DNN structure.

The phonological loop: The proposed network is 35% more computationally demanding than a RNN for a 5% improvement in performance. A 27% increase in performance is noted compared to a traditional fully connected feedforward ANN of the same size despite a more expensive training. This compromise is accentuated in the phonological similarity and word length effect tests, with the increase in training epochs averaging at 40% and an improvement up to 17% in accuracy compared to a RNN.

The multi-modal network: Comparing the proposed structure and algorithm to one composed by the widely adopted structures for visual, and phonological processing (CNN and RNN respectively) an improvement of about 4% in accuracy is noted at the expense of a 14% increase in training epochs. A homogeneous structure of DNNs witnessed a 13% drop in accuracy though requiring 32% less training epochs. The reader must keep in mind that the number of epochs does not necessarily reflect the computational time required: the time elapsed for a training epoch depends on the network structure as well as the hardware on which the network is deployed. In addition, speeding up the training is possible by optimizing the parallel implementation on a distributed platform.

Table 6.5: Datasets Summary

Dataset	# Classes	# Instances	Task
iLIDS-VID [216]	300	43800	Person Identification
Film Face	77	539	Person Identification
PETA [217]	8705	19000	Person Identification
Caviar [218]	2	65000	Abandoned luggage detection
UCF-Crime [219]	13	1900	Crime Classification

Memory Requirements: A first glance at the number of parameters stored indicates a clear advantage to the proposed structures over CNN, RNN and DNN. The savings in number of retained connections amount to 6.57, 2.84, 8.21, and 17.84 million parameters for the visual, phonological, central executive loops, and the overall network (compared with the least expensive artificial structure). On average, around 8.9 million less variables are needed - i.e. about 7.1 GB of storage space saved - a crucial aspect on platforms with limited storage.

6.2 The visual network: A case study on security applications

In this section, we test our visual network's ability to perform three security related tasks: person identification, abandoned luggage detection and classification of criminal behavior. The video frames were extracted and preprocessed into images to use for the classification tasks. The proposed network is compared against Fukushima's neogcognitron and four convolutional neural network architectures pretrained on Imagenet: VGG16, resnet, mobilenet, and inception.

Table **??** summarizes the performance of the tested architectures in training and testing stages measured as accuracy and time; in addition the average number of non-zero weights required to store the trained network (using a sparse representation) is recorded. All results are based on a 4 fold cross validation scheme.

As can be seen in table **??**, our proposed algorithm outperforms five architecture of convolutional neural networks for the film face and PETA datasets and is competitive with the best state of the art architecture on the iDLS dataset for identification tasks. On luggage detection tasks, BIVnet improves the state of the art accuracy achieved by inception by 2.4% for a slight increase in training time; compared to VGG16, BIVnet improves on accuracy in a considerable 8.8% for about 2.5× less training time. Our network exhibits a considerable

Table 6.6: Experimental Results Summary

Dataset	Network	Train. Acc.	Valid. Acc.	Test. Acc.	Train. Time (min)	# parameters
i-LIDS	VGG16	0.998	0.990	0.980	3,720	138M
	resnet	0.919	0.828	0.760	1,109	44M
	mobilenet	0.520	0.496	0.735	54	3.3M
	inception	0.834	0.918	0.965	165	6.7M
	Neocogn.	0.793	0.890	0.712	611	1.6M
	BIVNet	0.960	0.950	0.975	4,225	7.1M
Film Face	VGG16	0.370	0.409	0.385	174	138M
	resnet	0.680	0.790	0.750	55	44M
	mobilenet	0.657	0.545	0.651	3	3.3M
	inception	0.182	0.513	0.513	8	6.7M
	Neocog.	0.553	0.438	0.524	28	1.6M
	BIVNet	0.732	0.850	0.762	210	7.1M
PETA	VGG16	0.695	0.697	0.690	744	138M
	resnet	0.569	0.610	0.654	222	44M
	mobilenet	0.429	0.565	0.517	11	3.3M
	inception	0.567	0.717	0.510	33	6.7M
	Neocog.	0.379	0.492	0.501	122	1.6M
	BIVNet	0.729	0.780	0.750	845	7.1M
Caviar	VGG16	0.927	0.954	0.897	1564	138M
	resnet	0.882	0.920	0.925	1043	44M
	mobilenet	0.922	0.886	0.854	80	3.3M
	inception	0.974	0.910	0.961	485	6.7M
	Neocog.	0.849	0.851	0.825	582	1.6M
	BIVNet	0.964	0.990	0.985	612	7.1M
UCF-crime	VGG16	0.755	0.949	0.738	1778	138M
	resnet	0.737	0.764	0.810	1225	44M
	mobilenet	0.806	0.643	0.616	319	3.3M
	inception	0.938	0.692	0.811	645	6.7M
	Neocog.	0.758	0.637	0.619	733	1.6M
	BIVNet	0.794	0.774	0.865	843	7.1M

Table 6.7: Firing Threshold Sensitivity Analysis

Dataset	Firing Threshold	Test Accuracy	Training Time (min)	Number of parameters
i-LIDS	0.1	0.535	4911	7.7
	0.4	0.975	4032	7.1
	0.7	0.575	2252	4.3
	1	0.414	1701	1.6
Film Face	0.1	0.207	286	4.2
	0.4	0.762	199	4.0
	0.7	0.404	111	2.3
	1	0.160	79	2.0
PETA	0.1	0.651	1122	5.8
	0.4	0.750	806	5.2
	0.7	0.517	280	4.5
	1	0.331	224	5.1
Caviar	0.1	0.414	581	8.4
	0.4	0.985	612	7.1
	0.7	0.581	274	6.2
	1	0.581	274	6.2
UCF-crime	0.1	0.422	1534	8.5
	0.4	0.981	822	7.1
	0.7	0.603	385	6.2
	1	0.328	200	0.4

reduction in storage requirements as illustrated by the number of parameters with the exception of mobilenet - a network designed for low power mobile devices - and neocognitron which performance is considerably less than CNN and BIVnet. Conversely, the complexity of BIVnet presents a challenge in limited resource environments; with an increase in training of about 2×, 41×, 13×, and 3.5× compared with resnet, mobilenet, inception, and neocognitron respectively. However a reduction of 1.5× is noted when compared with VGG16.

Table 6.7 shows the effect of varying the firing threshold parameter on the performance of the proposed network by comparing the accuracy, training time and number of parameters obtained for values of the firing threshold ranging from 0.1 to 1. As can be seen in table 6.7 the optimal value of ϵ is about 0.4. A small firing threshold increases the number of parameters needed (more active connections) and increases the training time required with a noticeable decrease in performance while a large firing threshold reduces the network's sparsity (neurons are less prone to firing and hence competition between neurons is reduced) while degrading both the performance and the training time.

Chapter 7

Conclusion

This thesis presented a multi-modal computational model of working memory. The proposed model is rooted in its biological counterpart and outperforms artificial deep learning structure in all tested scenarios. A two-stage stochastic learning algorithm is proposed in which subpopulations of neurons reach a stable solution using a Hebbian based spike time dependent rule and larger associations are learned using a stochastic reinforcement learning strategy solved using a Bayesian inference approximation. The model is tested on an object recognition database for assisted living environments and achieved an average recognition rate of 98.25%.

Additionally, we presented an image processing deep network inspired by the brain's visual system. A stochastic plasticity dependent reinforcement learning algorithm is proposed to learn connections' weights. The network is tested on three surveillance tasks: person re-identification, abandoned luggage detection and crime classification. A superior performance is shown experimentally compared to state of the art models in addition to a marginal reduction in storage requirements at the expense of a moderate increase in training time.

Though the biological resemblance of our proposed model is limited; our approach constitutes a step towards bridging the gap between computational neuroscience and deep learning. While the former focuses on mathematical modeling of biological processes, the latter aims at creating complex artificial neural network structures capable of performing specific tasks at desired performance levels with little consideration to the neurological counterpart. A better approach to such goal entails a re-scoping of the problem towards a narrower task with clearer understanding of its execution in the brain. Perhaps a key strategy towards attaining that goal would be implementing smaller structures associated with simpler functions which interact in a much more complex manner than that described in this thesis.

In our opinion, an integration of neuroscience and deep learning relies on implementing a large scale structure analogous to brain which optimizes cost functions which are diverse and differ across substructures (brain areas) and evolve with time (development and learning). An architecture matched to the computational problem posed by a certain behavior executing that function would independently and efficiently achieve this task and be embedded within the large scale "brain" acting as a "subgoal" to the overall "goal". Our current knowledge of the brain functional anatomy allows for a range of implementations of goal assignment through multiple layers of neurons pointing towards the brain being a complex circuitry of specialized systems enabling efficient optimization. The brain is far from a homogeneous structure and hence a computational model faithful to the biological substrate must allow for a heterogeneous structure. Such approach allows for an interaction of multiple cost functions enabling an efficient data-driven learning.

The proposed algorithms in this thesis first attempted to derive a simple solution for a complex problem (algorithm 1) a task which proved to be insolvable. A closed form solution for such problem could not be computed, iterative and/or heuristic methods were resorted to for a numerical solution which did not guarantee optimality. Furthermore achieving a goal-subgoal strategy required a different approach. The approach then geared towards a more biologically and neurologically inspired learning via the STDP framework which was employed to implement a reinforcement learning strategy (algorithm 2) - a learning process still thought to be at the heart of human learning. The algorithm resulted in a successful learning of the large scale network without specific breaking down of the overall goal to subgoals. While a reinforcement learning strategy was implemented, individual loops couldn't be trained individually. Such limitation led to the conception of the two-stage algorithm (algorithm 3) anchored in the assumption that individual populations implement subgoals and collaborate towards the execution of the large goal. The algorithm allowed individual loop to implement visual processing and phonological processing functions and the overall network to implement a multi-modal working memory model. While our approach stems from our philosophy of bridging the gap between neuroscience and deep learning by implementing substructures with subgoals, our belief is that a better solution starts at the scale of smaller size populations and implementing a structure and an algorithm that matches the behavior observed in single cell recordings validated via biological data.

An important implication of a more biological extension of our approach could be crucial in shedding lights into the underlying phenomena governing neurological diseases and working memory disorders and could prove an important asset for the neuroscience and behavioral psychology communities. While closely observing the patterns of firing and communication of live brain

cells might pause several challenges (single cell recordings in vivo employ invasive techniques), a biologically faithful computational model can serve as an alternative in investigating a set of yet to be answered questions.

A more extreme approach recently gaining traction within the machine learning community argues towards knowledge driven modeling rather than data-driven learning. While our model relies on large amounts of data to learn its weights via an iterative algorithm requiring several iterations, its structure is prime for knowledge driven learning due to its ability to hierarchically extract and build increasingly complex representations of the input. Coupled with a knowledge based learning algorithm where insights are based on human understanding of the performed tasks, our method can be learned in "one shot" and can overcome several of the challenges of data driven approaches.

Conversely, neuromorphic computing - a field which emerged in the late 1980s - adopts a different but valid approach through implementing elementary programmable structures resembling neurons and constructing deep complex networks implementing various tasks. A direction to be investigated in the future presents itself in the form of implementing our proposed structure and algorithm on neuromorphic computing architectures.

Finally, the tremendous success deep learning has witnessed in the past decade relies heavily on learning from massive amounts of data. Computational models on the other hands, rely on behavior of neural populations and have yet to materialize into a model that can be employed for complex pattern recognition problems. Employing a biologically anchored model in real life prediction entails an in depth understanding of the mode of operation of neurons as well as knowledge of the large scale functionality of the brain - a challenge which in our opinion is yet to be fully conquered. The model proposed in this thesis achieves a working memory function by storing and processing visual and phonological loop and serves as a initial step towards a biologically inspired large scale model of the brain.

Bibliography

[1] N. Cowan, *Attention and memory*. Oxford University Press, 1997.

[2] C. Rottschy, R. Langner, I. Dogan, K. Reetz, A. R. Laird, J. B. Schulz, P. T. Fox, and S. B. Eickhoff, "Modelling neural correlates of working memory: a coordinate-based meta-analysis," *Neuroimage*, vol. 60, no. 1, pp. 830–846, 2012.

[3] D. E. Purves, G. J. Augustine, D. E. Fitzpatrick, L. C. Katz, *et al.*, "Neuroscience.," 1997.

[4] K. Zilles and K. Amunts, "Centenary of brodmann's map—conception and fate," *Nature Reviews Neuroscience*, vol. 11, no. 2, p. 139, 2010.

[5] T. Baltrušaitis, C. Ahuja, and L.-P. Morency, "Multimodal machine learning: A survey and taxonomy," *IEEE Transactions on Pattern Analysis and Machine Intelligence*, 2018.

[6] J. Ngiam, A. Khosla, M. Kim, J. Nam, H. Lee, and A. Y. Ng, "Multimodal deep learning," in *Proceedings of the 28th international conference on machine learning (ICML-11)*, pp. 689–696, 2011.

[7] W. Ouyang, X. Chu, and X. Wang, "Multi-source deep learning for human pose estimation," in *Proceedings of the IEEE Conference on Computer Vision and Pattern Recognition*, pp. 2329–2336, 2014.

[8] D. Wang, P. Cui, M. Ou, and W. Zhu, "Deep multimodal hashing with orthogonal regularization.," in *IJCAI*, vol. 367, pp. 2291–2297, 2015.

[9] N. Srivastava and R. R. Salakhutdinov, "Multimodal learning with deep boltzmann machines," in *Advances in neural information processing systems*, pp. 2222–2230, 2012.

[10] D. Bahdanau, K. Cho, and Y. Bengio, "Neural machine translation by jointly learning to align and translate," *arXiv preprint arXiv:1409.0473*, 2014.

[11] S. Venugopalan, H. Xu, J. Donahue, M. Rohrbach, R. Mooney, and K. Saenko, "Translating videos to natural language using deep recurrent neural networks," *arXiv preprint arXiv:1412.4729*, 2014.

[12] P. Cosi, E. M. Caldognetto, K. Vagges, G. A. Mian, and M. Contolini, "Bimodal recognition experiments with recurrent neural networks," in *Acoustics, Speech, and Signal Processing, 1994. ICASSP-94., 1994 IEEE International Conference on*, vol. 2, pp. II–553, IEEE, 1994.

[13] L. Deng, D. Yu, *et al.*, "Deep learning: methods and applications," *Foundations and Trends® in Signal Processing*, vol. 7, no. 3–4, pp. 197–387, 2014.

[14] B. P. Yuhas, M. H. Goldstein, and T. J. Sejnowski, "Integration of acoustic and visual speech signals using neural networks," *IEEE Communications Magazine*, vol. 27, no. 11, pp. 65–71, 1989.

[15] H. Bourlard and S. Dupont, "A mew asr approach based on independent processing and recombination of partial frequency bands," in *Spoken Language, 1996. ICSLP 96. Proceedings., Fourth International Conference on*, vol. 1, pp. 426–429, IEEE, 1996.

[16] M. Brand, N. Oliver, and A. Pentland, "Coupled hidden markov models for complex action recognition," in *Computer vision and pattern recognition, 1997. proceedings., 1997 ieee computer society conference on*, pp. 994–999, IEEE, 1997.

[17] P. K. Atrey, M. A. Hossain, A. El Saddik, and M. S. Kankanhalli, "Multimodal fusion for multimedia analysis: a survey," *Multimedia systems*, vol. 16, no. 6, pp. 345–379, 2010.

[18] G. Evangelopoulos, A. Zlatintsi, A. Potamianos, P. Maragos, K. Rapantzikos, G. Skoumas, and Y. Avrithis, "Multimodal saliency and fusion for movie summarization based on aural, visual, and textual attention," *IEEE Transactions on Multimedia*, vol. 15, no. 7, pp. 1553–1568, 2013.

[19] S. K. D'mello and J. Kory, "A review and meta-analysis of multimodal affect detection systems," *ACM Computing Surveys (CSUR)*, vol. 47, no. 3, p. 43, 2015.

[20] F. De la Torre and J. F. Cohn, "Facial expression analysis," in *Visual analysis of humans*, pp. 377–409, Springer, 2011.

[21] M. Hodosh, P. Young, and J. Hockenmaier, "Framing image description as a ranking task: Data, models and evaluation metrics," *Journal of Artificial Intelligence Research*, vol. 47, pp. 853–899, 2013.

[22] J. P. Bigham, C. Jayant, H. Ji, G. Little, A. Miller, R. C. Miller, R. Miller, A. Tatarowicz, B. White, S. White, *et al.*, "Vizwiz: nearly real-time answers to visual questions," in *Proceedings of the 23nd annual ACM symposium on User interface software and technology*, pp. 333–342, ACM, 2010.

[23] C.-A. Smarr, C. B. Fausset, and W. A. Rogers, "Understanding the potential for robot assistance for older adults in the home environment," tech. rep., Georgia Institute of Technology, 2011.

[24] R. Alami and D. Sidobre, "A mobile manipulator robot that brings objects to assist people," in *9th World Conference of Gerontechnology*, 2014.

[25] J. S. van't Schip, "Rolling aid for use by elderly and disabled people," Feb. 10 2004. US Patent 6,688,633.

[26] M. D. Anderson, "Knee scooter," May 10 2011. US Patent 7,938,413.

[27] K. Wada, T. Shibata, T. Musha, and S. Kimura, "Robot therapy for elders affected by dementia," *IEEE Engineering in medicine and biology magazine*, vol. 27, no. 4, 2008.

[28] R. Bemelmans, G. J. Gelderblom, P. Jonker, and L. De Witte, "Socially assistive robots in elderly care: A systematic review into effects and effectiveness," *Journal of the American Medical Directors Association*, vol. 13, no. 2, pp. 114–120, 2012.

[29] D. Hewson, C. Gutierrez Ruiz, and H. Michel, "Development of a multidimensional evaluation method for the use of a robotic companion as a function of care relationships," *Gerontechnology*, vol. 13, no. 2, p. 79, 2014.

[30] A. Ozguler, T. Loeb, and M. Baer, "Maintaining elderly people at home with a telemedicine platform solution: the quovadis project," *Gerontechnology*, vol. 13, no. 2, p. 80, 2014.

[31] T. S. Dahl and M. N. K. Boulos, "Robots in health and social care: A complementary technology to home care and telehealthcare?," *Robotics*, vol. 3, no. 1, pp. 1–21, 2013.

[32] S. T. Fiske, D. T. Gilbert, and G. Lindzey, *Handbook of social psychology*, vol. 2. John Wiley & Sons, 2010.

[33] A. D. Baddeley, G. Hitch, *et al.*, "Working memory," *The psychology of learning and motivation*, vol. 8, pp. 47–89, 1974.

[34] A. Baddeley, "The episodic buffer: a new component of working memory?," *Trends in cognitive sciences*, vol. 4, no. 11, pp. 417–423, 2000.

[35] A. Baddeley, *Working memory, thought, and action*, vol. 45. OUP Oxford, 2007.

[36] A. Krizhevsky, I. Sutskever, and G. E. Hinton, "Imagenet classification with deep convolutional neural networks," in *Advances in neural information processing systems*, pp. 1097–1105, 2012.

[37] Y. Wang, T. Bao, C. Ding, and M. Zhu, "Face recognition in real-world surveillance videos with deep learning method," in *Image, Vision and Computing (ICIVC), 2017 2nd International Conference on*, pp. 239–243, IEEE, 2017.

[38] Y. Akbulut, A. Şengür, and S. Ekici, "Gender recognition from face images with deep learning," in *Artificial Intelligence and Data Processing Symposium (IDAP), 2017 International*, pp. 1–4, IEEE, 2017.

[39] E. Ahmed, M. Jones, and T. K. Marks, "An improved deep learning architecture for person re-identification," in *Proceedings of the IEEE Conference on Computer Vision and Pattern Recognition*, pp. 3908–3916, 2015.

[40] D. Li, X. Chen, Z. Zhang, and K. Huang, "Learning deep context-aware features over body and latent parts for person re-identification," in *Proceedings of the IEEE Conference on Computer Vision and Pattern Recognition*, pp. 384–393, 2017.

[41] E. Ustinova, Y. Ganin, and V. Lempitsky, "Multi-region bilinear convolutional neural networks for person re-identification," in *Advanced Video and Signal Based Surveillance (AVSS), 2017 14th IEEE International Conference on*, pp. 1–6, IEEE, 2017.

[42] S. Smeureanu and R. T. Ionescu, "Real-time deep learning method for abandoned luggage detection in video," *arXiv preprint arXiv:1803.01160*, 2018.

[43] A. Islam, Y. Zhang, D. Yin, O. Camps, and R. J. Radke, "Correlating belongings with passengers in a simulated airport security checkpoint," in *Proceedings of the 12th International Conference on Distributed Smart Cameras*, p. 14, ACM, 2018.

[44] S. Pouyanfar and S.-C. Chen, "Automatic video event detection for imbalance data using enhanced ensemble deep learning," *International Journal of Semantic Computing*, vol. 11, no. 01, pp. 85–109, 2017.

[45] S. Bouindour, M. M. Hittawe, S. Mahfouz, and H. Snoussi, "Abnormal event detection using convolutional neural networks and 1-class svm classifier," 2017.

[46] M. H. de Boer, H. Bouma, M. C. Kruithof, F. B. ter Haar, N. M. Fischer, L. K. Hagendoorn, B. Joosten, and S. Raaijmakers, "Automatic analysis of online image data for law enforcement agencies by concept detection and instance search," in *Counterterrorism, Crime Fighting, Forensics, and Surveillance Technologies*, vol. 10441, p. 104410H, International Society for Optics and Photonics, 2017.

[47] P. Croskerry, "The importance of cognitive errors in diagnosis and strategies to minimize them," *Academic Medicine*, vol. 78, no. 8, pp. 775–780, 2003.

[48] J. A. Lenker and V. L. Paquet, "A review of conceptual models for assistive technology outcomes research and practice," *Assistive Technology*, vol. 15, no. 1, pp. 1–15, 2003.

[49] F. Paas and P. Ayres, "Cognitive load theory: A broader view on the role of memory in learning and education," *Educational Psychology Review*, vol. 26, no. 2, pp. 191–195, 2014.

[50] A. K. Engel, C. K. Moll, I. Fried, and G. A. Ojemann, "Invasive recordings from the human brain: clinical insights and beyond," *Nature Reviews Neuroscience*, vol. 6, no. 1, pp. 35–47, 2005.

[51] A. R. Conway, N. Cowan, and M. F. Bunting, "The cocktail party phenomenon revisited: The importance of working memory capacity," *Psychonomic bulletin & review*, vol. 8, no. 2, pp. 331–335, 2001.

[52] N. Cowan, "An embedded-processes model of working memory," *Models of working memory: Mechanisms of active maintenance and executive control*, vol. 20, p. 506, 1999.

[53] K. Pawlik and M. R. Rosenzweig, *The international handbook of psychology*. Sage, 2000.

[54] A. D. Baddeley, N. Thomson, and M. Buchanan, "Word length and the structure of short-term memory," *Journal of verbal learning and verbal behavior*, vol. 14, no. 6, pp. 575–589, 1975.

[55] A. D. Baddeley and J. D. Larsen, "The phonological loop unmasked? a comment on the evidence for a "perceptual-gestural" alternative," *The Quarterly Journal of Experimental Psychology*, vol. 60, no. 4, pp. 497–504, 2007.

[56] A. Baddeley, V. Lewis, and G. Vallar, "Exploring the articulatory loop," *The Quarterly journal of experimental psychology*, vol. 36, no. 2, pp. 233–252, 1984.

[57] D. M. Jones, R. W. Hughes, and W. J. Macken, "Perceptual organization masquerading as phonological storage: Further support for a perceptual-gestural view of short-term memory," *Journal of Memory and language*, vol. 54, no. 2, pp. 265–281, 2006.

[58] H. A. Colle and A. Welsh, "Acoustic masking in primary memory," *Journal of verbal learning and verbal behavior*, vol. 15, no. 1, pp. 17–31, 1976.

[59] P. Salamé and A. Baddeley, "Phonological factors in stm: Similarity and the unattended speech effect," *Bulletin of the Psychonomic Society*, vol. 24, no. 4, pp. 263–265, 1986.

[60] D. M. Jones and W. J. Macken, "Irrelevant tones produce an irrelevant speech effect: Implications for phonological coding in working memory.," *Journal of Experimental Psychology: Learning, Memory, and Cognition*, vol. 19, no. 2, p. 369, 1993.

[61] D. M. Jones and W. J. Macken, "Phonological similarity in the irrelevant speech effect: Within-or between-stream similarity?," *Journal of Experimental Psychology: Learning, Memory, and Cognition*, vol. 21, no. 1, p. 103, 1995.

[62] A. Baddeley, "Working memory: theories, models, and controversies," *Annual review of psychology*, vol. 63, pp. 1–29, 2012.

[63] K. S. Lashley, "The problem of serial order in behavior," in *Cerebral mechanisms in behavior*, pp. 112–136, 1951.

[64] G. D. Brown, T. Preece, and C. Hulme, "Oscillator-based memory for serial order.," *Psychological review*, vol. 107, no. 1, p. 127, 2000.

[65] N. Burgess and G. J. Hitch, "A revised model of short-term memory and long-term learning of verbal sequences," *Journal of Memory and Language*, vol. 55, no. 4, pp. 627–652, 2006.

[66] M. Page and D. Norris, "The primacy model: a new model of immediate serial recall.," *Psychological review*, vol. 105, no. 4, p. 761, 1998.

[67] A. Baddeley, S. Gathercole, and C. Papagno, "The phonological loop as a language learning device.," *Psychological review*, vol. 105, no. 1, p. 158, 1998.

[68] K. C. Klauer and Z. Zhao, "Double dissociations in visual and spatial short-term memory.," *Journal of Experimental Psychology: General*, vol. 133, no. 3, p. 355, 2004.

[69] R. H. Logie, "The functional organization and capacity limits of working memory," *Current Directions in Psychological Science*, vol. 20, no. 4, pp. 240–245, 2011.

[70] E. E. Smith and J. Jonides, "Working memory: A view from neuroimaging," *Cognitive psychology*, vol. 33, no. 1, pp. 5–42, 1997.

[71] A. Baddeley, G. Hitch, and R. Allen, "Working memory and binding in sentence recall," *Journal of Memory and Language*, vol. 61, no. 3, pp. 438–456, 2009.

[72] N. Cowan, *Working memory capacity*. Psychology press, 2012.

[73] N. Cowan, "Evolving conceptions of memory storage, selective attention, and their mutual constraints within the human information-processing system.," *Psychological bulletin*, vol. 104, no. 2, p. 163, 1988.

[74] N. Cowan, "On short and long auditory stores.," *Psychological bulletin*, vol. 96, no. 2, p. 341, 1984.

[75] N. Wood and N. Cowan, "The cocktail party phenomenon revisited: how frequent are attention shifts to one's name in an irrelevant auditory channel?," *Journal of Experimental Psychology: Learning, Memory, and Cognition*, vol. 21, no. 1, p. 255, 1995.

[76] N. Cowan, "Metatheory of storage capacity limits," *Behavioral and brain sciences*, vol. 24, no. 01, pp. 154–176, 2001.

[77] C. C. Morey and N. Cowan, "When visual and verbal memories compete: Evidence of cross-domain limits in working memory," *Psychonomic bulletin & review*, vol. 11, no. 2, pp. 296–301, 2004.

[78] K. A. Ericsson and W. Kintsch, "Long-term working memory.," *Psychological review*, vol. 102, no. 2, p. 211, 1995.

[79] *Models of working memory: Mechanisms of active maintenance and executive control*, ch. Long-term working memory as an alternative to capacity models of working memory in everyday skilled performance. Cambridge University Press, 1999.

[80] P. Barrouillet, N. Gavens, E. Vergauwe, V. Gaillard, and V. Camos, "Working memory span development: a time-based resource-sharing model account.," *Developmental psychology*, vol. 45, no. 2, p. 477, 2009.

[81] P. Barrouillet and V. Camos, "The time-based resource-sharing model of working memory," *The cognitive neuroscience of working memory*, pp. 59–80, 2007.

[82] P. Barrouillet and V. Camos, "As time goes by temporal constraints in working memory," *Current Directions in Psychological Science*, vol. 21, no. 6, pp. 413–419, 2012.

[83] P. Barrouillet and V. Camos, "Working memory and executive control: A time-based resource-sharing account," *Psychologica Belgica*, vol. 50, no. 3-4, 2010.

[84] C. Donkin, R. M. Nosofsky, J. M. Gold, and R. M. Shiffrin, "Discrete-slots models of visual working-memory response times.," *Psychological Review*, vol. 120, no. 4, p. 873, 2013.

[85] J. N. Rouder, R. D. Morey, N. Cowan, C. E. Zwilling, C. C. Morey, and M. S. Pratte, "An assessment of fixed-capacity models of visual working memory," *Proceedings of the National Academy of Sciences*, vol. 105, no. 16, pp. 5975–5979, 2008.

[86] M. J. Kane, M. K. Bleckley, A. R. Conway, and R. W. Engle, "A controlled-attention view of working-memory capacity.," *Journal of Experimental Psychology: General*, vol. 130, no. 2, p. 169, 2001.

[87] J. R. Anderson, D. Bothell, M. D. Byrne, S. Douglass, C. Lebiere, and Y. Qin, "An integrated theory of the mind.," *Psychological review*, vol. 111, no. 4, p. 1036, 2004.

[88] D. E. Kieras and D. E. Meyer, "An overview of the epic architecture for cognition and performance with application to human-computer interaction," *Human-computer interaction*, vol. 12, no. 4, pp. 391–438, 1997.

[89] J. E. Laird, A. Newell, and P. S. Rosenbloom, "Soar: An architecture for general intelligence," *Artificial intelligence*, vol. 33, no. 1, pp. 1–64, 1987.

[90] P. J. Barnard and J. D. Teasdale, "Interacting cognitive subsystems: A systemic approach to cognitive-affective interaction and change," *Cognition & Emotion*, vol. 5, no. 1, pp. 1–39, 1991.

[91] E. Fedorenko, E. Gibson, and D. Rohde, "The nature of working memory capacity in sentence comprehension: Evidence against domain-specific working memory resources," *Journal of Memory and Language*, vol. 54, no. 4, pp. 541–553, 2006.

[92] E. Vergauwe, P. Barrouillet, and V. Camos, "Do mental processes share a domain-general resource?," *Psychological Science*, vol. 21, no. 3, pp. 384–390, 2010.

[93] J. M. Chein, A. B. Moore, and A. R. Conway, "Domain-general mechanisms of complex working memory span," *NeuroImage*, vol. 54, no. 1, pp. 550–559, 2011.

[94] G. Cocchini, R. H. Logie, S. Della Sala, S. E. MacPherson, and A. D. Baddeley, "Concurrent performance of two memory tasks: Evidence for domain-specific working memory systems," *Memory & Cognition*, vol. 30, no. 7, pp. 1086–1095, 2002.

[95] N. Cowan, "The magical mystery four: How is working memory capacity limited, and why?," *Current directions in psychological science*, vol. 19, no. 1, pp. 51–57, 2010.

[96] G. A. Miller, "The magical number seven, plus or minus two: some limits on our capacity for processing information.," *Psychological review*, vol. 63, no. 2, p. 81, 1956.

[97] N. Cowan, T. D. Johnson, and J. Scott Saults, "Capacity limits in list item recognition: Evidence from proactive interference," *Memory*, vol. 13, no. 3-4, pp. 293–299, 2005.

[98] S. J. Luck and E. K. Vogel, "The capacity of visual working memory for features and conjunctions," *Nature*, vol. 390, no. 6657, p. 279, 1997.

[99] S. J. Luck and E. K. Vogel, "Visual working memory capacity: from psychophysics and neurobiology to individual differences," *Trends in cognitive sciences*, vol. 17, no. 8, pp. 391–400, 2013.

[100] O. Barak, M. Tsodyks, and R. Romo, "Neuronal population coding of parametric working memory," *Journal of Neuroscience*, vol. 30, no. 28, pp. 9424–9430, 2010.

[101] K. K. Sreenivasan, C. E. Curtis, and M. D'Esposito, "Revisiting the role of persistent neural activity during working memory," *Trends in cognitive sciences*, vol. 18, no. 2, pp. 82–89, 2014.

[102] M. Wang, Y. Yang, C.-J. Wang, N. J. Gamo, L. E. Jin, J. A. Mazer, J. H. Morrison, X.-J. Wang, and A. F. Arnsten, "Nmda receptors subserve persistent neuronal firing during working memory in dorsolateral prefrontal cortex," *Neuron*, vol. 77, no. 4, pp. 736–749, 2013.

[103] R. Pascanu and H. Jaeger, "A neurodynamical model for working memory," *Neural networks*, vol. 24, no. 2, pp. 199–207, 2011.

[104] H. Sanders, M. Berends, G. Major, M. S. Goldman, and J. E. Lisman, "Nmda and gabab (kir) conductances: the "perfect couple" for bistability," *Journal of Neuroscience*, vol. 33, no. 2, pp. 424–429, 2013.

[105] J. J. Hopfield, "Neural networks and physical systems with emergent collective computational abilities," *Proceedings of the national academy of sciences*, vol. 79, no. 8, pp. 2554–2558, 1982.

[106] D. J. Amit and N. Brunel, "Learning internal representations in an attractor neural network with analogue neurons," *Network: Computation in Neural Systems*, vol. 6, no. 3, pp. 359–388, 1995.

[107] D. J. Amit and N. Brunel, "Model of global spontaneous activity and local structured activity during delay periods in the cerebral cortex.," *Cerebral cortex*, vol. 7, no. 3, pp. 237–252, 1997.

[108] D. J. Amit and M. Tsodyks, "Quantitative study of attractor neural networks retrieving at low spike rates: Ii. low-rate retrieval in symmetric networks," *Network: Computation in Neural Systems*, vol. 2, no. 3, pp. 275–294, 1991.

[109] B. Tahvildari, M. Wölfel, A. Duque, and D. A. McCormick, "Selective functional interactions between excitatory and inhibitory cortical neurons and differential contribution to persistent activity of the slow oscillation," *Journal of Neuroscience*, vol. 32, no. 35, pp. 12165–12179, 2012.

[110] T. P. Vogels, H. Sprekeler, F. Zenke, C. Clopath, and W. Gerstner, "Inhibitory plasticity balances excitation and inhibition in sensory pathways and memory networks," *Science*, vol. 334, no. 6062, pp. 1569–1573, 2011.

[111] M. V. Sanchez-Vives, M. Mattia, A. Compte, M. Perez-Zabalza, M. Winograd, V. F. Descalzo, and R. Reig, "Inhibitory modulation of cortical up states," *Journal of neurophysiology*, vol. 104, no. 3, pp. 1314–1324, 2010.

[112] Z. P. Kilpatrick, B. Ermentrout, and B. Doiron, "Optimizing working memory with heterogeneity of recurrent cortical excitation," *Journal of neuroscience*, vol. 33, no. 48, pp. 18999–19011, 2013.

[113] M. Abeles, *Corticonics: Neural circuits of the cerebral cortex*. Cambridge University Press, 1991.

[114] M. Diesmann, M.-O. Gewaltig, and A. Aertsen, "Stable propagation of synchronous spiking in cortical neural networks," *Nature*, vol. 402, no. 6761, pp. 529–533, 1999.

[115] K. Kitano, H. Câteau, and T. Fukai, "Self-organization of memory activity through spike-timing-dependent plasticity," *Neuroreport*, vol. 13, no. 6, pp. 795–798, 2002.

[116] K. Kitano, H. Okamoto, and T. Fukai, "Time representing cortical activities: two models inspired by prefrontal persistent activity," *Biological cybernetics*, vol. 88, no. 5, pp. 387–394, 2003.

[117] N. F. Hardy and D. V. Buonomano, "Neurocomputational models of interval and pattern timing," *Current Opinion in Behavioral Sciences*, vol. 8, pp. 250–257, 2016.

[118] Z. Wang, A. T. Sornborger, and L. Tao, "Graded, dynamically routable information processing with synfire-gated synfire chains," *PLoS Comput Biol*, vol. 12, no. 6, p. e1004979, 2016.

[119] A. Riehle, S. Grün, M. Diesmann, and A. Aertsen, "Spike synchronization and rate modulation differentially involved in motor cortical function," *Science*, vol. 278, no. 5345, pp. 1950–1953, 1997.

[120] X.-J. Wang, "Synaptic basis of cortical persistent activity: the importance of nmda receptors to working memory," *Journal of Neuroscience*, vol. 19, no. 21, pp. 9587–9603, 1999.

[121] A. Compte, N. Brunel, P. S. Goldman-Rakic, and X.-J. Wang, "Synaptic mechanisms and network dynamics underlying spatial working memory in a cortical network model," *Cerebral Cortex*, vol. 10, no. 9, pp. 910–923, 2000.

[122] M. Domjan, *The principles of learning and behavior*. Nelson Education, 2014.

[123] A. Miyake and P. Shah, *Models of working memory: Mechanisms of active maintenance and executive control*. Cambridge University Press, 1999.

[124] E. Guigon, B. Dorizzi, Y. Burnod, and W. Schultz, "Neural correlates of learning in the prefrontal cortex of the monkey: a predictive model," *Cerebral Cortex*, vol. 5, no. 2, pp. 135–147, 1995.

[125] J. E. Lisman, J.-M. Fellous, and X.-J. Wang, "A role for nmda-receptor channels in working memory," *Nature neuroscience*, vol. 1, no. 4, pp. 273–275, 1998.

[126] E. Marder, L. Abbott, G. G. Turrigiano, Z. Liu, and J. Golowasch, "Memory from the dynamics of intrinsic membrane currents," *Proceedings of the national academy of sciences*, vol. 93, no. 24, pp. 13481–13486, 1996.

[127] M. Camperi and X.-J. Wang, "A model of visuospatial working memory in prefrontal cortex: recurrent network and cellular bistability," *Journal of computational neuroscience*, vol. 5, no. 4, pp. 383–405, 1998.

[128] D. Durstewitz and J. Seamans, "Beyond bistability: biophysics and temporal dynamics of working memory," *Neuroscience*, vol. 139, no. 1, pp. 119–133, 2006.

[129] D. Trubutschek, S. Marti, A. Ojeda, J.-R. King, Y. Mi, M. Tsodyks, and S. Dehaene, "A theory of working memory without consciousness or sustained activity," *bioRxiv*, p. 093815, 2016.

[130] M. G. Stokes, "'activity-silent'working memory in prefrontal cortex: a dynamic coding framework," *Trends in Cognitive Sciences*, vol. 19, no. 7, pp. 394–405, 2015.

[131] G. Mongillo, O. Barak, and M. Tsodyks, "Synaptic theory of working memory," *Science*, vol. 319, no. 5869, pp. 1543–1546, 2008.

[132] S. Hochreiter and J. Schmidhuber, "Long short-term memory," *Neural computation*, vol. 9, no. 8, pp. 1735–1780, 1997.

[133] F. A. Gers, J. Schmidhuber, and F. Cummins, "Learning to forget: Continual prediction with lstm," *Neural computation*, vol. 12, no. 10, pp. 2451–2471, 2000.

[134] F. A. Gers, N. N. Schraudolph, and J. Schmidhuber, "Learning precise timing with lstm recurrent networks," *Journal of machine learning research*, vol. 3, no. Aug, pp. 115–143, 2002.

[135] H. Sak, A. W. Senior, and F. Beaufays, "Long short-term memory recurrent neural network architectures for large scale acoustic modeling.," in *Interspeech*, pp. 338–342, 2014.

[136] R. C. O'Reilly and M. J. Frank, "Making working memory work: a computational model of learning in the prefrontal cortex and basal ganglia," *Neural computation*, vol. 18, no. 2, pp. 283–328, 2006.

[137] M. Takac and A. Knott, "A neural network model of episode representations in working memory," *Cognitive Computation*, vol. 7, no. 5, pp. 509–525, 2015.

[138] F. G. Ashby, S. W. Ell, V. V. Valentin, and M. B. Casale, "Frost: a distributed neurocomputational model of working memory maintenance," *Journal of cognitive neuroscience*, vol. 17, no. 11, pp. 1728–1743, 2005.

[139] K. Oberauer, S. Lewandowsky, S. Farrell, C. Jarrold, and M. Greaves, "Modeling working memory: An interference model of complex span," *Psychonomic bulletin & review*, vol. 19, no. 5, pp. 779–819, 2012.

[140] D. Monroe, "Neuromorphic computing gets ready for the (really) big time," *Communications of the ACM*, vol. 57, no. 6, pp. 13–15, 2014.

[141] W. Zhao, G. Agnus, V. Derycke, A. Filoramo, J. Bourgoin, and C. Gamrat, "Nanotube devices based crossbar architecture: toward neuromorphic computing," *Nanotechnology*, vol. 21, no. 17, p. 175202, 2010.

[142] M. M. Waldrop, "Brain in a box," *Nature*, vol. 482, no. 7386, p. 456, 2012.

[143] P. Gang and S. Feng, *Eastward Flows the Great River: Festschrift in Honor of Professor William SY. Wang on His 80th Birthday*. City University of HK Press, 2013.

[144] J. Makino, T. Fukushige, M. Koga, and K. Namura, "Grape-6: Massively-parallel special-purpose computer for astrophysical particle simulations," *Publications of the Astronomical Society of Japan*, vol. 55, no. 6, pp. 1163–1187, 2003.

[145] K. Boahen, "Neurogrid: emulating a million neurons in the cortex," in *Conf. proc. ieee eng. med. biol. soc*, p. 6702, 2006.

[146] B. V. Benjamin, P. Gao, E. McQuinn, S. Choudhary, A. R. Chandrasekaran, J.-M. Bussat, R. Alvarez-Icaza, J. V. Arthur, P. A. Merolla, and K. Boahen, "Neurogrid: A mixed-analog-digital multichip system for large-scale neural simulations," *Proceedings of the IEEE*, vol. 102, no. 5, pp. 699–716, 2014.

[147] A. Calimera, E. Macii, and M. Poncino, "The human brain project and neuromorphic computing," *Functional neurology*, vol. 28, no. 3, p. 191, 2013.

[148] T. Sharp, F. Galluppi, A. Rast, and S. Furber, "Power-efficient simulation of detailed cortical microcircuits on spinnaker," *Journal of neuroscience methods*, vol. 210, no. 1, pp. 110–118, 2012.

[149] E. I. Guerra-Hernandez, A. Espinal, P. Batres-Mendoza, C. H. Garcia-Capulin, R. D. J. Romero-Troncoso, and H. Rostro-Gonzalez, "A fpga-based neuromorphic locomotion system for multi-legged robots," *IEEE Access*, vol. 5, pp. 8301–8312, 2017.

[150] V. Menon, "Large-scale brain networks and psychopathology: a unifying triple network model," *Trends in cognitive sciences*, vol. 15, no. 10, pp. 483–506, 2011.

[151] V. Menon, "Large-scale brain networks in cognition: Emerging principles," *Analysis and function of large-scale brain networks*, p. 43, 2010.

[152] A. M. Owen, K. M. McMillan, A. R. Laird, and E. Bullmore, "N-back working memory paradigm: A meta-analysis of normative functional neuroimaging studies," *Human brain mapping*, vol. 25, no. 1, pp. 46–59, 2005.

[153] M. I. Posner, S. PETERSEN, P. FOX, and M. RAICHLE, "Localization of cognitive operations in the human brain," *Science*, vol. 240, no. 4859, pp. 1627–1631, 1988.

[154] M. A. Kim, E. Tura, S. G. Potkin, J. H. Fallon, D. S. Manoach, V. D. Calhoun, J. A. Turner, *et al.*, "Working memory circuitry in schizophrenia shows widespread cortical inefficiency and compensation," *Schizophrenia research*, vol. 117, no. 1, pp. 42–51, 2010.

[155] M. Bayerl, T. F. Dielentheis, G. Vucurevic, T. Gesierich, F. Vogel, C. Fehr, P. Stoeter, M. Huss, and A. Konrad, "Disturbed brain activation during a working memory task in drug-naive adult patients with adhd," *Neuroreport*, vol. 21, no. 6, pp. 442–446, 2010.

[156] R. Peters, "The prevention of dementia," *International journal of geriatric psychiatry*, vol. 24, no. 5, pp. 452–458, 2009.

[157] G. L. Shulman, D. L. Pope, S. V. Astafiev, M. P. McAvoy, A. Z. Snyder, and M. Corbetta, "Right hemisphere dominance during spatial selective attention and target detection occurs outside the dorsal frontoparietal network," *Journal of Neuroscience*, vol. 30, no. 10, pp. 3640–3651, 2010.

[158] M. Marangon, S. Jacobs, and S. H. Frey, "Evidence for context sensitivity of grasp representations in human parietal and premotor cortices," *Journal of neurophysiology*, vol. 105, no. 5, pp. 2536–2546, 2011.

[159] M. Bortoletto and R. Cunnington, "Motor timing and motor sequencing contribute differently to the preparation for voluntary movement," *Neuroimage*, vol. 49, no. 4, pp. 3338–3348, 2010.

[160] F. Collette and M. Van der Linden, "Brain imaging of the central executive component of working memory," *Neuroscience & Biobehavioral Reviews*, vol. 26, no. 2, pp. 105–125, 2002.

[161] J. M. Palva, S. Monto, S. Kulashekhar, and S. Palva, "Neuronal synchrony reveals working memory networks and predicts individual memory capacity," *Proceedings of the National Academy of Sciences*, vol. 107, no. 16, pp. 7580–7585, 2010.

[162] N. Müller and R. Knight, "The functional neuroanatomy of working memory: contributions of human brain lesion studies," *Neuroscience*, vol. 139, no. 1, pp. 51–58, 2006.

[163] J. Bergmann, E. Genç, A. Kohler, W. Singer, and J. Pearson, "Neural anatomy of primary visual cortex limits visual working memory," *Cerebral cortex*, vol. 26, no. 1, pp. 43–50, 2014.

[164] B. Voytek and R. T. Knight, "Prefrontal cortex and basal ganglia contributions to visual working memory," *Proceedings of the National Academy of Sciences*, vol. 107, no. 42, pp. 18167–18172, 2010.

[165] L. J. Kasper, R. M. Alderson, and K. L. Hudec, "Moderators of working memory deficits in children with attention-deficit/hyperactivity disorder (adhd): a meta-analytic review," *Clinical psychology review*, vol. 32, no. 7, pp. 605–617, 2012.

[166] G. Vallar and T. Shallice, *Neuropsychological impairments of short-term memory*. Cambridge University Press, 2007.

[167] H. L. Pincham, "The neural correlates of working memory impairment in attention-deficit/hyperactivity disorder," *Journal of Neuroscience*, vol. 34, no. 17, pp. 5735–5737, 2014.

[168] T. S. Eich, D. E. Nee, C. Insel, C. Malapani, and E. E. Smith, "Neural correlates of impaired cognitive control over working memory in schizophrenia," *Biological psychiatry*, vol. 76, no. 2, pp. 146–153, 2014.

[169] M. D'esposito and B. R. Postle, "The cognitive neuroscience of working memory," *Annual review of psychology*, vol. 66, 2015.

[170] N. Cowan, "Working memory underpins cognitive development, learning, and education," *Educational Psychology Review*, vol. 26, no. 2, pp. 197–223, 2014.

[171] S. E. Gathercole and A. D. Baddeley, *Working memory and language*. Psychology Press, 2014.

[172] G. S. Halford, N. Cowan, and G. Andrews, "Separating cognitive capacity from knowledge: A new hypothesis," *Trends in cognitive sciences*, vol. 11, no. 6, pp. 236–242, 2007.

[173] E. Kyndt, E. Cascallar, and F. Dochy, "Individual differences in working memory capacity and attention, and their relationship with students' approaches to learning," *Higher Education*, vol. 64, no. 3, pp. 285–297, 2012.

[174] C. Hulme and S. Mackenzie, *Working Memory and Severe Learning Difficulties (PLE: Memory)*. Psychology Press, 2014.

[175] M. Melby-Lervåg and C. Hulme, "Is working memory training effective? a meta-analytic review.," *Developmental psychology*, vol. 49, no. 2, p. 270, 2013.

[176] M. Spencer-Smith and T. Klingberg, "Working memory training," *The Wiley Handbook of Cognitive Control*, pp. 491–512, 2017.

[177] W. Knight, "What happens when you give an ai a working memory?," in *Intelligent Machines*, MIT Technology review, 2016.

[178] R. H. Logie, K. J. Gilhooly, and V. Wynn, "Counting on working memory in arithmetic problem solving," *Memory & cognition*, vol. 22, no. 4, pp. 395–410, 1994.

[179] C. L. Forgy, "Rete: A fast algorithm for the many pattern/many object pattern match problem," *Artificial intelligence*, vol. 19, no. 1, pp. 17–37, 1982.

[180] A. Fletcher, "Action potential: generation and propagation," *Anaesthesia & Intensive Care Medicine*, vol. 15, no. 6, pp. 287–291, 2014.

[181] A. H. Rezvani, "Involvement of the nmda system in learning and memory," *Animal models of cognitive impairment*, pp. 37–48, 2006.

[182] K. J. Staley, B. L. Soldo, W. R. Proctor, *et al.*, "Ionic mechanisms of neuronal excitation by inhibitory gabaa receptors," *SCIENCE-NEW YORK THEN WASHINGTON-*, pp. 977–977, 1995.

[183] V. B. Mountcastle, "The columnar organization of the neocortex.," *Brain: a journal of neurology*, vol. 120, no. 4, pp. 701–722, 1997.

[184] *Neural Circuit Development and Function in the Brain*, ch. Cortical Columns. Comprehensive Developmental Neuroscience, 2013.

[185] D. Barbour, "Auditory cortex structure and circuitry," 2009.

[186] T. A. Hackett, "Anatomical organization of the auditory cortex," *Journal of the American Academy of Audiology*, vol. 19, no. 10, pp. 774–779, 2008.

[187] C. E. Collins, D. C. Airey, N. A. Young, D. B. Leitch, and J. H. Kaas, "Neuron densities vary across and within cortical areas in primates," *Proceedings of the National Academy of Sciences*, vol. 107, no. 36, pp. 15927–15932, 2010.

[188] R. H. Masland, "The neuronal organization of the retina," *Neuron*, vol. 76, no. 2, pp. 266–280, 2012.

[189] J. Nolte, "The human brain: an introduction to its functional anatomy," 2002.

[190] Y. LeCun, Y. Bengio, *et al.*, "Convolutional networks for images, speech, and time series," *The handbook of brain theory and neural networks*, vol. 3361, no. 10, p. 1995, 1995.

[191] K. Fukushima, "Neocognitron: A hierarchical neural network capable of visual pattern recognition," *Neural networks*, vol. 1, no. 2, pp. 119–130, 1988.

[192] K. Fukushima and S. Miyake, "Neocognitron: A self-organizing neural network model for a mechanism of visual pattern recognition," in *Competition and cooperation in neural nets*, pp. 267–285, Springer, 1982.

[193] K. Fukushima, S. Miyake, and T. Ito, "Neocognitron: A neural network model for a mechanism of visual pattern recognition," *IEEE transactions on systems, man, and cybernetics*, no. 5, pp. 826–834, 1983.

[194] A. G. Hashmi and M. H. Lipasti, "Cortical columns: Building blocks for intelligent systems," in *Computational Intelligence for Multimedia Signal and Vision Processing, 2009. CIMSVP'09. IEEE Symposium on*, pp. 21–28, IEEE, 2009.

[195] A. Hashmi, H. Berry, O. Temam, and M. Lipasti, "Automatic abstraction and fault tolerance in cortical microachitectures," in *ACM SIGARCH computer architecture news*, vol. 39, pp. 1–10, ACM, 2011.

[196] A. Hashmi and M. H. Lipasti, "Discovering cortical algorithms.," in *IJCCI (ICFC-ICNC)*, pp. 196–204, 2010.

[197] J. Yelnik, "Functional anatomy of the basal ganglia," *Movement disorders*, vol. 17, no. S3, 2002.

[198] A. S. Karlsen and B. Pakkenberg, "Total numbers of neurons and glial cells in cortex and basal ganglia of aged brains with down syndrome—a stereological study," *Cerebral cortex*, vol. 21, no. 11, pp. 2519–2524, 2011.

[199] D. V. Buonomano and M. M. Merzenich, "Cortical plasticity: from synapses to maps," *Annual review of neuroscience*, vol. 21, no. 1, pp. 149–186, 1998.

[200] W. Gerstner and W. M. Kistler, "Mathematical formulations of hebbian learning," *Biological cybernetics*, vol. 87, no. 5-6, pp. 404–415, 2002.

[201] F. Zenke, W. Gerstner, and S. Ganguli, "The temporal paradox of hebbian learning and homeostatic plasticity," *Current opinion in neurobiology*, vol. 43, pp. 166–176, 2017.

[202] D. O. Hebb, *The Organizations of Behavior: a Neuropsychological Theory*. Lawrence Erlbaum, 1963.

[203] N. Caporale and Y. Dan, "Spike timing–dependent plasticity: a hebbian learning rule," *Annu. Rev. Neurosci.*, vol. 31, pp. 25–46, 2008.

[204] K. M. Diederen, H. Ziauddeen, M. D. Vestergaard, T. Spencer, W. Schultz, and P. C. Fletcher, "Dopamine modulates adaptive prediction error coding in the human midbrain and striatum," *Journal of Neuroscience*, vol. 37, no. 7, pp. 1708–1720, 2017.

[205] J. P. O'Doherty, "Reward representations and reward-related learning in the human brain: insights from neuroimaging," *Current opinion in neurobiology*, vol. 14, no. 6, pp. 769–776, 2004.

[206] P. Dayan and N. D. Daw, "Decision theory, reinforcement learning, and the brain," *Cognitive, Affective, & Behavioral Neuroscience*, vol. 8, no. 4, pp. 429–453, 2008.

[207] M. Ito and K. Doya, "Multiple representations and algorithms for reinforcement learning in the cortico-basal ganglia circuit," *Current opinion in neurobiology*, vol. 21, no. 3, pp. 368–373, 2011.

[208] Q. J. Huys, T. V. Maia, and M. J. Frank, "Computational psychiatry as a bridge from neuroscience to clinical applications," *Nature neuroscience*, vol. 19, no. 3, p. 404, 2016.

[209] S. Palminteri and M. Pessiglione, "Opponent brain systems for reward and punishment learning: causal evidence from drug and lesion studies in humans," in *Decision Neuroscience*, pp. 291–303, Elsevier, 2017.

[210] J. Baxter and P. L. Bartlett, "Direct gradient-based reinforcement learning," in *Circuits and Systems, 2000. Proceedings. ISCAS 2000 Geneva. The 2000 IEEE International Symposium on*, vol. 3, pp. 271–274, IEEE, 2000.

[211] S. Sahara, Y. Yanagawa, D. D. O'Leary, and C. F. Stevens, "The fraction of cortical gabaergic neurons is constant from near the start of cortical neurogenesis to adulthood," *Journal of Neuroscience*, vol. 32, no. 14, pp. 4755–4761, 2012.

[212] M. Toussaint, "Robot trajectory optimization using approximate inference," in *Proceedings of the 26th annual international conference on machine learning*, pp. 1049–1056, ACM, 2009.

[213] J. Deng, W. Dong, R. Socher, L.-J. Li, K. Li, and L. Fei-Fei, "Imagenet: A large-scale hierarchical image database," in *Computer Vision and Pattern*

Recognition, 2009. CVPR 2009. IEEE Conference on, pp. 248–255, Ieee, 2009.

[214] F. France, "projet shtooka."

[215] C. McCool, S. Marcel, A. Hadid, M. Pietikäinen, P. Matejka, J. Cernockỳ, N. Poh, J. Kittler, A. Larcher, C. Levy, *et al.*, "Bi-modal person recognition on a mobile phone: using mobile phone data," in *Multimedia and Expo Workshops (ICMEW), 2012 IEEE International Conference on*, pp. 635–640, IEEE, 2012.

[216] M. Li, X. Zhu, and S. Gong, "Unsupervised person re-identification by deep learning tracklet association," *arXiv preprint arXiv:1809.02874*, 2018.

[217] Y. Deng, P. Luo, C. C. Loy, and X. Tang, "Pedestrian attribute recognition at far distance," in *Proceedings of the 22nd ACM international conference on Multimedia*, pp. 789–792, ACM, 2014.

[218] R. Fisher, J. Santos-Victor, and J. Crowley, "Context aware vision using image-based active recognition," *EC's Information Society Technology's Programme Project IST2001-3754*, 2001.

[219] W. Sultani, C. Chen, and M. Shah, "Real-world anomaly detection in surveillance videos," *Center for Research in Computer Vision (CRCV), University of Central Florida (UCF)*, 2018.